Time dependent behavior of discontinuities and its relationship with long-term strength

March 2019

LIU ANG

Abstract

Rock mass, as an engineering material, is a complex geological material containing numerous discontinuities such as geological faults, joints, fractures, etc. Discontinuities are among the most important factors that governing the mechanical behavior of a rock mass. Investigated data has demonstrated that the failure of the rock engineering along discontinuities is always not a brittle behavior but progressive damage after years or decades by creep and stress relaxation. Currently, intensive emphasis has been put on studying the time-dependent behaviors of rock masses through laboratory creep tests. However, stress relaxation behaviors and its correlation with long-term strength has been rarely investigated.

A series of conventional shear tests, shear creep tests and shear relaxation tests under different normal stresses were performed on artificial discontinuities with different Joint Roughness Coefficient (JRC). Special interests of this study are given to understand the time dependent behaviors of discontinuities, especially stress relaxation behaviors, and their relationship with long-term strength of discontinuities.

The main research contents are as follows:

1) A series of conventional shear tests on discontinuities with various normal stresses and JRC were conducted to explore the shear mechanical behaviors impacted by normal stress and JRC.

2）A series of stepwise shear creep tests of discontinuities were conducted, and evolutions of creep and creep rates are analyzed. Accordingly, an improved K-B model was proposed to describe the creep characteristics of discontinuities, and the fitting results present a good agreement with test results.

3) The isostress cyclic loading method (ICLM) was proposed to study the shear stress relaxation behaviors of discontinuities. The evolutions of stress relaxation curves under different normal stress as well as cyclic loading were analyzed. Accordingly, a nonlinear model (H-K-M) was proposed to describe the stress relaxation characteristics of discontinuities, and the fitting results agree well with test results.

4) Correlation between stress relaxation behavior and long-term strength, as well as between creep behaviors and long-term strength are analyzed. Stress relaxation method is put forward and

proposed to determine long-term strength of discontinuities, from which the obtained long-term strengths present a good agreement with Mohr-Coulomb shear formula. Besides, long-term strengths were also obtained by creep tests. Differences between these methods were compared, which shows that stress relaxation method is more accurate.

Key words： discontinuities, artificial rocks, creep, stress relaxation, long-term strength

Contents

Chapter 1 Introduction

1.1 Background

Safety is very important for surrounding rock in underground excavations of transportation tunnel, mine and energy storage, as well as nuclear waste disposal (Brouard et al. 2013; Damjanac and Fairhurst 2010; Lacroix and Amitrano 2013; Main 2000; Miura et al. 2003; Mortazavi and Molladavoodi 2012; Nara et al. 2010; Tsai 2007). In the safety assessment of such projects the behavior of strength is inevitably of concern. As the failure of the rocks under loading is not a sudden brittle failure but progressive damaged after years or decades by stress relaxation and creep, this kind of strength or stability behavior is, of course, not only in the conventional sense, but also must be related with time. In addition, rock mass met in engineering is a complex geological material containing numerous discontinuities. These discontinuities usually have various mechanical characteristics due to the combinatorial effects of environmental conditions, such as field stress and groundwater conditions (Zhang et al. 2012, 2013). Barton (2013) pointed out that the stability of rock engineering mainly depends on the development of these discontinuities and their mechanical properties.

1.2 Current research

1.2.1 Creep and stress relaxation behaviors

Rock mass, as an engineering material, is a complex geological material containing numerous discontinuities such as geological faults, joints, fractures, etc. Discontinuities are among the most important factors that governing the mechanical behavior of a rock mass. The shear behavior of a discontinuity is a combination of complicated phenomena, which might suffer from complicated kinematic interactions associating with dilatancy, asperity crushing, and energy is dissipated by these kinematic interactions of contacted asperities on the surface of the discontinuities. Investigated data has demonstrated that the failure of the rock engineering under loading is always not a brittle behavior but progressive damage after years or decades by creep and stress relaxation

(Malan, 1999). Meanwhile, viscosity values measured on an engineering scale are much greater than those determined from intact rocks (Chin et al, 1987; Malan, 1987) It is reasonable to assume that the time-dependent behavior of rock masses will be controlled by the time-dependent behaviors that occur along discontinuities. To this end, emphasizing on time-dependent behavior of discontinuities is of great significance for rock engineering (Bieniawski Z T, 1967a, b; Shao J F et al, 2003). On the other hand, discontinuities in natural rocks are usually complicated and changeable, it is extremely difficult to collect and process natural rock masses with a homogenous discontinuity. Hence, replicas of natural discontinuities using cement mortar are preferred by many researchers for investigating the mechanical properties of discontinuities (Zhang et al. 2011, 2012).

Time-dependent behavior is a general term encompassing concepts like e.g. creep, stress relaxation, etc. Creep is defined as a state caused by prescribed boundary forces, while relaxation represents the state caused by prescribed boundary displacements (Spence and Hult J. 1973). Creep and relaxation are two intrinsic time-dependent behaviors of material caused by different boundary conditions (Goodman, 1989). The redistribution of stresses and displacements brought about in a rock mass when a pre-existing equilibrium is disturbed by such as excavation or in situ fracturing etc., is a time-dependent process involving a considerable time of months or years. If without reinforcement or supporting, the rock mass will suffer from creep and may eventually collapse over time. While the deformation is constrained by reinforcement or supporting, the rock mass will suffer from stress relaxation and may also eventually fail over time. Understanding the progressive failure induced by creep or stress relaxation behaviors would supply theorical support for retaining design. Intensive emphasis has been put on studying the time-dependent failure behaviors of rock masses through laboratory creep tests. However, while conducting the creep tests, it is extremely difficult to maintain a constant load during the tertiary stage where the rock mass starts to fail rapidly. As a result, limited information is available on the knowledge about time-dependent properties in this post-failure region. On the other hand, relaxation test under a constant strain could be an alternative to overcome the challenge posed in the creep tests to study time-dependent properties of rock mass (Peng 1973; Peng and Podnieks 1972). To data, however, rare studies have been conducted on the time-dependent behaviors of rock mass from the

perspective of stress relaxation properties. More relaxation study is worth trying to improve the rheological theory and verify the consistence between creep and stress relaxation.

1.2.2 Constitutive model

The constitutive model of rheological properties for rock mass has been investigated by many investigators encompass creep tests or theoretical analysis, but limited from the viewpoint of stress relaxation. Generally, rheological models can be divided into three categories: empirical, component, and mechanism-based constitutive. The empirical models are normally defined using a logarithmic function, a power function, and other differential equations (Molladavoodi and Mortazavi 2011; Zhang et al. 2012; Chen et al. 2014) to reproduce the stages of brittle creep of rocks with relatively few parameters and are widely used in practical engineering. However, the inherent physical mechanisms related to creep deformation are not accommodated in empirical models, so the key mechanical parameters remain physically unclear. As for component models, in practice, the separation of deformation into elastic, plastic, and viscous components can be difficult to achieve (Tsai et al. 2008). The creep behavior of brittle rock is found to be highly dependent on the subcritical cracking process, and rock rupture generally takes place soon after the appearance of accelerated creep strain (Salganik and Gotlib 2000). So finding a tractable way to link small-scale microcrack growth, which could be described with damage, with its macroscopic manifestation, i.e., creep strain and shear fracture is the essence of the problem in modeling creep (Brantut et al. 2012), coupled the sliding wing crack model of Ashby and Sammis (1990) with the Charles (1958) description of subcritical crack growth to describe time-dependent brittle creep of water-saturated rocks under triaxial stress conditions. Macroscopic brittle creep is modeled on the basis of micro crack extension under compressive stresses caused by subcritical crack growth (Atkinson 1984). When the stress intensity factor at crack tips is lower than the fracture toughness, subcritical crack growth (Atkinson 1984) occurs and eventually results in macroscopic faulting of the rock. In addition, stress corrosion was considered as one deformation micro mechanism explaining the macroscopic behavior of rocks in the brittle creep regime, and the associated model was also proposed (Lockner 1993; Costin 1985). Heap et al. (2015) also considered stress corrosion as one main mechanism for subcritical crack growth under upper crustal conditions. Although great effort has been made to model the rock creep and the proposed models have successfully reproduced the behavior of different types of rocks under a variety of loading conditions, currently there are few models that could include all the physical mechanisms and observations in a realistic way.

1.2.3 Long-term strength

A stress threshold, which is widely accepted as correct, could be observed during the creep process of rock mass, when the applied stress is higher than the stress threshold, the rock mass will fail in a limited time, even if the loading rate remains constant and when the applied stress is below the stress threshold, the creep deformation can be stabilized over time. This stress threshold is usually defined as long-term strength. Previous researches have shown that the failure strength of rock mass under long-term loading is clearly lower than that under conventional loading (Fabre and Pellet 2006; Zhang et al. 2011a, b). Liu and Xu (2000) carried out the rheological test on plaster samples and concluded that the long-term strength of anhydrite is approximately 66% of the conventional strength. Read (2004) considered that the in situ long-term strength of rocks is 50 % smaller than that obtained by a uniaxial compression test. Zhang et al. (2015) tested the mechanical behavior of weak discontinuity s through shear creep tests and found that the long-term strength of weak discontinuity s was approximately 80% of the conventional strength. Obviously, long-term strength is more reasonable that be adopted in the design of rock engineering to ensure its long-term stability.

As for determination of long-term strength, the most direct testing method is to use a single-stage constant load test under a series of different stress levels, which can accurately and directly obtain the long-term strength value. This value is the lowest loading value that experiences a sufficiently long loading time before the failure of the rock mass. Although this method is reasonable in theory, it is difficult to use in actual operation because the testing time is excessively long (Liu 1994). Since the behaviors of creep and stress relaxation both present strong association with long-term strength, we can use the different variation law in creep or stress relaxation tests before and after the long-term strength to determine its value. Currently, Stress relation properties and its relation to long-term strength were reported rarely (Ang 2015), most determination methods of the long-term strength are based on the creep test currently, which is conducted by stepwise increasing the loading stress. Bieniawski (1967) suggested that the long-term uniaxial compressive strength of rock could be determined by the inflection point of the volumetric curve that marked the transition from stable to unstable crack propagation. Munday et al. (1977) investigated the long-term strength of sandstone, marble, granodiorite, and granite through the variations of volume expansion and Poisson's ratio during creep process, and found that the long-term strength obtained based on Poisson's ratio was higher than that based on volume expansion. Martin and Chandler (1994) proposed that the long-term strength of rocks corresponds to the stress at which microscopic damage begins to induce dilation. Chandler (2013) defined long-term rock strength as the value of deviatoric

stress at volume strain reversal.

Although numerous endeavors have been done in determining long-term strength, it is still not enough to accurately describe the time-dependent strength for the different definition of long-term strength, and most of determinations of long-term strength are from the viewpoint of creep. In present study, a series of shear stress relaxation tests and shear creep tests were performed on discontinuities, firstly, a new method on basis of stress relaxation properties is put forward, which can more accurately and simply determine long-term strength, and then the evolution laws of creep rate under different stress levels and isochronous stress-strain curves are utilized to determine long-term strength of rock mass respectively, and their rationalities are discussed. Eventually, the results of long-term strengths determined by three aforementioned methods are comparatively analyzed.

1.3 The objective of this research

This research selected artificial joint surfaces poured by cement mortar based on Barton's ten standard lines of 1st, 4th, 6th and 10th to study its rheological properties through shear test under different stress levels, shear creep test and shear stress relaxation test. The size of the samples used was 10 by 10 by 10 cm.

Main research contents are as follows.

1. The mechanical properties of intact sample and shear strength and deformation on shear direction was studied based on uniaxial compression test of intact sample and instantaneous shear test of 1th,4^{th} and 10^{th} discontinuity under different normal stress;

2. Creep rate law of discontinuity and shear creep properties of discontinuity were studied based on shear creep test of 1th, 4^{th} and 10^{th} discontinuity under different normal stress which is conducted by multi-stage loading method;

3. K-B model was selected to describe creep properties based on the test result, furthermore a improved K-B model was built which has better result to study its properties. The evolution laws of K-B model's parameters were analyzed from views of creep mechanism and the parameter influence on creep curve respectively.

4. The stress relaxation mechanism, stress relaxation law and stress relaxation properties under different stress, different discontinuity and cyclic loading condition were studied based on shear relaxation test of 4^{th}, 6^{th} and 10^{th} discontinuity which is conducted by isostress cyclic loading method (ICLM) under different stress value.

5. Burgers models was selected to describe stress relaxation properties of discontinuity,

furthermore a improve models named H-K-M model was suggested to describe its properties which obtained better result. The evolution laws of model's parameters in this two were analyzed from views of creep mechanism and the parameter influence on creep curve respectively.

6. Time-effect properties of rock mass were analyzed. The principle of different method to determine long-term strength was studied and theirs advantages and disadvantages were compared. A new method to determine long-term strength was proposed based on shear stress relaxation result, which is better than existed method.

Chapter 2 Shear properties of discontinuities

2.1 Samples preparation

Discontinuity is a joint name of various types of geological interface like geological stratum and fault, joint, cleavage etc., which are formed in geological process in rock mass. Rock mass as multiple cracks material cut by discontinuities depend on its difference of other materials, discontinuities always control the deformation and damage of rock mass, therefore the mechanical mechanism of discontinuities is directly related to safe and stability of rock engineering.

The morphology of discontinuities as a complicated factor has very important influence to mechanical behaviors of rock mass, but current research result also cannot give an accurate evaluation effecting in the mechanic properties of rock mass. Barton first come up with a concept of JRC to describe the morphological influence of discontinuities in the mechanical behaviors of rock mass based on numerous shear tests, then he cooperated with Choubey and gave out ten typical discontinuity lines, whose JRC value is from 0 to 20. Lately, International Society for Rock Mechanics (ISRM) redefined these discontinuity section lines (Figure 2.1) based on Barton etc., which effectively promotes to investigated the impact of discontinuities on mechanical behaviors of rock mass widely and deeply.

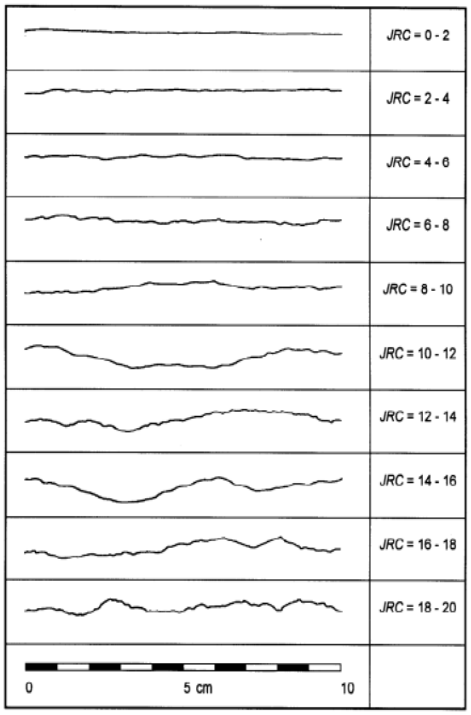

Figure 2.1 Ten standard roughness profiles suggested by Barton and Choubey (1977)

In this work, since it is extremely difficult to collect and process natural rock mass with a discontinuity, this test selected steel mold (Figure 2.2) and used appropriate materials to manually pour a cube model with a discontinuity (Figure 2.2), which can guarantee the relative homogeneity of the sample. In this test, No. 325 cement, sand, and water were selected as model materials, at a mixing ratio of 2:4:1. The 4th and 10th discontinuity lines from Barton′s ten standard lines (Figure 2.3) were selected to pour the sample, at a size of 10 by 10 by 10 cm. After pouring the cube model, the mold was opened when the model is formed (statically stored for 24 h); finally, the model was stored under constant temperature and humidity (temperature: 20±0.2℃; humidity: Over 95 %) for 28 days.

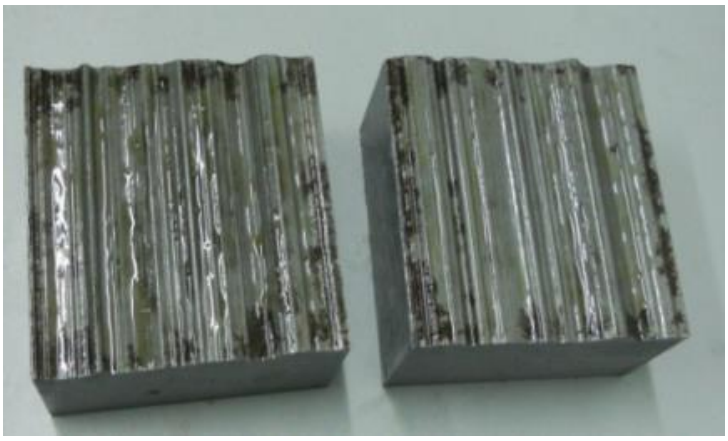

Figure 2.2 Steel mold used in pouring structural sample

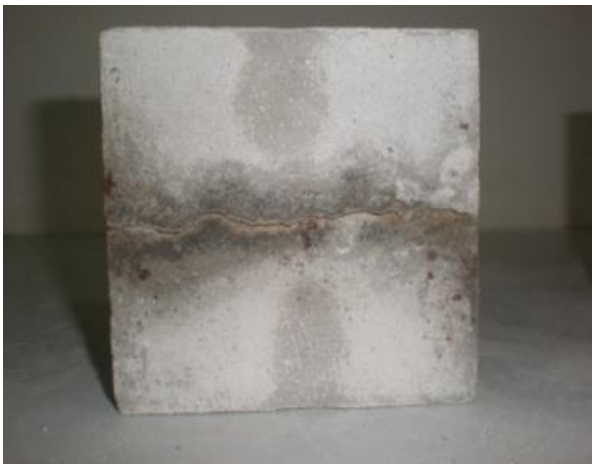

Figure 2.3 Artificial sample of discontinuity

2.2 Testing equipment

A CSS-1950 biaxial shear rheological testing equipment (shown in Figure 2.4) with servo

control was used for the test. This equipment is mainly composed of three parts, host machine, electric cabinet and computer. It can conduct uniaxial compressive test, biaxial compressive test, uniaxial rheological test and shear rheological test on rocks and concrete. This machine can use a built-in software system to control the test process and test parameters, automatically collect the data, and set the acquisition precision according to the requirements. The largest vertical axis compression load is 500 kN, and the largest horizontal axis compression load is 300 kN. Loading system is screw loading, loading rate can be controlled in two manners, stress rate and strain rate. Deformation in two directions can be measured, and its precision can up to 0.001mm.

Figure 2.4 CSS-1950 biaxial shear rheological testing equipment

2.3 Loading procedures and test conditions

Laboratory tests related to the shear properties in this chapter are listed as follows.

1) Firstly, a series of uniaxial compression tests were conducted, and the strength value of test materials as well as the relation of loading and deformation were obtained whose loading rate is 0.2KN/s, the relationship between loading stress and deformation can be obtained to study the properties of this material's strength .etc. 10%, 15%, 20%,30% and 40% of strength value were selected as the preparing value of shear test in the following study.

2) Conducting shear test on intact sample and 1th, 4^{th}, 6^{th} and 10^{th} structural surface sample in which normal force is 10%,15%,20%,30% and 40% of strength value respectively, shear strength

and the relationship between shear stress and deformation in shear direction can be obtained. In the process of the test, normal stress is loaded firstly, keep it as a constant through the whole test when the loading value up to predetermined value, and then apply the shear stress until the sample is broken, the loading rate is still 0.2KN/s.

3) Based on the relationship between shear strength and shear deformation and M-C shear strength formula, $\tau = c + \sigma_n \tan\varphi$, cohesion force c and internal friction angle φ can be obtained , and the relationship with JRC of them was studied. In addition, the change laws of shear deformation curves are summarized.

After shear stress test under different normal stress on the intact sample and structural sample which is poured based on the 1st, 4th, 6th and 10th section line of Barton's then standard section line, shear strength, cohesion force and internal friction angle of these sample can be got, the relationship between these three parameters and JRC is analyzed. The shear deformation properties effected by stress and JRC is studied, which could give fundamental parameters for the shear rheological test.

2.4 Strength properties of discontinuities

2.4.1 Uniaxial compressing test on intact sample

Five intact samples were conducted uniaxial compressing test, most of them perform columnar or pyramid shaped damage, and parts of them perform necking damage. Typical damage can be seen from Figure 2.5. The load deformation curve is shown in Figure 2.6.

From Figure 2.6, stress-strain curve can be divided to four stages, compression stage, elastic stage, plastic stage and damage stage, which is similar with stress-strain curve in rock mechanic theory. It also can testify that using cement mortar as artificial material can reflect the properties of rock mechanic well.

Through uniaxial compression test, strength value can obtain as follows 22.85 MPa, 22.34 MPa, 17.77 MPa, 26.84 MPa and18.86 MPa. Obtained data did not appear obvious difference, and the average value of them were taken as uniaxial compressing strength, 21.73MPa.

Figure 2.5 Typical failure pattern of intact samples

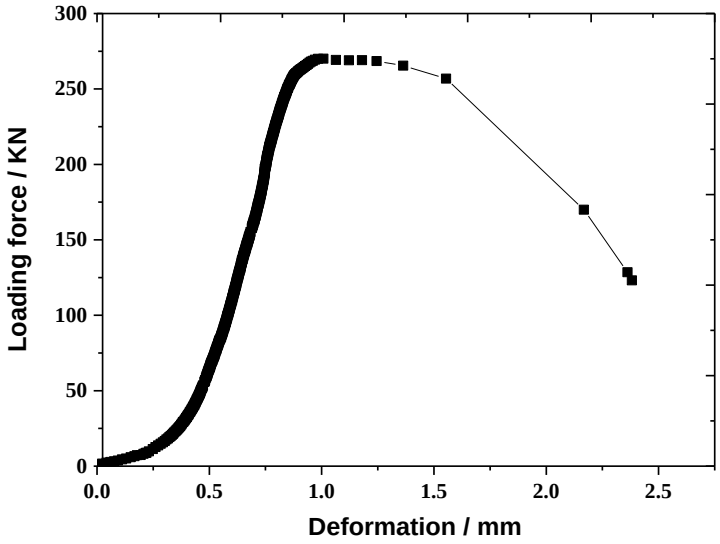

Figure 2.6 Typical loading-displacement curve of intact samples

2.4.2 Shear test results on intact sample and sample with discontinuity

From 2.4.1, strength value of intact sample under uniaxial loading was obtained, take 10%, 15%, 20%, 30% and 40% of the value, 2.17MPa, 3.26 MPa, 4.35 MPa, 6.52 MPa and 8.69 MPa in turn, as the normal loading stress using in shear test. Five groups of shear test on each discontinuity were conducted, and shear strengths are shown as Table 2.1.

From Table 2.2, comparing with sample with discontinuity, shear strength of intact sample has a significantly improve. Shear strength of intact sample is 6.21MPa, while the value of sample with 10^{th} discontinuity is 3.15 which is only 50.7% of the intact sample.

Table 2.1 Shear strength of tested discontinuities

NO.	JRC	Normal stress/ MPa				
		2.17	3.26	4.35	6.52	8.69
1st	1	1.76	2.83	3.89	5.52	6.89
4th	7	2.21	3.20	4.54	6.03	8.32
6th	11	2.55	3.65	4.77	6.57	9.37
10th	19	3.15	4.34	5.62	8.50	10.21
Intact sample	—	6.21	7.21	8.25	10.26	12.28

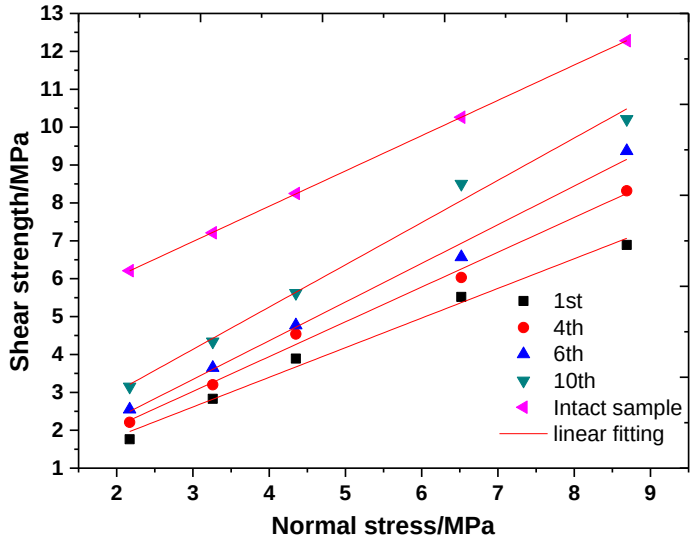

Figure 2.7 Relationship between shear strength and normal strength

The linear relationship of shear strength and normal stress can be drawn as Figure 2.7, which illustrate that material used in the sample has good mechanic property with the linear correlation

coefficient all reached 0.99.

Cohesive force and internal friction angle can be calculated as shown in Table 2.2 following M-C formula.

Table 2.2 Fitting parameters by Mohr Coulomb

Discontinuities	Cohesive Force MPa	Internal friction angle °	R^2
1st	0.268	37.46	0.995
4th	0.271	42.58	0.996
6th	0.281	45.60	0.995
10th	0.790	47.48	0.999
Intact sample	4.185	43.00	0.996

From Figure 2.7 and Table 2.2 it can be seen that:

1) Cohesive force increase with the increasing of JRC and 10^{th} discontinuity has an obvious increasing comparing to 6^{th} discontinuity, which is caused by the change of the shear failure mechanism with the increasing of JRC (explained in detail in 2.3). Shear strength of intact sample mostly depend on the cohesive force which has a significantly increase comparing to sample with discontinuity.

2) The relationship between internal friction angel and JRC can describe in linear form shown in Figure 2.8 and the correlation coefficient is up to 0.995, expression is $\varphi=0.553JRC+38.2$.

The shear strength also increases with the increasing of JRC under same normal stress, and a linear relationship whose correlation coefficient is up to 0.95 between them can be established as follow (Eq. 2.1 & Figure 2.9).

$$\tau = mJRC + n \qquad (2.1)$$

Where, m and n is fitting coefficient.

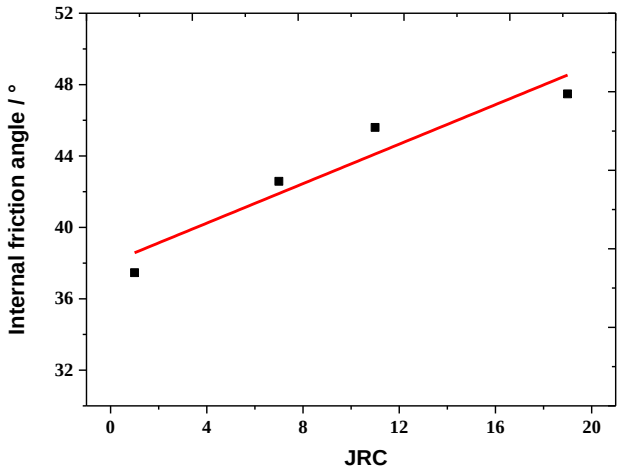

Figure 2.8 Relationship between JRC and internal friction angle

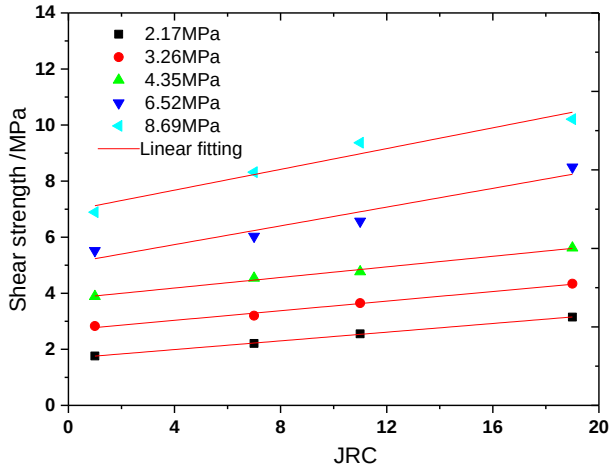

Figure 2.9 Relationship between shear strength and JRC

From Figure 2.9 it can be seen that:

1) *m* increases with the increasing of normal stress, as seen in Figure 2.10. The increasing trend is slowly when the stress level is relatively slow, and then entrance to a rapid increasing stage, lastly slow down again. The reason is also relate to the change of shear failure mechanic.

2) *n* has a linear relationship with normal stress (see Figure 2.11), which meet the following formula $n = 0.782\sigma_n + 0.127$.

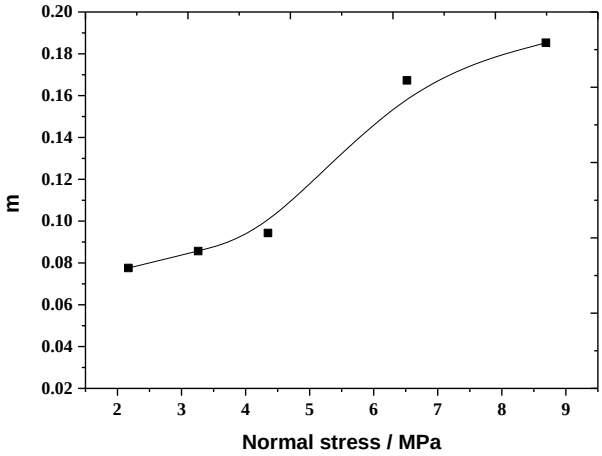

Figure 2.10 Relationship between m and normal stress

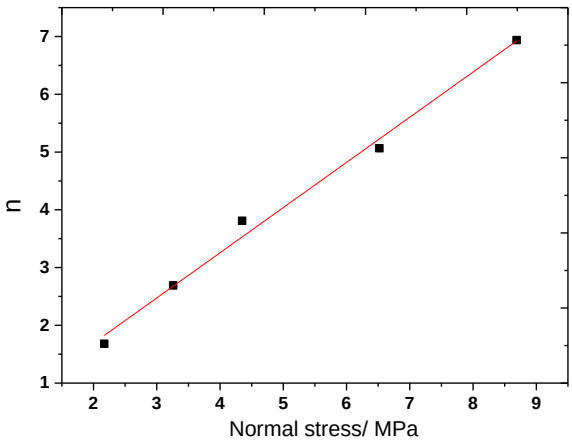

Figure 2.11 Relationship between n and normal stress

Based on the analysis above, the value of shear strength is related to both normal stress and JRC, shear strength increase with the increasing of both normal stress and JRC and has linear relationship with them. The slopes of the fitting line are 0.959 and 0.106 respectively, which illustrate that shear strength is affected by the normal stress more obvious.

2.5 Deformation properties of discontinuities

2.5.1 Shearing mechanism of discontinuities

The mechanic properties of rock mass with discontinuity mainly include shear strength,

deformation property and constitutive relation, and the deformation property usually uses the relationship between shear strength and shear deformation to describe. The current study focusing on the deformation property is relative less, while mostly focus on the strength property and the parameters relating to the strength of sample with discontinuity, which is mainly attribute to the large difference of shear deformation curves.

Shear stress-strain curve obtained through shear strength test present different forms. In views of mechanism, generally, there are two damage forms, hard failure and frictional movement, hard failure is in term of shearing down the main raised position locating on the surface of discontinuity, and frictional movement happen between side walls of discontinuity. Usually, hard failure happens along with a larger stress fluctuation and frictional movement happens along with a relative larger deformation. Generally, both two forms work in the process of shearing test, and one of them predominate.

From section 2.4.2, the shearing property is affected by both normal stress and JRC. As the sample with discontinuity used in the test is continuous, first choice of deformation would be in term of frictional movement presenting normal capacity and the main factors limiting the deformation in shear direction would be the normal stress and the shape of protruding on the structural surface. If the shear stress along the tilt angle of the protruding is not big enough to overcome the sum stress of normal force component along the shape of the protruding and the frication stress between the side walls of discontinuity, the shear stress would accumulate in this area with the increasing loading till its value is big enough to cut down the protruding. (see Figure 2.12)

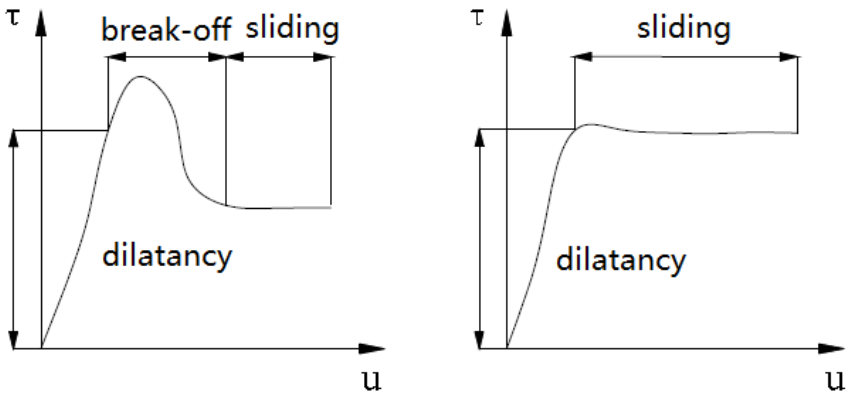

Figure 2.12 Break-off failure and grinding failure

From Figure 2.12, the former part of these two forms is similar, which successively experience consolidation stage, elastic deformation stage and yield deformation phase, and finally is up to the peak strength. The curve law changes after the peak strength, for the difference of deformation mechanism.

2.5.2 Test results

Based on test results, stress-deformation curves of a same discontinuity under different normal stress can be drew as follow (see Figure 2.13).

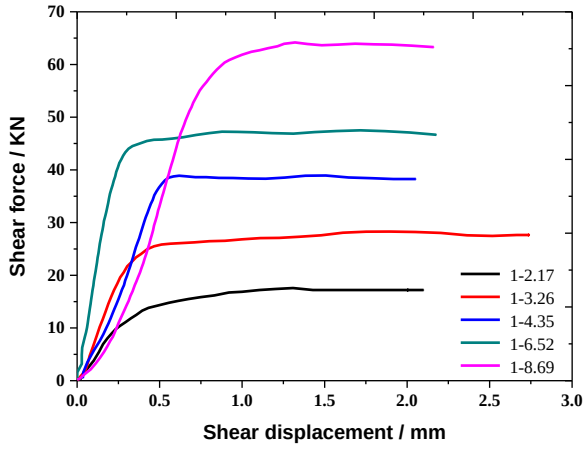

a. 1st discontinuity

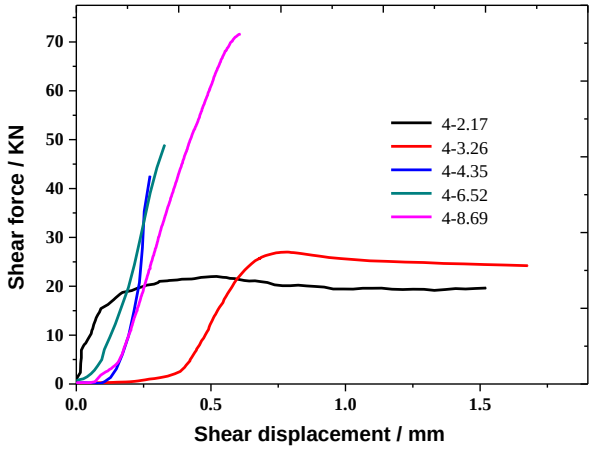

b. 4th discontinuity

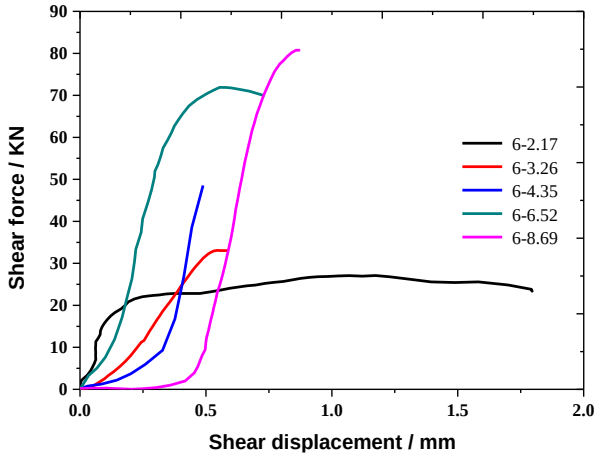

c. 6th discontinuity

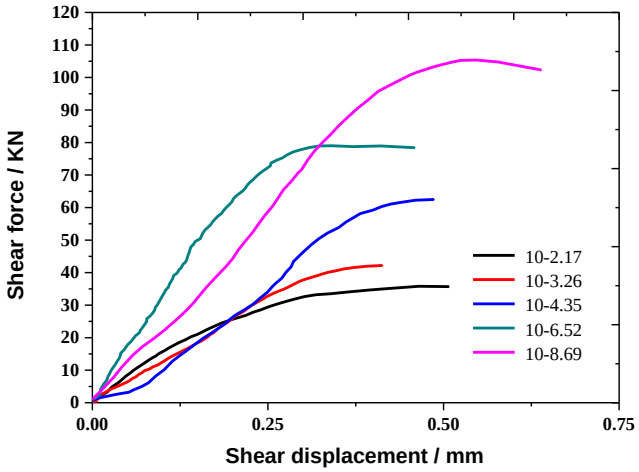

d. 10th discontinuity

Figure 2.13 Shear force-displacement curve

From Figure 2.13 it can be seen that:

1) Two mentioned types of curves in term of break-off type and grinding type curve were observed in the shear deformation-stress curve. Nothing that the break-off type curve in the post-peak regime is not well observed resulting in the stuffiness of test equipment. According to the statistics, there are 8 shear deformation curves failed in term of grinding, while 12 shear deformation curves failed in term of break-off.

2) Part of curves present a larger shear deformation at the initial stage (e.g. 4-8.69 and 6-8.69), it is considered resulting from adjusting of discontinuities which are not well matched to each other.

3）As shown in figure 2-13, the 1st discontinuity are failed by grinding, the 4th discontinuity

under relatively low normal stress are failed by grinding and are failed by break-off under relatively high normal stress, and the 6th and 10th discontinuities is dominated by break-off failure. It is indicated that, with the increase of JRC, the failure pattern transit from grinding type to break-off type.

On the basis of Figure 2.13, the relationship between the shear force and shear displacement with different JRC under same normal stress could be drawn in Figure 2.14. From which, it is observed that while the normal stress is equal to 2.17MPa the failure pattern of the 1st ,4th and 10th discontinuities are controlled by grinding type and the 10th discontinuity is controlled by break-off type. With the increasing of normal stress, the failure pattern are gradually controlled by break-off type. When the normal stress is increased to 4.35, 6.52 and 8.69MPa, the 1st discontinuities presents grinding failure and the others are controlled by break-off failure.

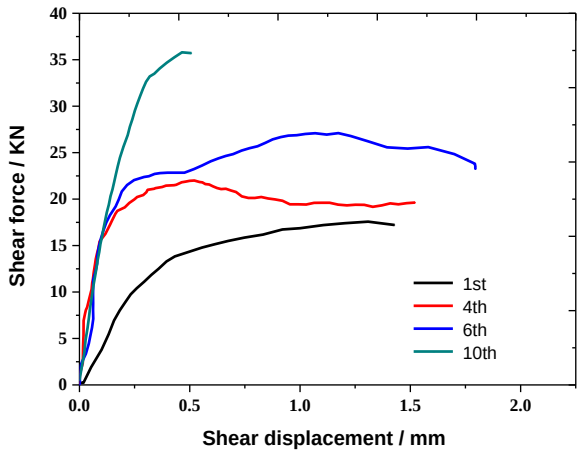

a. Normal stress 2.17MPa

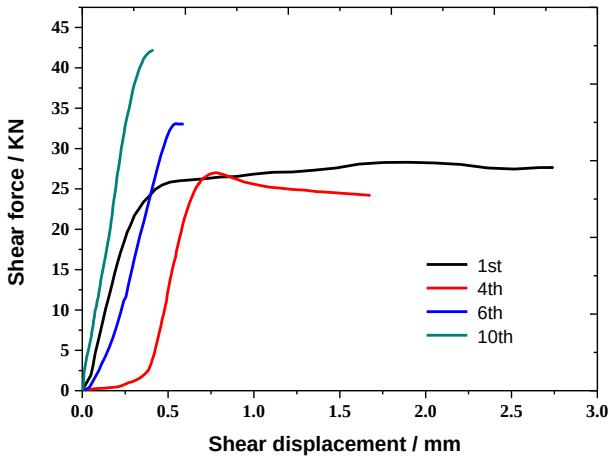

b. Normal stress 3.26MPa

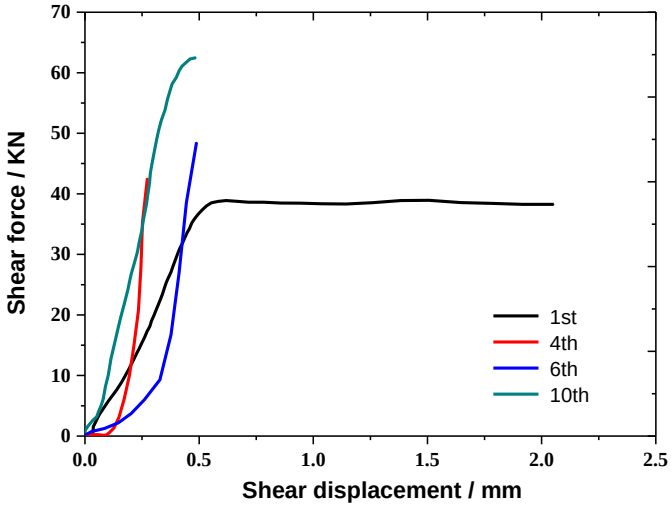

c. normal stress 4.35MPa

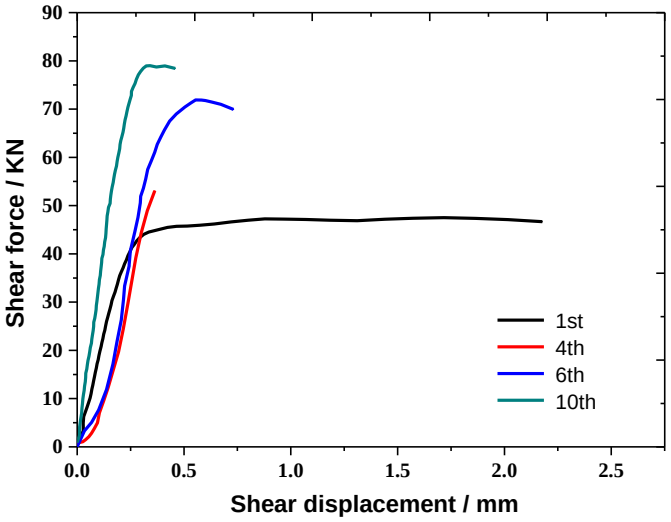

d. Normal stress 6.52MPa

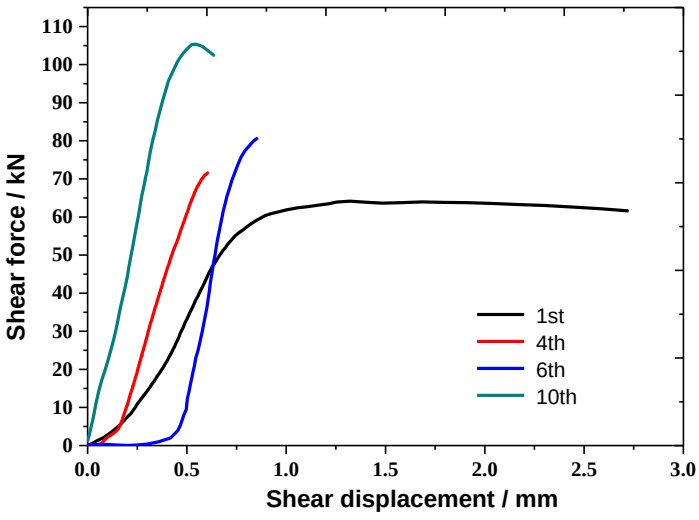

e. Normal stress 8.69MPa

Figure 2.14 Shear force- displacement curve

2.6 Summary

In this chapter, conventional shear test on artificial discontinuities with different JRC were conducted and the corresponding shear force-deformation curves were obtained. The main conclusions can be drawn as follow.

1）The shear deformation curves could be divided into two types, i.e. break-off type and grinding type, which is depended on the applied normal stress and the JRC value of tested discontinuities. Generally, with the increase of both normal stress and JRC, the type of shear-deformation curve is transferring from grinding type to break-off type.

2）For the discontinuities with same JRC, shear strength increase linearly with the normal stress increase. For the shear test conducted under same normal stresses, the shear stress linearly increases with the JRC increases.

3) The mechanical parameters, cohesive force and internal friction angle, are obtained from Molar coulomb's formula. The friction angle linearly increases with the increase of JRC, while the shear strength of intact sample is mainly depended on its cohesive force.

Chapter 3 Creep properties of discontinuities

In engineering practice, the time-dependent failure of rock masses is not induced by the internal rheology, but by the structural rheology. Generally, the rheological damage of discontinuities is not an instantaneous moment, but a progressive process that caused under the long-term compression-shear manifested as creep and relaxation behaviors. Therefore, it is of significance to study the creep behavior of samples with discontinuity under compression-shear condition.

Since the rheological constitutive model is one of the important parts of creep study, numerous researchers have done plenty of contributions on it. The present models mainly include empirical model, and element combination model, etc. In which, empirical model can accurately describe the creep behaviors in a single engineering practice but fail in others, because its involved parameters do not have clear physical meaning. On the other hand, though the involved parameters in element combination models in describing creep have clear physical meaning, it needs an accurate cognition on the rheological mechanism. As a result, those element combination models established basing on an inaccurate mechanism would have same issues as empirical model. In addition, there also exist literatures to show that the elasticity modulus, viscosity coefficient, etc. are not constant but varied with the testing time. In view of these, the fundamental method to solve the problem of establishing constitutive model is to correlate the relationship among rheological parameters, stress and time. Unfortunately, rare efforts have been made on this subject, and a great quantity of work is still desired.

In this chapter, a series of shear creep tests were conducted on discontinuities of the 1st, 4th and 10th discontinuity of Barton's standard section line. The creep properties basing on whole process creep curve, multi-stage loading creep curves, multi-stage loading creep rate curves and isochronous curves were studied, and Nishihara model was proposed to describe the creep properties of discontinuity. With this, a new model based on NISHIHARA model, which can give a better description to creep properties, was suggested, and the evolution of its involved parameters were analyzed from the perspectives of creep mechanism and the sensibility of the parameters respectively.

3.1 Loading procedure and test conditions

The samples used in the creep test is poured by cement mortar and the structural plans based on the 1st, 4th and 10th discontinuities from the ten standard section plane of Barton were selected, as also mentioned in Chapter 2. The test equipment also used the CSS-1950 rock biaxial rheological apparatus (see 2.1.1 & 2.1.2).

The loading method (see Figure 3.1) called Chen loading method was used, which can obtain more test date through one sample, and the fundamental principle of it can memory the loading history and avoid the influence of the difference of samples. Three groups of each discontinuity under different normal stress were used to conduct the shear creep test. Each sample is named: the No. of discontinuity-normal stress, for example, 1-2.17 refers to the test of 1st discontinuity under the normal stress of 2.17MPa.

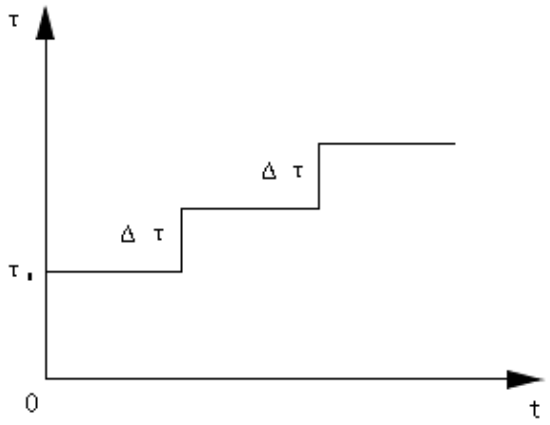

Figure 3.1 Illustration of stepwise loading procedure

Details about the test procedures are shown as follows:

1) Firstly, apply the normal stress (with a loading rate of 0.2 kN/s) on the sample until the deformation becomes unchanged. In which, the normal stresses in each creep test were adopted to be the 10%, 20% and 30% of the averaged shear strength of the intact sample obtained in chapter 2.2.1 (i.e. 21.73 MPa). Therefore, the normal stresses were 2.17 MPa, 4.35 MPa and 6.52 MPa, respectively.

2) Secondly, apply the shear stress to the predetermined value after the normal deformation tends to be stable, with the loading rate of 0.2 kN/s, and then conduct the shear creep test. In which,

the shear values for each test were selected to be the 50 %, 60 %, 70 %, 80 %, 90 % and 95 % of the shear strength of the rock sample under the corresponding normal stress.

3) Each level of creep tests was kept for 72h until its broken, and each sample was tested for 5 ~ 6 levels. During the test, the temperature and the humidity of the laboratory room were remained constant, and the ambient vibration was avoided.

Details about the testing conditions for the creep tests are shown in Table 3.1.

Table 3.1 Creep test conditions

Sample	JRC	levels	Shear stress /MPa	Shear stress/shear strength	Time per level/h	Times/h
1-2.17	1	1	0.88	0.5	71.33	356.11
		2	1.06	0.6	71.15	
		3	1.23	0.7	71.15	
		4	1.41	0.8	71.33	
		5	1.58	0.9	71.15	
1-4.35	1	1	1.95	0.5	71.51	430.04
		2	2.33	0.6	71.84	
		3	2.72	0.7	71.67	
		4	3.11	0.8	71.67	
		5	3.5	0.9	71.66	
		6	3.7	0.95	71.68	
1-6.25	1	1	2.37	0.5	71.89	429.99
		2	2.84	0.6	71.65	
		3	3.31	0.7	71.66	
		4	3.78	0.8	71.66	
		5	4.26	0.9	71.48	
		6	4.49	0.95	71.65	
4-2.17	7	1	1.1	0.5	71.00	366.14
		2	1.32	0.6	73.12	
		3	1.54	0.7	73.33	
		4	1.76	0.8	74.79	
		5	1.98	0.9	73.90	
4-4.35	7	1	2.27	0.5	72.40	359.27
		2	2.72	0.6	71.65	
		3	3.18	0.7	71.14	
		4	3.63	0.8	71.42	
		5	4.09	0.9	72.66	
4-6.52	7	1	2.66	0.5	71.33	357.42
		2	3.19	0.6	70.67	

		3	3.72	0.7	71.53	
		4	4.25	0.8	72.71	
		5	4.78	0.9	71.18	
10-2.17	19	1	1.79	0.5	71.67	359.18
		2	2.15	0.6	71.67	
		3	2.51	0.7	71.84	
		4	2.86	0.8	71.90	
		5	3.22	0.9	72.10	
10-4.35	19	1	3.13	0.5	71.71	358.93
		2	3.75	0.6	71.70	
		3	4.38	0.7	71.88	
		4	5	0.8	71.87	
		5	5.63	0.9	71.77	
10-6.52	19	1	3.95	0.5	71.86	429.95
		2	4.74	0.6	71.69	
		3	5.53	0.7	71.71	
		4	6.32	0.8	71.31	
		5	7.11	0.9	71.69	
		6	7.51	0.95	71.69	

3.2 Whole process of creep curves

3.2.1 Creep mechanism

The process of creep can be divided into three stages (see Figure 3.2), i.e. the primary creep stage, the stable (secondary) creep stage and the accelerated (tertiary) creep stage.

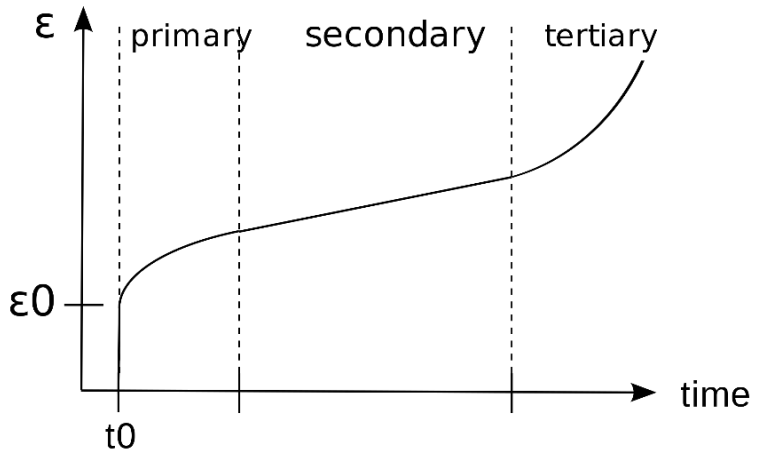

Figure 3.2 Typical creep curves and its division

1) In the primary creep stage, the creep rate gradually tends to a stable value or 0, its duration mostly depends on the stress level and the viscous-elasticity property of the rock. In this stage, if unload the stress, instantaneous elastic deformation would be released firstly, and then viscoelastic deformation showing the hysteresis effect would recover gradually over time, a certain amount of residual plastic deformations cannot be recovered, as shown in dotted line B-C in Figure 3.2.

2) In the stable creep stage B-D, the creep curve presents as an approximately linear manner, and the creep rate is a constant. This stage of creep is resulted from the progressive damage of either the rock or the discontinuity; the creep rate and the duration of this stage are greatly influenced by the stress level. Unloading the sample in this stage, the instantaneous elastic deformation would firstly recovered, followed by the gradually recovery of the viscoelastic deformation with the elapsing time. In addition to the remaining part of the instantaneous plastic deformation, part of the sticky plastic deformation will be permanent residual deformation, as shown in the dotted D-E in Figure 3.2;

3) In accelerated creep stage, the creep rate would increase rapidly and the rock would be damage eventually. In this stage, the creep curve evolves nonlinearly, which is caused by the extension of the macro cracks, as well as the rheological damage of the rock. Currently, instructive summaries regarding this stage are still limited.

3.2.2 The whole process of creep curves

A series of creep shear tests on discontinuities of 1st, 4th and 10th Barton's line were conducted under different normal stresses of 2.17 MPa、4.35 MPa and 6.52 MPa. Based on their test results, the whole process of creep curves could be obtained, as shown in Figure 3.3 to Figure 3.11.

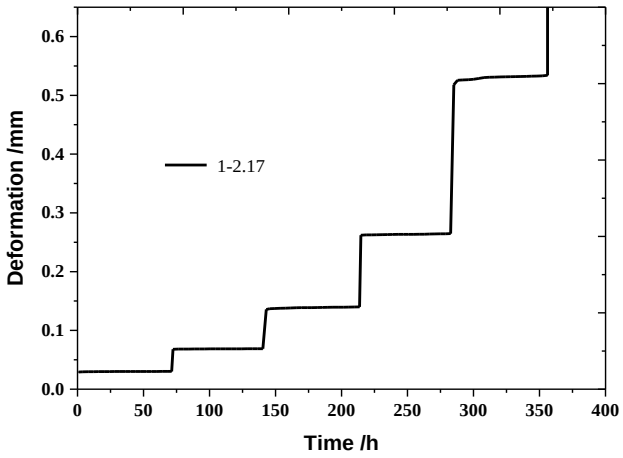

Figure 3.3 Whole process of creep curves under stepwise loading（1-2.17）

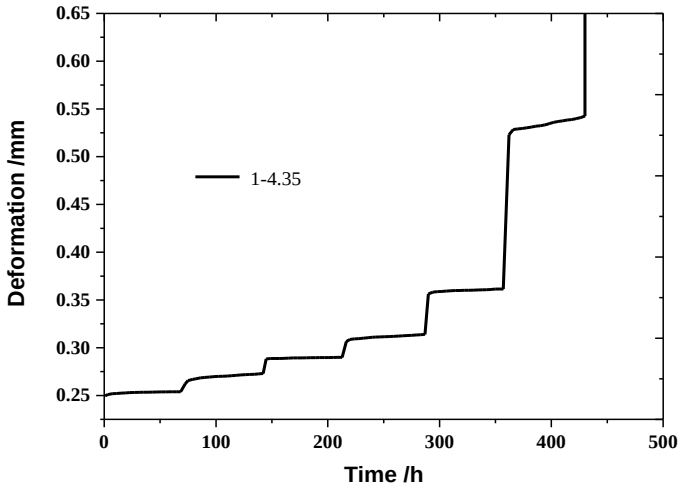

Figure 3.4 Whole process of creep curves under stepwise loading（1-4.35）

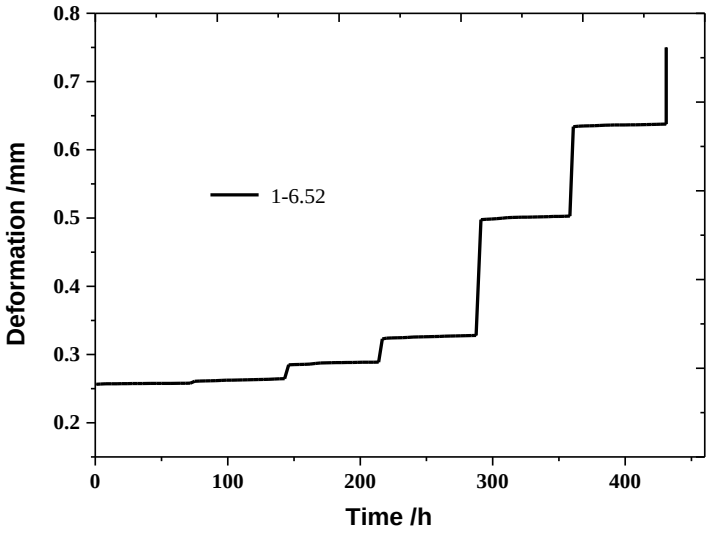

Figure 3.5 Whole process of creep curves under stepwise loading（1-6.52）

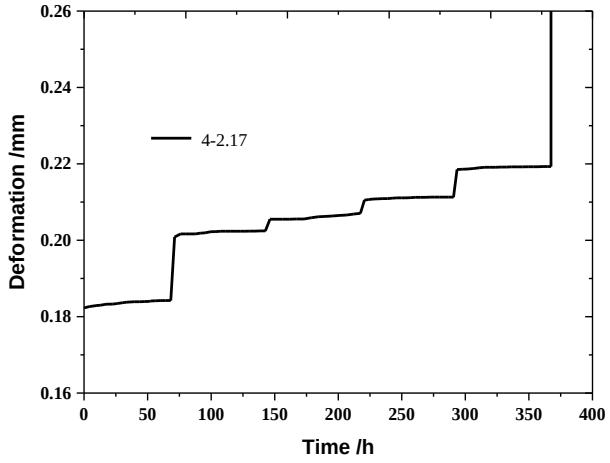

Figure 3.6 Whole process of creep curves under stepwise loading（4-2.17）

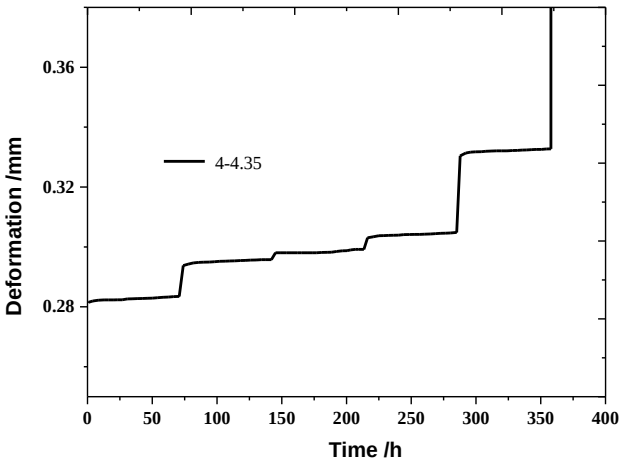

Figure 3.7 Whole process of creep curves under stepwise loading（4- 4.35）

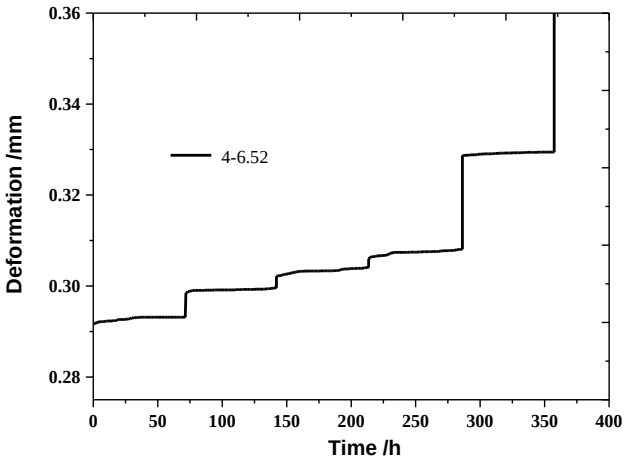

Figure 3.8 Whole process of creep curves under stepwise loading（4-6.52）

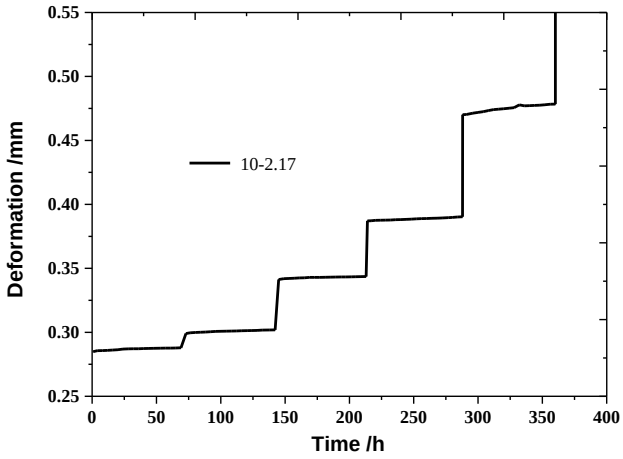

Figure 3.9 Whole process of creep curves under stepwise loading（10-2.17）

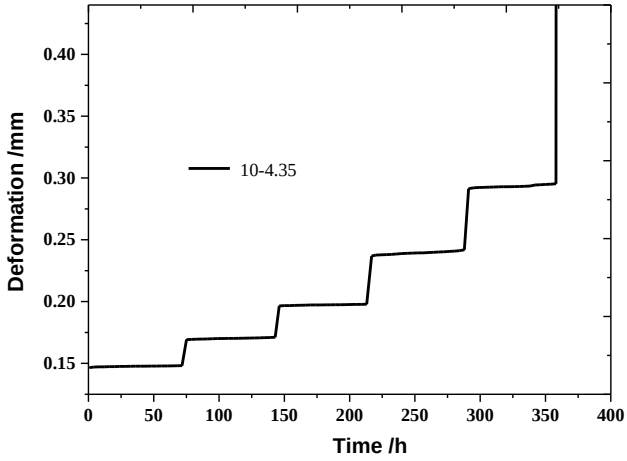

Figure 3.10 Whole process of creep curves under stepwise loading（10-4.35）

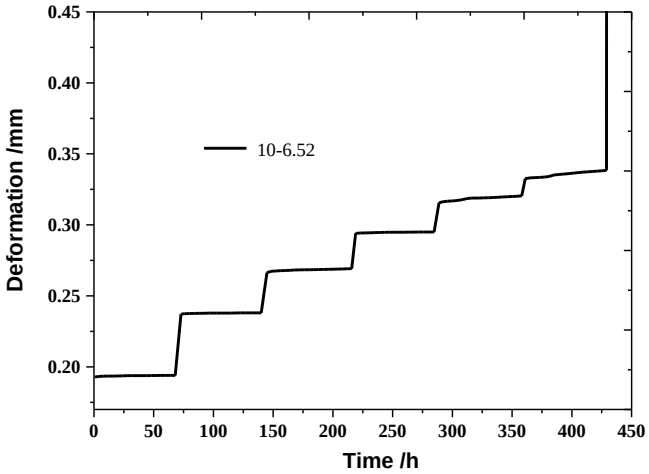

Figure 3.11 Whole process of creep curves under stepwise loading（10-6.52）

From Figures 3.3 to 3.11, it is observed that:

1) The first loading level in each curve is larger, which is due mainly to the manufacture issue of the sample where the discontinuities were not close very well. Most of the deformation is not caused by the essential deformation of the sample itself but by the closing of the gap between two discontinuity s.

2) Most of the samples were failed in the last loading level accompanying with the third creep stage (i.e. accelerated creep stage) except the sample 1-4.35, which is broken under a constant stress, but also show an instantaneous damage along with a large deformation. It can be seen that the damage feature during the accelerated creep stage is very different between the structural surface and intact rock. Creep damage of an intact rock subjected to a constant stress is a process of the gradual development and accumulation of micro cracks, which finally coalescent into macro-cracks along with the viscous friction effect between cracks, leading to the catastrophic failure of the sample. While for those samples with discontinuities, the sample is already under coalescence, when the stress level has reached a certain value, viscous resistance inclines to reduce quickly, leading to a relatively instantaneous failure in the accelerated creep stage.

3.3 The properties of stepwise creep curve

Based on the results of the whole process of creep curves, the grade creep curve could be obtained after using the Boltzmann superposition principle, which could consider the influence of historical loading. With this, the creep properties and the isochronous curve features under different stress levels were studied.

3.3.1 Multi-grade creep curves

To study the evolution of creep curves under different stress levels, the corresponding grade creep curves were obtained by superposition the results obtained in the whole creep curves. The results were shown in Figures 3.12~3.20.

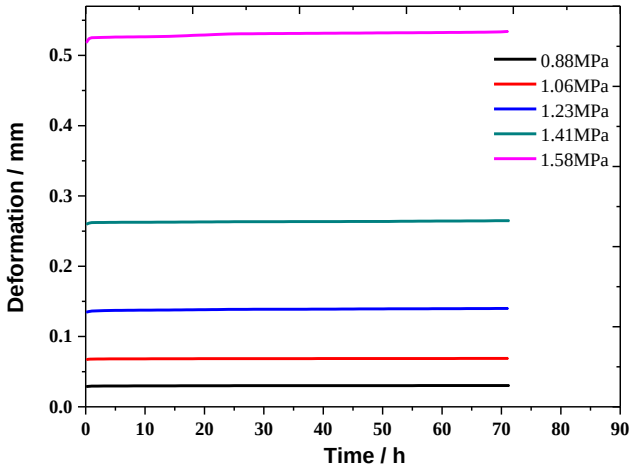

Figure 3.12 Multi-grade creep curves（1-2.17）

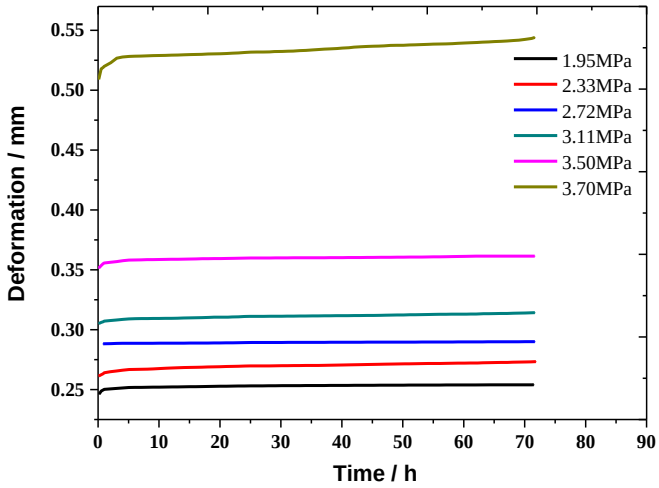

Figure 3.13 Multi-grade creep curves（1-4.35）

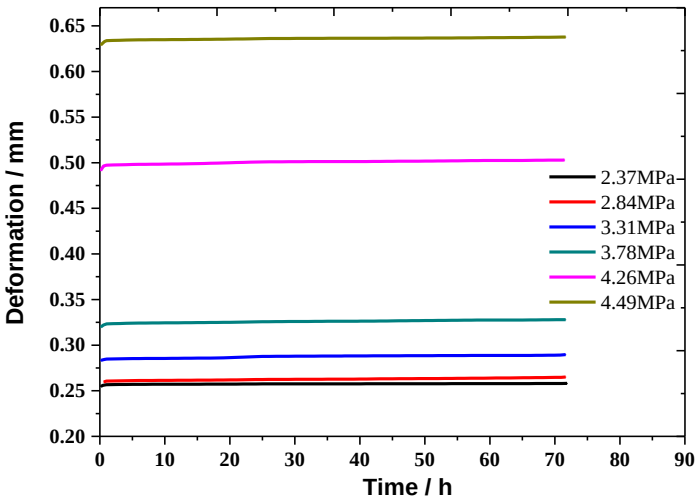

Figure 3.14 Multi-grade creep curves（1-6.52）

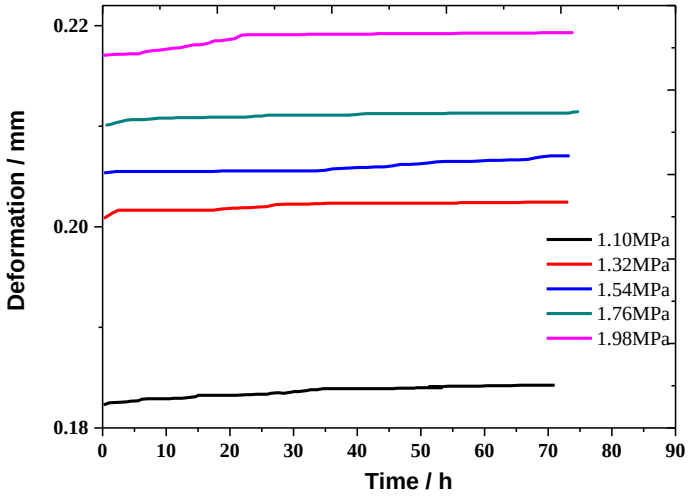

Figure 3.15 Multi-grade creep curves（4-2.17）

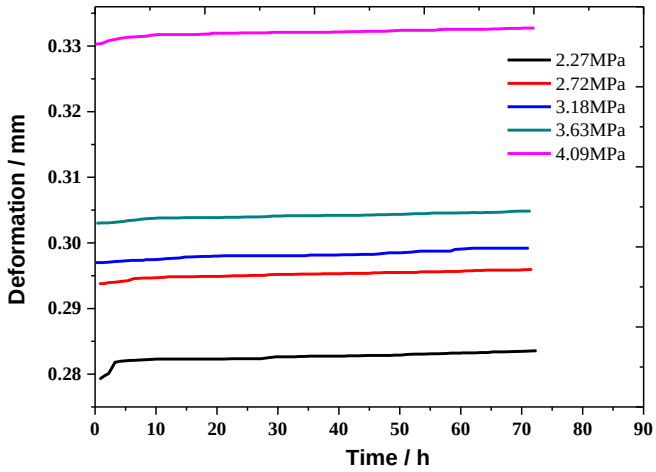

Figure 3.16 Multi-grade creep curves（4-4.35）

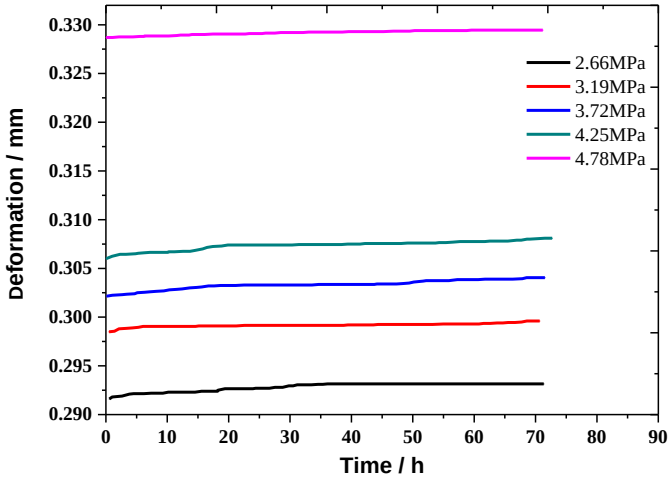

Figure 3.17 Multi-grade creep curves（4-6.52）

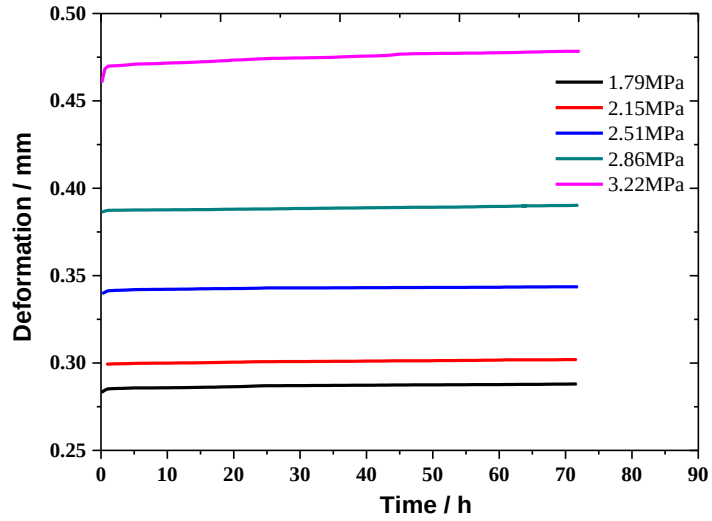

Figure 3.18 Multi-grade creep curves（10-2.17）

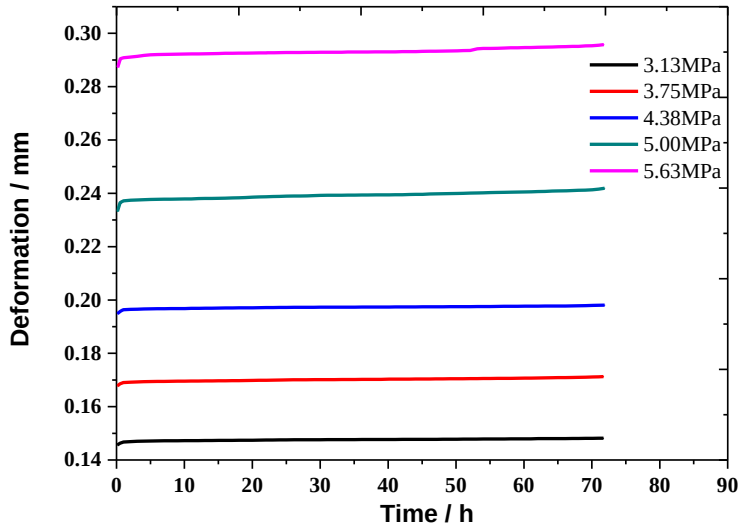

Figure 3.19 Multi-grade creep curves（10-4.35）

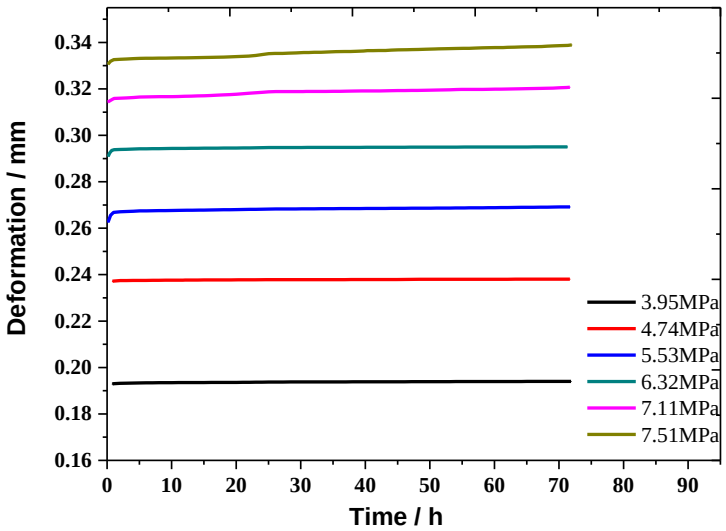

Figure 3.20 Multi-grade creep curves（10-6.52）

From Figures 3.12~3.20, it could be observed that the total deformation includes the instantaneous deformation and the creep deformation. By processing the data, the proportion of each deformation to the total deformation could be obtained, as shown in Table 3.2.

Table 3.2 The component of deformation

Sample	levels	Normal stress	Shear stress	instantaneous deformation	Creep deformation	Total deformation	Ratio of creep %
		MPa	MPa	mm	mm	mm	
1-2.17	1	2.17	0.88	0.0289	0.0014	0.0303	4.62
	2	2.17	1.06	0.0673	0.0016	0.0689	2.25
	3	2.17	1.23	0.1347	0.0053	0.1400	3.79
	4	2.17	1.41	0.2599	0.0050	0.2649	1.88
	5	2.17	1.58	0.5181	0.0160	0.5341	3.00
1-4.35	1	4.35	1.95	0.2462	0.0079	0.2541	3.09
	2	4.35	2.33	0.2613	0.0121	0.2734	4.43
	3	4.35	2.72	0.2882	0.0119	0.2900	4.10
	4	4.35	3.11	0.3052	0.0091	0.3143	2.89
	5	4.35	3.50	0.3515	0.0100	0.3615	2.76
	6	4.35	3.70	0.5091	0.0350	0.5441	6.43
1-6.52	1	6.52	2.37	0.2548	0.0033	0.2581	1.28
	2	6.52	2.84	0.2597	0.0054	0.2651	2.04
	3	6.52	3.31	0.2834	0.0063	0.2897	2.19
	4	6.52	3.78	0.3199	0.0081	0.3280	2.47
	5	6.52	4.26	0.4914	0.0116	0.5030	2.30
	6	6.52	4.49	0.6291	0.0087	0.6378	1.37
4-2.17	1	2.17	1.10	0.1823	0.0020	0.1843	1.06
	2	2.17	1.32	0.2009	0.0016	0.2025	0.79
	3	2.17	1.54	0.2054	0.0017	0.2071	0.82
	4	2.17	1.76	0.2101	0.0014	0.2115	0.64
	5	2.17	1.98	0.2171	0.0023	0.2193	1.03
4-6.52	1	6.52	2.66	0.2916	0.0016	0.2932	0.53
	2	6.52	3.19	0.2986	0.0011	0.2996	0.35
	3	6.52	3.72	0.3022	0.0019	0.3041	0.62
	4	6.52	4.25	0.306	0.0021	0.3081	0.68
	5	6.52	4.78	0.3287	0.0008	0.3295	0.23
10-2.17	1	2.17	1.79	0.2832	0.0047	0.288	1.65
	2	2.17	2.15	0.2991	0.0029	0.302	0.96
	3	2.17	2.51	0.3397	0.0039	0.3436	1.12
	4	2.17	2.86	0.3863	0.004	0.3903	1.02
	5	2.17	3.22	0.4605	0.0179	0.4784	3.74
10-4.35	1	4.35	3.13	0.1457	0.0025	0.1482	1.69
	2	4.35	3.75	0.1678	0.0035	0.1713	2.04
	3	4.35	4.38	0.1949	0.0032	0.1981	1.62
	4	4.35	5	0.2332	0.0087	0.2419	3.58
	5	4.35	5.63	0.2872	0.0086	0.2958	2.9

10-6.52	1	6.52	3.95	0.1929	0.0011	0.194	0.59
	2	6.52	4.74	0.2371	0.001	0.2381	0.42
	3	6.52	5.53	0.2625	0.0067	0.2692	2.48
	4	6.52	6.32	0.2909	0.0041	0.295	1.39
	5	6.52	7.11	0.3144	0.0063	0.3207	1.98
	6	6.52	7.51	0.3306	0.0083	0.3389	2.45

The results from Figures 3.12~3.20 and Table 3.2 show that:

1) Generally, the instantaneous deformation is mainly impacted by the shear stress level, which increases with the increase of the shear stress. In the 1st level of loading, the instantaneous deformation is relative large, which is mainly due to the closure of the gap between the discontinuities. The instantaneous deformations occurred in the following loading levels of 2nd to 4th are observed to increase linearly with the increased shear stress. However, as the progress of increasing shear stress, the instantaneous deformation increases more rapidly in the 5th and 6th loading level, because the stress levels that is larger than the yield stress has caused partial plastic deformation of the discontinuity to develop, so called strain softening properties.

2) Creep deformation is also mainly impacted by the shear stress level, which also increases with the increasing shear stress. However, the impact of different JRC on the creep deformation is relatively small.

3) The proportion of creep deformation to the total deformation is within 0.23% ~ 6.43%. For a given sample, the proportion of creep deformations is generally tending to reduce initially followed by an increasing manner. It should be noted that, the required testing time for creep test is relatively longer than normal test. Since the testing time for each loading level are quite equivalent to each other, the creep deformation still tends to develop even at the end of the 4th, 5th and 6th loading level.

3.3.2 Creep of discontinuities under different shear stresses

Since the creep properties under different shear stresses are quite different, the author discusses on this issue. To this end, some typical creep curves under low shear stresses of the 1st and 2nd loading levels and under high shear stresses of the 4th and 5th loading levels were selected for

illustration, as shown in Figures 3.21~3.23 and Figures 3.24~3.26 respectively.

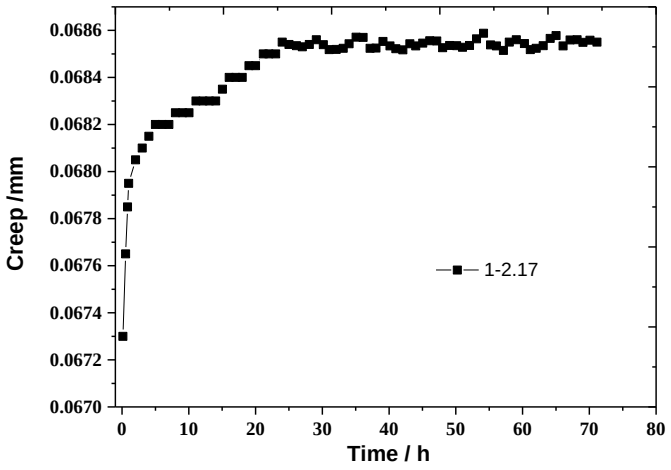

Figure 3.21 Creep curve in the second level（1-2.17）

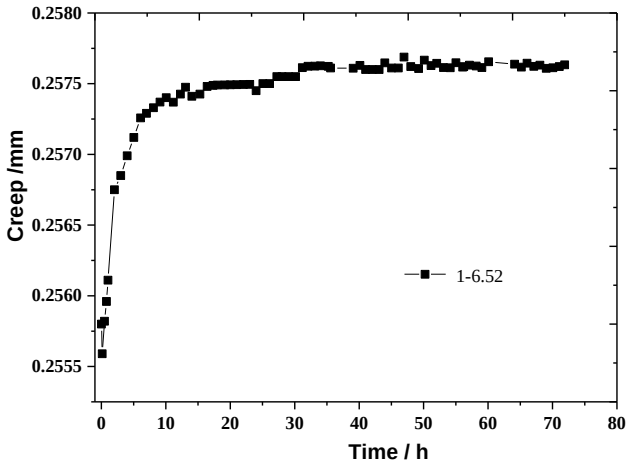

Figure 3.22 Creep curve in the first level（1-6.52）

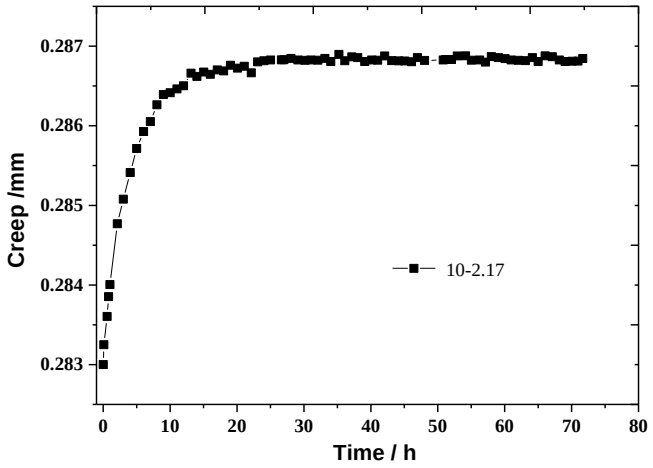

Figure 3.23 Creep curve in the first level（10-2.17）

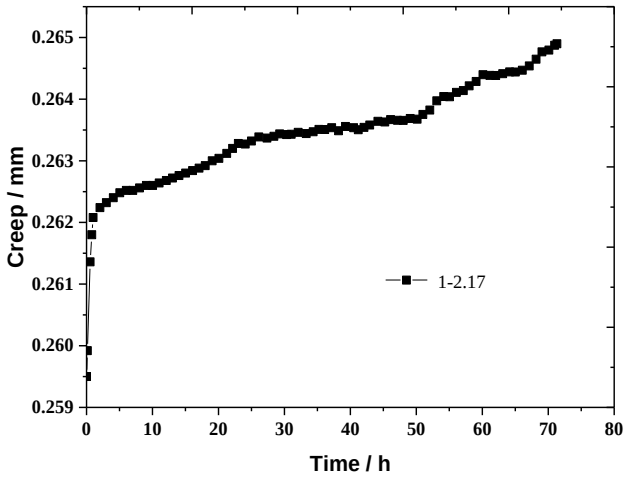

Figure 3.24 Creep curve in the fourth level（1-2.17）

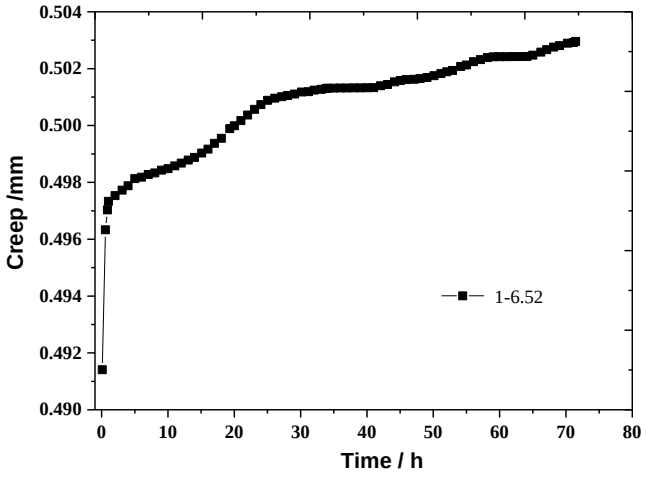

Figure 3.25 Creep curve in the fifth level（1-6.52）

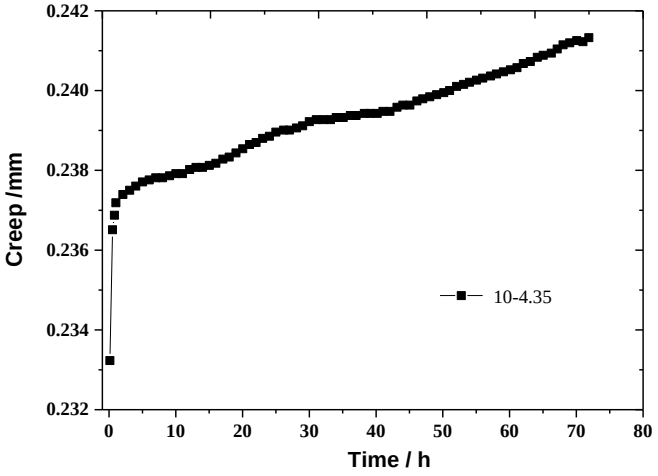

Figure 3.26 Creep curve in the fourth level（10-4.35）

The results show that:

1) Under the low shear stress, as shown in Figures 3.21 ~ 3.23, the creep curve manifests as attenuation creep type in which the deformation tends to subside to a constant value over time.

2) While under high shear stress, the creep curve presents as the stable creep type in which the creep rate keeps as a constant greater than 0, and the creep deformation increases almost linearly, as can be seen from Figures 3.24~3.26. Theoretically, in addition to attenuation creep stage, a sample under high shear stress levels would also undergo through the stable creep stage and the accelerated creep stage, and leading to the final failure over time. However, since the testing time for each loading level is not long enough to observe such stages, the sample was almost failed instantaneously.

3) The duration of attenuation creep stage under the low shear stress is longer than that under the high shear stress. Take the results of test 1-2.17 as an illustration, the corresponding duration times for the 1st loading level and the 4th loading level are to be around 15 h and 2h, respectively, as respectively shown in Figures 3.21 and 3.24. The main reason is considered to be the viscous deformation of the sample which could be more fully developed under a low shear stress.

4) From Figures 3.24 ~ 3.26, it is observed that under high shear stresses, the creep curve undergoing the stable creep stage is not a strictly straight line but with some fluctuations. It is caused by the different properties of intact sample and sample with discontinuities. The crack existed in the samples conducted in this thesis is already under the coalescence status, i.e. the discontinuity, and the concentrated stress is mainly distributed in the discontinuities where the damage gradually develop with the increasing stress. Some asperities would firstly break off, leading to the fluctuation of the creep rate. As a result, the creep curve presents as a non-uniformed ladder creep type.

3.4 Creep rate properties

Understanding the evolution of creep rate during each creep stage has a great significance to the practical engineering. For example, for original tunnel, the mature timing for the 2nd time of lining the tunnel wall is after the creep rate of the shaped wall decays to a certain value after several days. In this section, the evolution of the creep rate is concluded and an empirical formula to

describe its behavior is suggested. Since the creep properties in the failure stage undergoing the accelerated creep stage behaves instantaneously, only the evolutions of the creep rates during the attenuation creep stage and stable creep stage will be analyzed.

3.4.1 Basic law

Take the derivation of each point at the creep curves, the creep rate curves could be obtained, and the typical creep rate curves are shown in Figures 3.27~3.28.

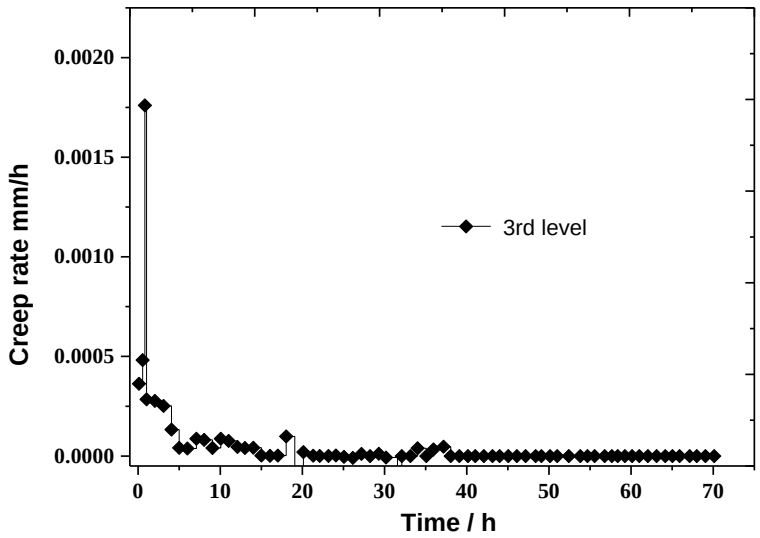

Figure 3.27 Creep rate curve in the 3rd level（1-2.17）

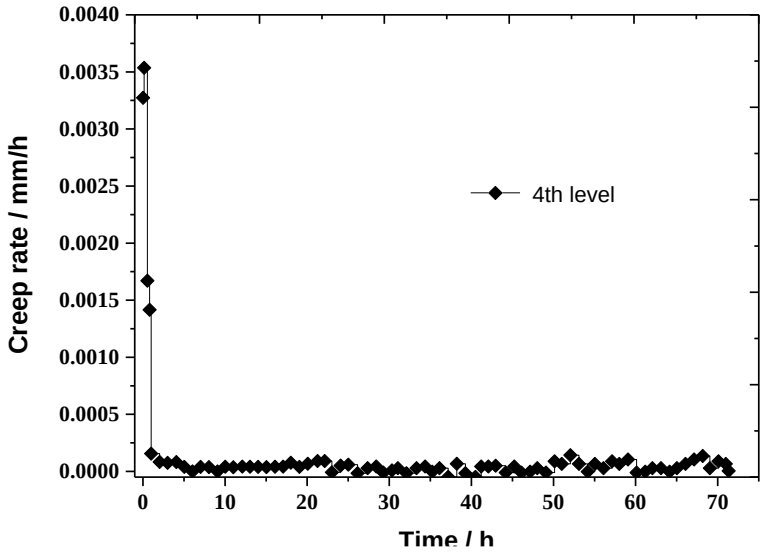

Figure 3.28 Creep rate curve in the 4th level（1-2.17）

Form Figures 3.27 ~ 3.28, it can be seen that the evolution of the creep rate during the 3rd and 4th loading levels behaves similarly to each other, which reduces firstly and then tends to subsides to an equivalent value. While the creep rate in the 3rd loading level eventually tends to 0 (Figure 3.27), it subsides to a stable value that is slightly greater than 0 in the 4th loading level (Figure 3.28).

Theoretically, when the sample is subjected to a high shear stress, its creep process could be divided into three stages in terms of attenuation creep stage, stable creep stage and accelerated creep stage. During the attenuation stage, the creep rate reduces gradually with the elapsing time, which then tends to a stable value greater than 0 in the stable stage. The creep rate finally enters into the accelerated stage and leads to the failure of the sample. For the case of intact rocks, when the damage accumulates to a critical value, micro-cracks would be initiated and extended, which finally coalesces to the macro-structure failure. While for the case of discontinuity, the capacity of the shearing resistance gradually reduces with the increase of the cumulative damage induced by viscous-plastic deformation. As a result, when the applied shear stress exceeds its shearing resistance, stick-slip would occur, causing the creep rate to increase subsequently. A relatively rapid failure is therefore followed.

3.4.2 Empirical formula

As stated above, the creep rate is observed decreasing with time and finally tending to a stable value. The following empirical formula in Eq. 3.1 is therefore suggested to describe the evolution of the creep rate.

$$v = \frac{m}{t^n} \qquad (3.1)$$

Where, v is the creep rate, t represents the elapsing time, m is a fitting parameter that mainly related to the stress levels, and n is the fitting parameter mainly related to the property of the testing material.

It could be observed that the fitting curves based on Eq. 3.1 have a good consistence with the testing results. Take the results obtained from the sample 1-6.52 as examples, as shown in Figures 3.29~3.34. Besides, the fitting parameters are also obtained, as shown in Table 3.3.

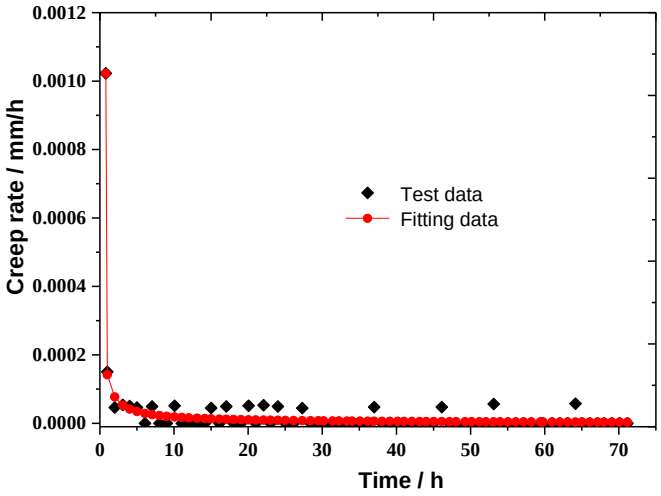

Figure 3.29 Fitting curve of creep rate（1st level）

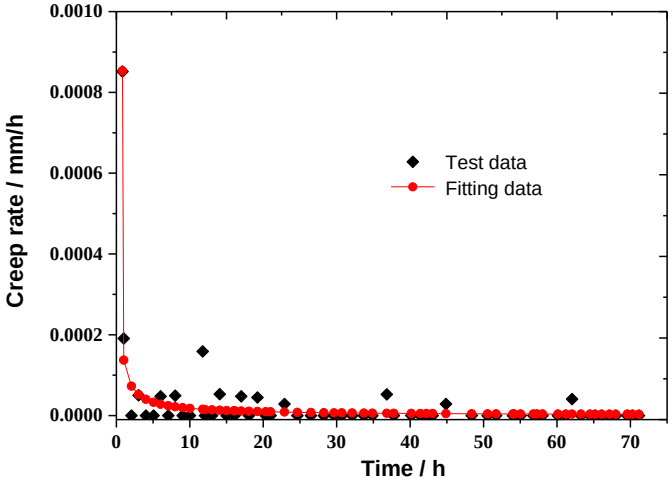

Figure 3.30 Fitting curve of creep rate（2nd level）

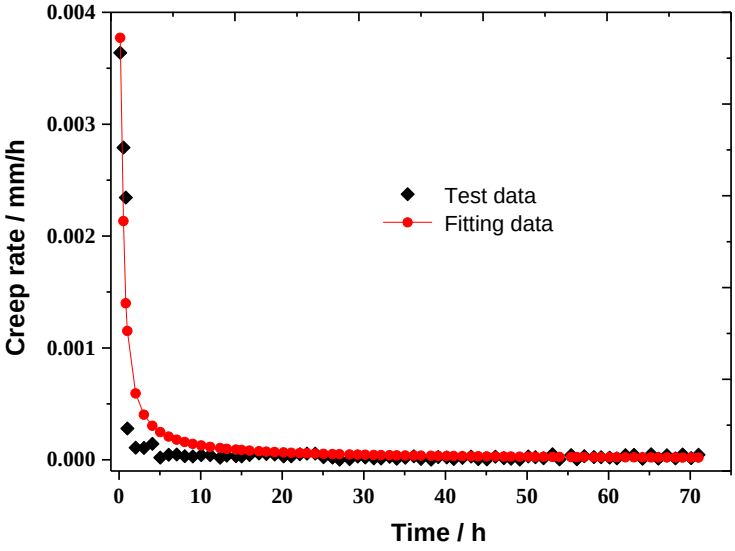

Figure 3.31 Fitting curve of creep rate（3rd level）

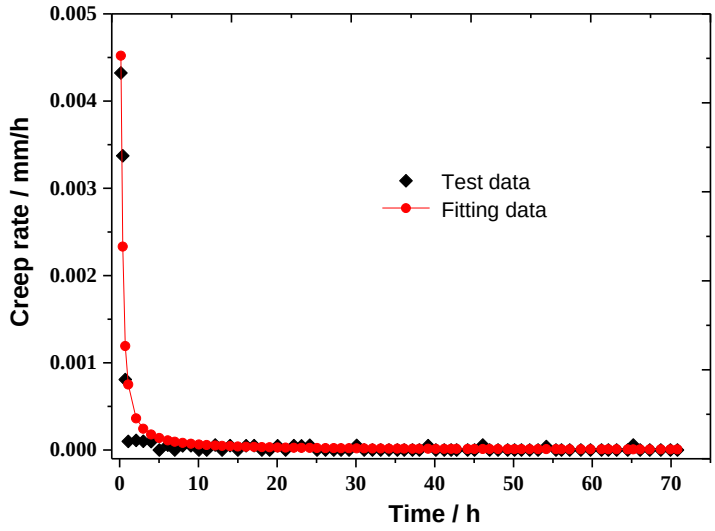

Figure 3.32 Fitting curve of creep rate（4th level）

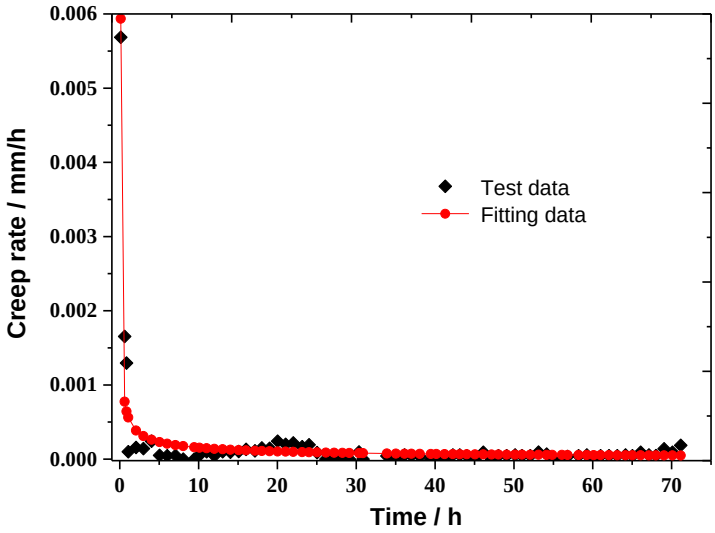

Figure 3.33 Fitting curve of creep rate（5th level）

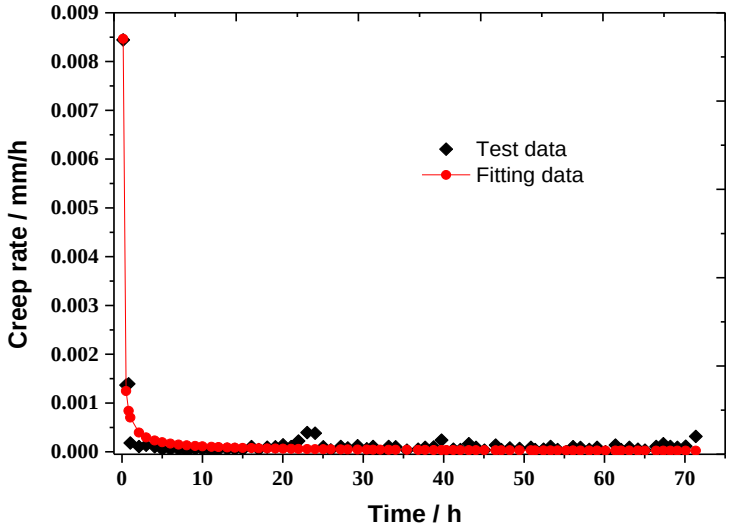

Figure 3.34 Fitting curve of creep rate（6th level）

Table 3.3 Parameter of empirical formula

sample	Loading level	*m*	*n*	Mean value of n	correlation coefficient R
1-2.17	1	0.000182	0.589177	0.747792	0.85
	2	0.000238	0.683909		0.90
	3	0.000584	0.693404		0.88
	4	0.00069	0.842676		0.96
	5	0.00154	0.929794		0.86
1-4.35	1	0.001246	0.981941	0.741218	0.89
	2	0.000174	0.594603		0.87
	3	0.000127	0.630897		0.90
	4	0.000846	0.714588		0.86
	5	0.001474	0.631309		0.89
	6	0.003078	0.893972		0.93
1-6.52	1	0.000553	0.861711	0.778135	0.97
	2	0.000364	0.766453		0.95
	3	0.000652	0.582749		0.9
	4	0.001201	0.759368		0.85
	5	0.001161	0.979271		0.83
	6	0.001565	0.71926		0.87
4-2.17	1	0.000111	0.462067	0.713279	0.79
	2	0.000141	0.709825		0.84
	3	0.000185	0.77201		0.95
	4	0.000321	0.791226		0.88
	5	0.000784	0.831268		0.93
4-4.35	1	0.000737	0.844551	0.811534	0.83
	2	0.00011	0.775107		0.82
	3	0.000143	0.750075		0.86
	4	0.000177	0.846885		0.89
	5	0.000285	0.841054		0.80
4-6.52	1	0.000233	0.587516	0.758468	0.80
	2	0.000104	0.579343		0.82
	3	0.000171	0.775245		0.88
	4	0.000291	0.917326		0.83
	5	0.000408	0.93291		0.81
10-2.17	1	0.000569	0.682964	0.836911	0.89
	2	0.00066	0.911083		0.98
	3	0.000709	0.770495		0.90
	4	0.000943	0.799167		0.88
	5	0.001769	1.020846		0.99
10-4.35	1	0.000398	0.673913	0.847824	0.87
	2	0.00047	0.716095		0.83

	3	0.000541	0.717105		0.88
	4	0.00065	1.230743		0.92
	5	0.001544	0.901265		0.91
10-6.52	1	0.000142	0.881879	0.937549	0.98
	2	0.000138	0.886566		0.97
	3	0.000473	0.959803		0.98
	4	0.000826	1.110186		0.98
	5	0.001089	0.978703		0.89
	6	0.001721	0.808155		0.95

It can be seen from Table 3.3 that

1) *m* depends mainly on the shear stress level, which gradually increases with the increase of the shear stress, and at an increasing rate. Take the result from the sample 1-2.17 as an example: the difference between the 1st and the 2nd levels is 0.000056, while the difference increases to 0.00085 between the 4th and the 5th levels.

2) *n* varies slightly and almost keeps as a stable value with the increase of the shear stress, it illustrates that *n* is independent of the shear stress level and might be depends on the property of the material itself.

3.4.3 Creep rate under different stress levels

Based on Eq. 3.1, the fitting curves of the evolution of creep rates under different shear stress levels could be obtained. In order to clearly show the difference of the evolution in the initial stage, the corresponding fitting curves were plotted in logarithm scale, i.e. creep rate-log *t*, as shown in Figures 3.35~3.43.

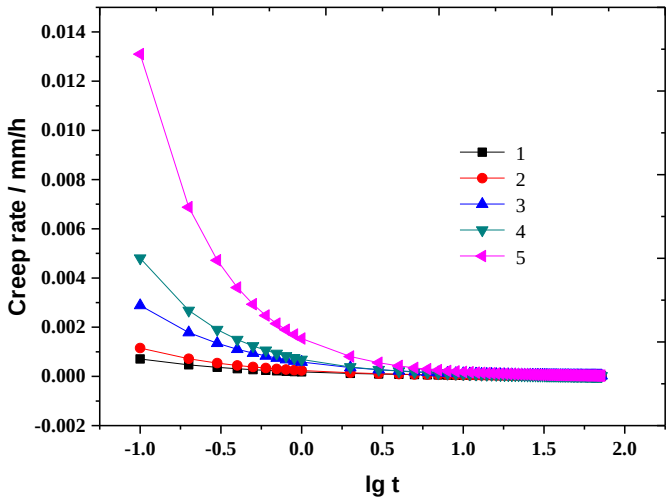

Figure 3.35 lgt-creep rate curve（1-2.17）

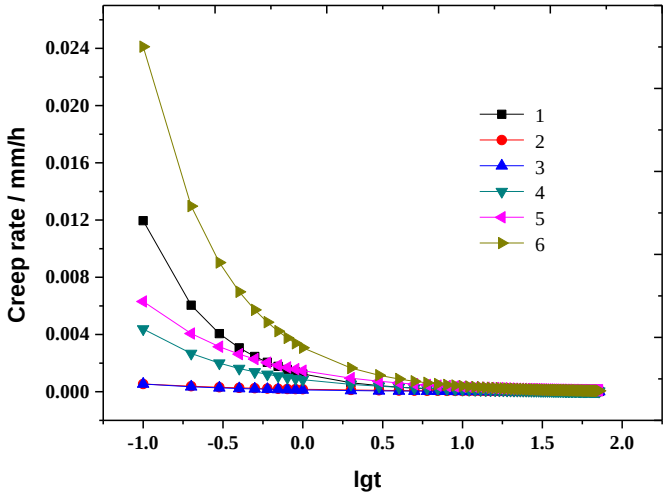

Figure 3.36 lgt-creep rate curve（1-4.35）

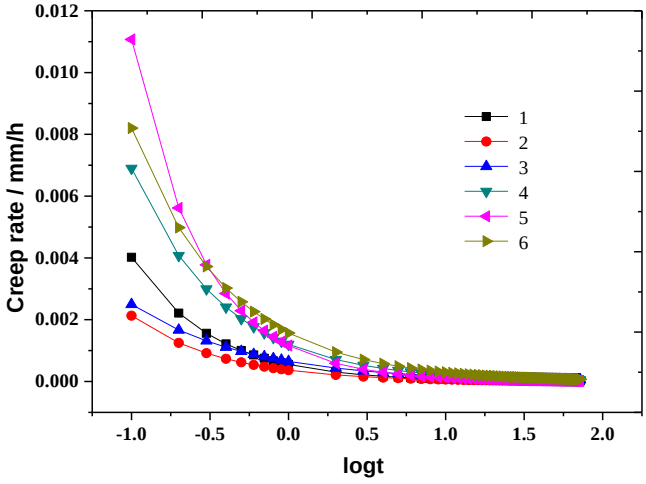

Figure 3.37 lgt-creep rate curve（1-6.52）

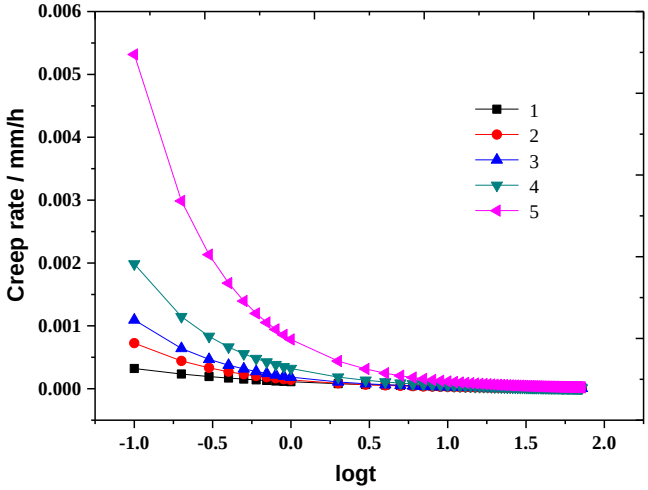

Figure 3.38 lgt-creep rate curve（4-2.17）

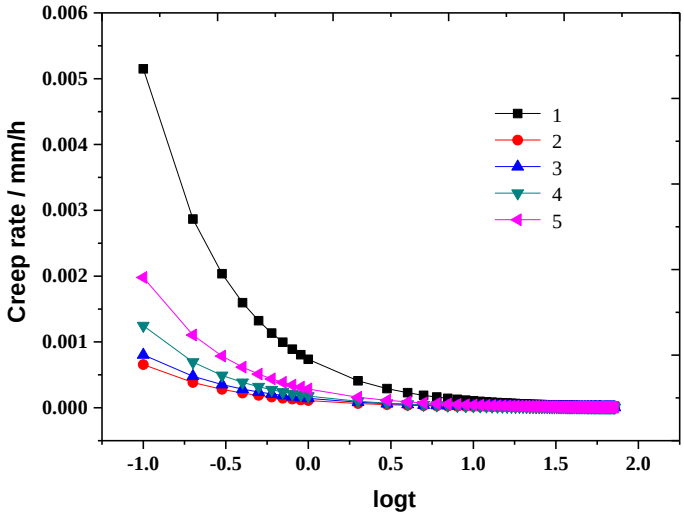

Figure 3.39 lgt-creep rate curve（4-4.35）

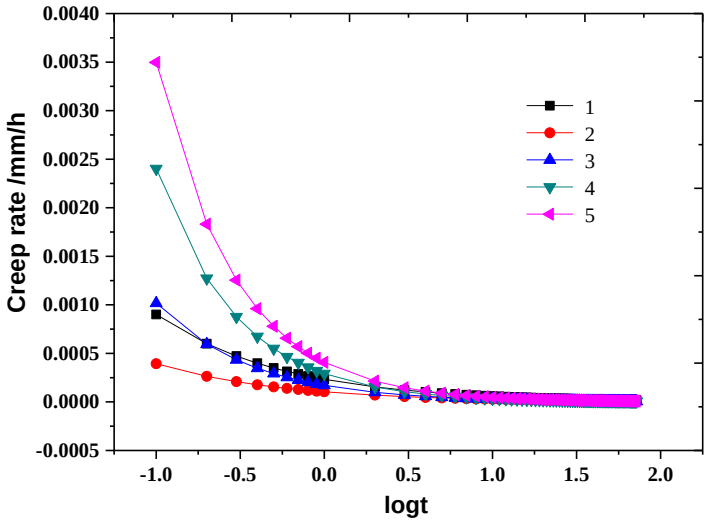

Figure 3.40 lgt-creep rate curve（4-6.52）

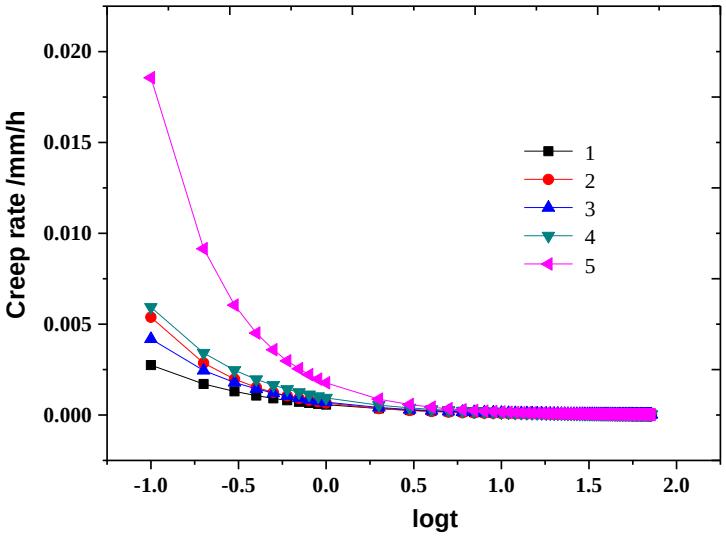

Figure 3.41 lgt-creep rate curve（10-2.17）

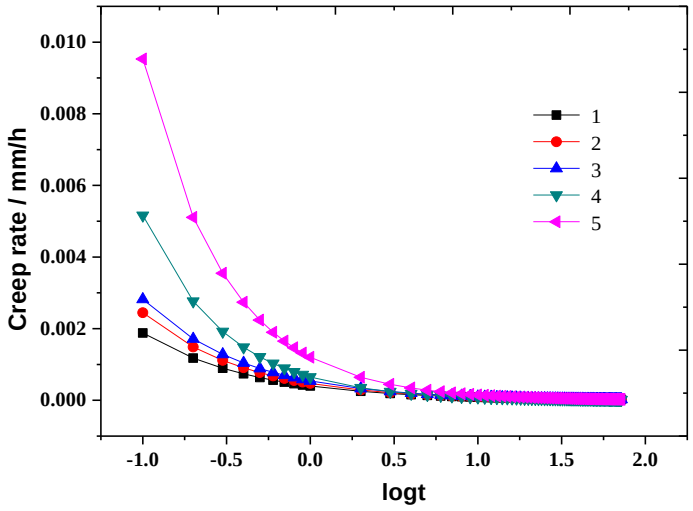

Figure 3.42 lgt-creep rate curve（10-4.35）

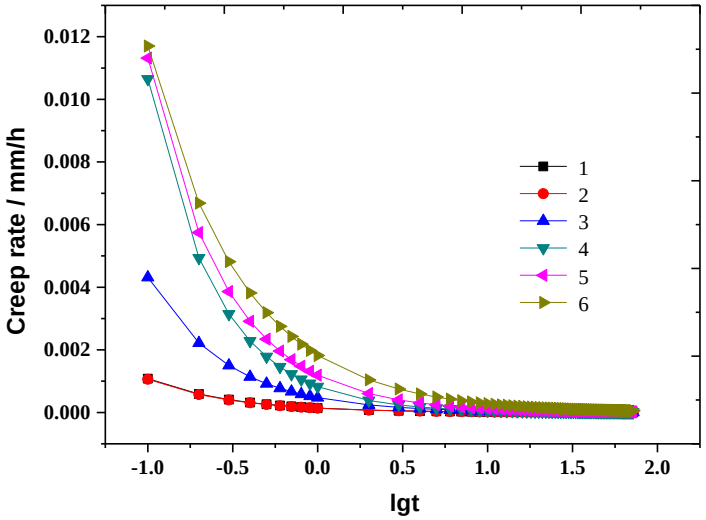

Figure 3.43 lgt-creep rate curve（10-6.52）

From Figures 3.35~3.43, it is observed that:

1) The initial creep rate mainly depends on the shear stress level, which increases with the increase of the shear stress level. Take the result from sample 1-2.17 as an example, when t = 0.1 h, the creep rates for each loading levels are 0.00071 mm/h, 0.0012 mm/h, 0.0029 mm/h, 0.0048 mm/h and 0.0121mm/h respectively.

2) However, exceptions also exist for some samples where the creep rate in the 1st level is larger than that in the 2nd and 3rd levels, as shown in for example, Figure 3.40. This phenomenon is attributing to the manufacture issue of the sample itself, where the artificial discontinuities might be not perfectly matched, and a gap might exist between these two brought-together discontinuities. Therefore, significant deformations caused by the closure of the gap would be occurred in the 1st loading level and counted into the creep deformation, leading to a relatively large creep rate. This reason is also accounted for some exceptions that existed in the m values obtained from the fitting curves, where the m values in the 1st level of some testing cases are found larger than those in the 2nd and 3rd levels.

3.5 Creep Constitutive study: NISHIHARA model

Building the constitutive relationship, which reflects the creep properties through building the mathematical relationship of stress, strain and time, is an important part to study rheological property. Since the creep tests are time consuming, the constitutive relation is usually built and generalized through a few tests on individual rocks, and then applies it on the rock engineering.

Currently the most widely method to build a constitutive relation is component modeling, which describes the creep properties under different shear stress levels and rock material properties. Three main kinds of components are widely used, i.e. the elastic Hook body, the Newton body and the Saint Venant plastic body. These components are usually assembled in series or parallel manner. When the components are in series, they own equivalent shear stress but generally different strains, and the total strain is the sum of the strains at each component. On the other hand, when the components are in parallel, they own equivalent strain but generally different shear stresses, and the total shear stress is the sum of the stress at each component. Since each component assembled

in the model has a clear physical meaning, it is very meaningful for understanding the mechanical behavior of rock materials.

In this section, based on the test results, NISHIHARA model was selected to describe the creep properties, and the evolutions of the parameters used in this model were studied.

3.5.1 Nishihara model

From previous testing results of the creep curves under different shear stress, some conclusions could be drawn as follow.

1) The main deformation during the creep process is elastic deformation; therefore, a Hook body should be included.

2) All of the tested samples have underwent through the attenuation creep stage where the creep rate attenuates to a relative stable value; therefore, Kelvin model was selected to describe this process, representing viscous-elastic creep behavior.

3) The evolution of creep curves under high shear stress is greatly different with that under low shear stress. In which, under low shear stress level, creep would eventually become stable, while under high shear stress, creep would continuously develop even after reaching the stable creep stage; therefore, the viscous-plastic body was selected to describe these creep behaviors under different shear stresses.

It is worth noted that the generalized Kelvin model which assembles the Hook body and Kelvin model in series, could describe the creep behavior that under low shear stress, where the creep would eventually stabilize. Thereafter, Nishihara further extended the generalized Kelvin model into a completed NISHIHARA model, also called Bingham-vogt model, by additionally assembling a viscous-plastic body in series, in order to describe the creep behavior under high shear stress. The NISHIHARA model includes a Hook body, a Kelvin body and a Viscous-plastic body and five components as shown in Figure 3.44. In which, the plastic component in the viscous-plastic body acts as a stress valve, i.e. when the shear stress is larger than the long-term stress, the plastic deformation will develop infinitely, while when the shear stress is smaller than the long-term strength, the model will degenerate into a generalized Kelvin model.

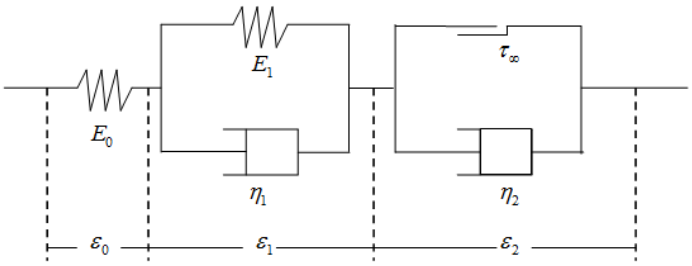

Figure 3.44 Nishihara model

In this model, the shear stress for the three parts of the model are equivalent to each other, while the corresponding strains are generally different, and the total strain is the sum of the stains of these three parts.

$$\sigma = \sigma_0 = \sigma_1 = \sigma_2 \tag{3.2}$$

$$\varepsilon = \varepsilon_0 + \varepsilon_1 + \varepsilon_2 \tag{3.3}$$

Hook model can be described by the following constitutive relation:

$$\varepsilon_0 = \sigma_0 / E_0 \tag{3.4}$$

Kelvin body is a parallel combination of a viscous component and an elastic component whose strains are equivalent but corresponding shear stresses are different. The total shear stress of this body is the sum of the stress of these two components, as shown in Eq.3.5.

$$\sigma = \sigma_1 = \sigma_{1v} + \sigma_{1h} = \eta_1 \dot{\varepsilon}_1 + E_1 \varepsilon_1 \tag{3.5}$$

Viscous-plastic body is a parallel combination of a viscous component and a plastic component. Similar to the Kelvin body, the strains for these two components are equal and the total shear stress is the sum of their corresponding shear stress.

$$\sigma = \sigma_2 = \sigma_{2v} + \sigma_{2p} \tag{3.6}$$

When the shear stress is smaller than the long-term strength, the viscous-plastic body would be invalid. On the other hand, when the shear stress is larger than the long-term strength, the shear stress could be described as Eq.3.7.

$$\sigma_2 - \sigma_\infty = \eta_2 \dot{\varepsilon}_2 \tag{3.7}$$

Combining Eq. 3.3, Eq.3.4 and Eq.3.5, the constitutive formula of Kelvin model could be obtained as follow:

$$\frac{E_0\eta_1}{E_0+E_1}\dot{\varepsilon}+\frac{E_0E_1}{E_0+E_1}\varepsilon=\frac{\eta_1}{E_0+E_1}\dot{\sigma}+\sigma \tag{3.8}$$

Similarly, combining the Eq. 3.3, Eq.3.4, Eq.3.5 and Eq.3.6, the complete NISHIHARA model could be obtained and the constitutive formula is shown as follow:

$$\eta_2\dot{\varepsilon}+\frac{\eta_2\eta_1}{E_1}\ddot{\varepsilon}=\frac{\eta_2\eta_1}{E_0E_1}\ddot{\sigma}+(\frac{\eta_2}{E_0}+\frac{\eta_2+\eta_1}{E_1})\dot{\sigma}+(\sigma-\sigma_\infty) \tag{3.9}$$

Based on the formula 3.4, 3.5 and 3.7, the creep constitutive formula of each part can be obtained as follows:

$$\varepsilon_0=\frac{\sigma}{E_0} \tag{3.10}$$

$$\varepsilon_1=\frac{\sigma}{E_1}[1-\exp(-\frac{E_1}{\eta_1}t)] \tag{3.11}$$

The viscous-plastic body will appear in two cases when the shear stress is either larger or small than the long-term strength.

$$\varepsilon_2=0 \qquad \sigma\le\sigma_\infty \tag{3.12}$$

$$\varepsilon_2=\frac{\sigma-\sigma_\infty}{\eta_2}t \qquad \sigma\ge\sigma_\infty \tag{3.13}$$

Therefore, the creep constitutive relationship in the NISHIHARA model can be given as below.

$$\varepsilon=\frac{\sigma}{E_0}+\frac{\sigma}{E_1}[1-\exp(-\frac{E_1}{\eta_1}t)] \qquad \sigma\le\sigma_\infty \tag{3.14}$$

$$\varepsilon=\frac{\sigma}{E_0}+\frac{\sigma}{E_1}[1-\exp(-\frac{E_1}{\eta_1}t)]+\frac{\sigma-\sigma_\infty}{\eta_2}t \qquad \sigma\ge\sigma_\infty \tag{3.15}$$

Similarly, the stress relaxation constitutive relations could be also obtained as follows.

When $\sigma\leqslant\sigma_\infty$,

$$\sigma=(E_0-\frac{E_1E_0}{E_1+E_0})\varepsilon_0\exp(-\frac{E_0+E_1}{\eta_1}t)+\frac{E_1E_0\varepsilon_0}{E_0+E_1} \tag{3.16}$$

When $t\to\infty$, $\sigma\to E_\infty\varepsilon_0$. In which $E_\infty=\frac{E_1E_0}{E_1+E_0}$。

When $\sigma \geqslant \sigma_\infty$,

$$\sigma = \frac{q_2 \varepsilon_0}{p_2(a_1 - a_2)}\left[(\frac{q_1}{q_2} - a_2)\exp(-a_2 t) - (\frac{q_1}{q_2} - a_1)\exp(-a_1 t)\right] + \sigma_\infty \quad (3.17)$$

In which, $a_1 = \frac{p_1 + \sqrt{p_1^2 - 4p_2}}{2p_2}$, $a_2 = \frac{p_1 - \sqrt{p_1^2 - 4p_2}}{2p_2}$。

$p_1 = (\frac{\eta_2}{E_0} + \frac{\eta_2}{E_1} + \frac{\eta_1}{E_1})$, $p_2 = \frac{\eta_2 \eta_1}{E_0 E_1}$, $q_1 = \eta_2$, $q_2 = \frac{\eta_2 \eta_1}{E_1}$。

Since NISHIHARA model uses the plastic element in the viscous-plastic body as stress valve, it allows the parameters involved in the model to vary before and after reaching the long-term strength. Therefore, it could solve the parameters' nonlinear problem to some extent, and has been widely used in rheological practices. However, this model still did not give reasonable exploration on the nonlinear trend of the involved parameters.

3.5.2 Model fitting and the involved parameter evolution analysis

According to the creep curves obtained under different shear stress levels, it is observed that the creep curves under the shear stress levels of 0.5 τ, 0.6 τ and 0.7 τ would eventually levels off, exhibiting as attenuation creep characteristics; while when the stress levels are 0.8 τ, 0.9 τ and 0.95 τ, creep would continuously develop without showing a leveling off in the stable creep stage. Therefore, the creep behavior under relatively low shear stress level of 0.5 τ, 0.6 τ, and 0.7 τ could be described by the generalized Kelvin model, while when the shear stress level is relatively high, e.g. 0.8 τ, 0.9 τ, and 0.95 τ, the complete NISHIHARA model is applicable for description.

By curve fitting method, the NISHIHARA model fitting curves could be obtained, as shown in Figures 3.45~3.50. Meanwhile, the values of involved parameters in the NISHIHARA model could be also obtained, as shown in Table 3.6. Since E_0 is mainly induced by the instantaneous deformation, it could be obtained by calculating the slope of the straight line segment from the test data, while other parameters could be obtained by the optimal solution method through the software of 1stOpt.

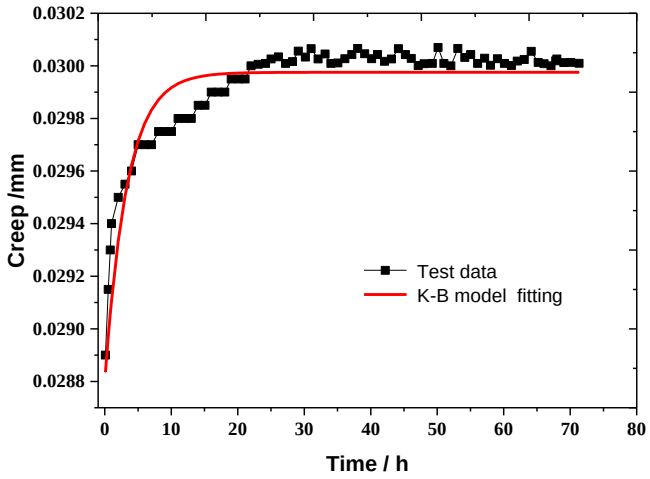

Figure 3.45 Fitting result by Nishihara model（1-2.17, 1st level）

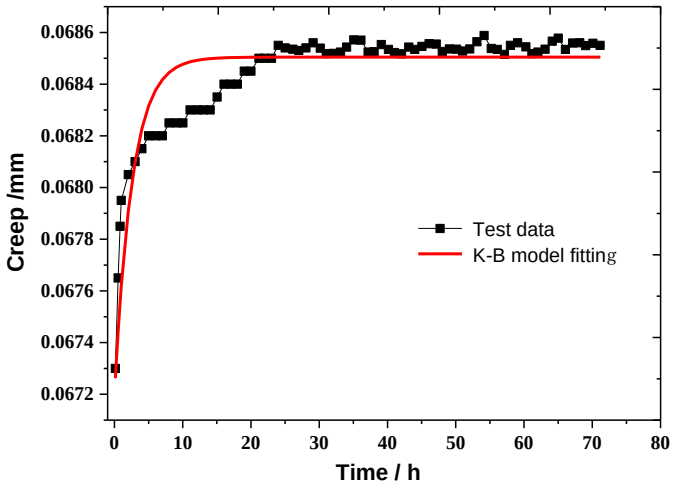

Figure 3.46 Fitting result by Nishihara model（1-2.17, 2nd level）

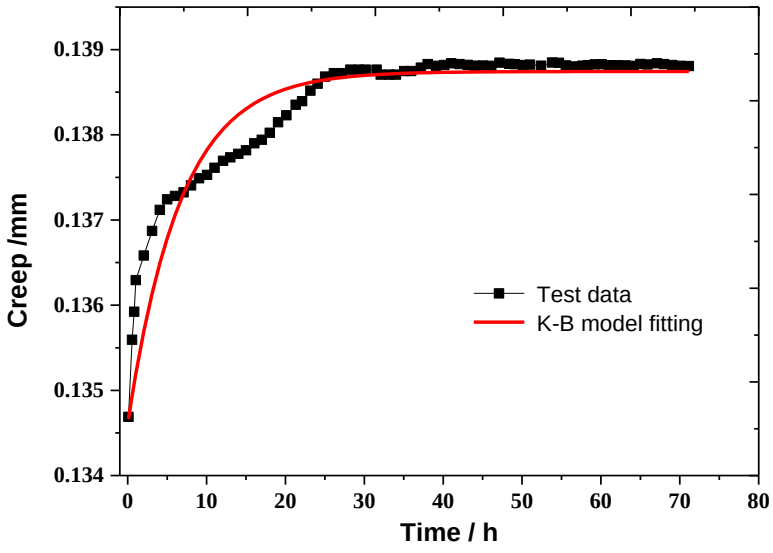

Figure 3.47 Fitting result by Nishihara model（1-2.17, 3rd level）

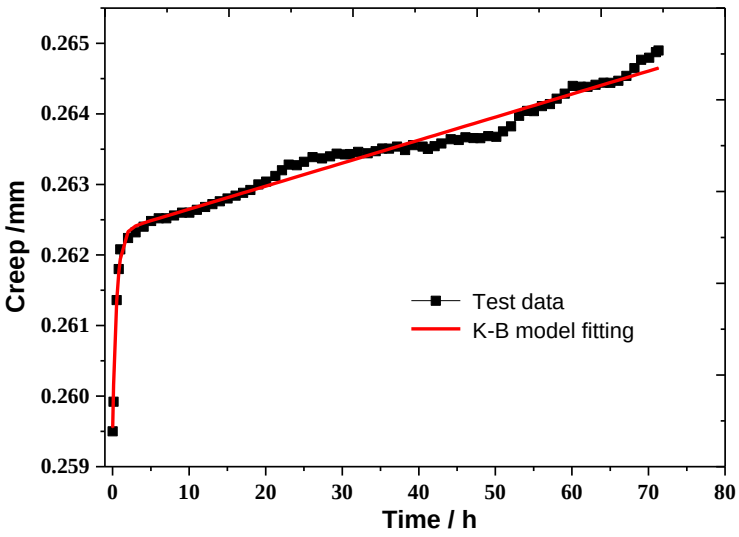

Figure 3.48 Fitting result by Nishihara model（1-2.17, 4th level）

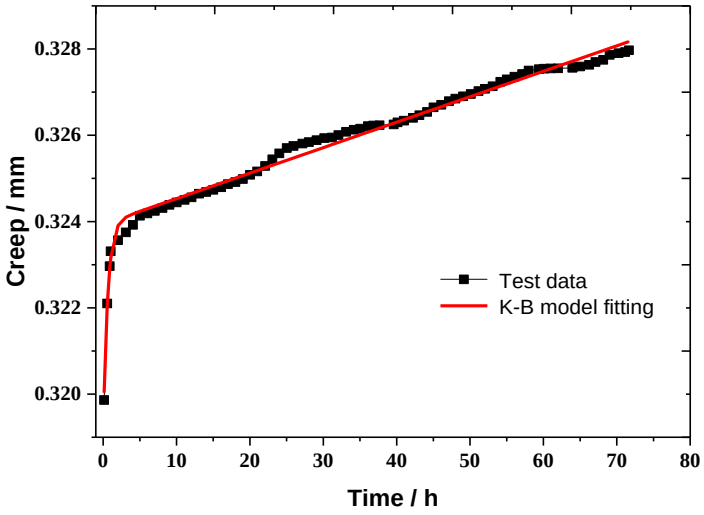

Figure 3.49 Fitting result by Nishihara model（1-6.52, 4th model）

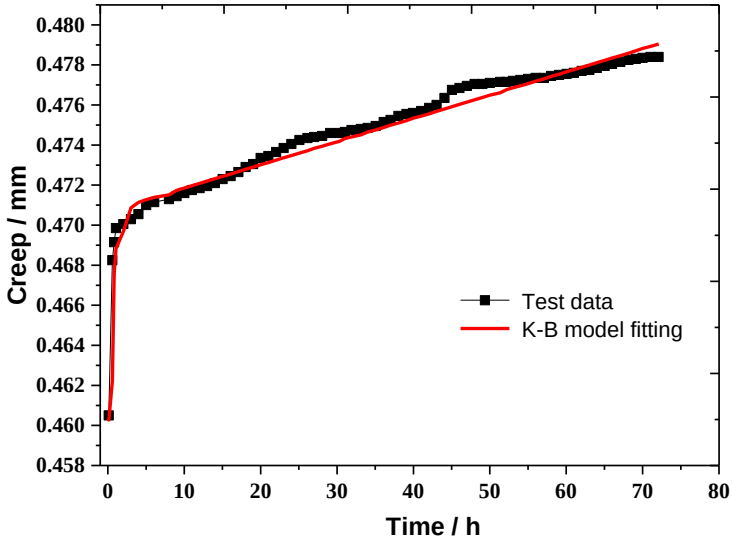

Figure 3.50 Fitting result by Nishihara model（10-2.17, 5th level）

Table 3.6 Parameters of Nishihara model

Sample	Loading level	τ /MPa	E_0 /GPa	E_1 /GPa	η_1 /(GPa.h)	η_2 /(GPa.h)	Correlation coefficients R
1-2.17	1	0.88	30.56	501.15	712.62	—	0.820
	2	1.06	15.78	327.75	1064.2	—	0.810
	3	1.23	9.13	219.55	1559.51	—	0.900
	4	1.41	5.43	499.46	260.9	2701.16	0.991
	5	1.58	3.06	166.22	84.99	2359.05	0.972
1-4.35	1	1.95	7.89	267.12	616.8	—	0.880
	2	2.33	8.96	196.68	1704.56	—	0.920
	3	2.72	9.46	294.91	2036.2	—	0.850
	4	3.11	10.2	779.75	1483.91	12792.94	0.996
	5	3.5	9.97	478.2	612.82	12253.18	0.991
	6	3.7	7.28	202.09	185.96	3520.98	0.996
1-6.52	1	2.37	9.27	856.72	1221.56	—	0.830
	2	2.84	10.99	398.85	933.39	—	0.850
	3	3.31	11.86	366.1	2301.3	—	0.840
	4	3.78	11.85	765.65	450.56	14007.46	0.996
	5	4.26	8.68	580.38	316.03	10132.12	0.974
	6	4.49	7.15	806.99	570.93	22433.23	0.985
4-2.17	1	1.1	6.06	295.28	1632.22	—	0.780
	2	1.32	6.6	393.84	861.96	—	0.720
	3	1.54	7.5	396.31	1627.44	—	0.850
	4	1.76	8.38	1303.75	1039.47	11961.23	0.968
	5	1.98	9.21	1601.27	1241.35	16807.62	0.968
4-4.35	1	2.27	8.14	471.84	1519.12	—	0.860
	2	2.72	9.30	802.2	3869.37	—	0.800
	3	3.18	10.76	891.15	7057.3	—	0.740
	4	3.63	11.98	1245.29	170.91	11425.4	0.970
	5	4.09	12.41	3212.61	13459.69	43160.02	0.995
4-6.52	1	2.66	9.16	800.35	2427.17	—	0.650
	2	3.19	10.7	1267.31	2703.25	—	0.650
	3	3.72	12.36	1059.05	4598.92	—	0.720
	4	4.25	13.98	1598.09	36.31	13487.98	0.937
	5	4.78	14.58	2633.46	45.16	75740.45	0.943
10-2.17	1	1.79	6.33	347.43	1590.93	—	0.830
	2	2.15	7.22	361.22	351.95	—	0.710
	3	2.51	7.40	627.56	2673.38	—	0.880
	4	2.86	7.41	1288.87	247.22	4956.33	0.996
	5	3.22	6.99	297.86	147.97	4648.33	0.992
10-4.35	1	3.13	21.53	1142.17	2651.49	—	0.710
	2	3.75	22.40	1314.79	1225.15	—	0.750
	3	4.38	22.44	760.06	1228.46	—	0.650

	4	5.00	21.46	1124.51	495.33	5981.82	0.995
	5	5.63	19.62	1257.66	698.03	18944.53	0.976
10-6.52	1	3.95	20.57	1208.76	884.77	—	0.870
	2	4.74	20.08	2556.37	3128.99	—	0.810
	3	5.53	21.11	894.88	771.26	—	0.850
	4	6.32	21.79	1478.72	729.85	32687.87	0.990
	5	7.11	22.64	2044.51	1301.6	19800.35	0.978
	6	7.51	22.76	2924.37	1215.83	17790.87	0.993

From Figures 3.45 ~ 3.50 and Table 3.6, it is observed that:

1) The NISHIHARA model can reasonably describe the creep characteristics of the discontinuity, where the correlation coefficients of the fitting curve are all above 0.70. Particularly, when the stress level is relatively high, the correlation coefficients of the fitting curves could be larger than 0.90.

2) E_0 reflects the behavior of instantaneous deformation of testing samples. It can be seen from the curve fitting results that with the same discontinuity and same normal stress, E_0 varies slightly regardless of different applied shear stress. However, as for the same discontinuity, E_0 increases with the increase of the normal stress; and increases gradually with the increase of JCR for different structure planes subjected to the same normal stress. Note that the increase amount induced by different JCR is smaller compared to that induced by different normal stress. It is therefore concluded that the instantaneous deformation of the discontinuity subjected to shear creep depends greatly on the applied normal stress and the JCR of the discontinuity, and the effect of normal stress is greater than the effect of JCR.

3) E_1 reflects the elastic modulus in the viscous-elastic creep, which has a great influence on the creep behavior including the total creep deformation, creep rate and creep duration, during the attenuation creep stage. From Table 3.6, it is found that under the same discontinuity and the same normal force, E_1 decreases initially and then tends to increase with the increase of shear stress, suggesting that both the creep deformation and the creep duration developed during the attenuation creep stage present as an initial increase followed by a decrease manner. This is additionally consistent to the realistic observations. As for the same discontinuity subjected to different normal

stresses, the averaged E_1 increases gradually with the increased normal stress. While when subjected to the same normal force, the averaged E_1 increases slightly with the increase of JCR of the structural surface. However, the variation of JCR has a relatively smaller effect on the creep behavior, compared to the variation of shear stress. These evolutions of E_1 to the increased normal stresses and JCR are closely related to the weakening effect of the structure planes on the mechanical properties of the rock material.

4) η_1 represents the viscosity coefficient of the viscoelastic deformation part. Its variation r has no effect on the total amount of the creep deformation, while it do has a great influence on the creep evolutions in terms of the creep rate and creep duration during the attenuation creep stage. It can be seen from the Table 3.6 that when the shear stress is relatively low, for the same discontinuity subjected to the same normal force, a higher shear stress yields a larger η_1 value, suggesting that the creep duration in the attenuation creep stage is longer. While when the shear stress level is relatively large, η_1 will reduce rapidly and the creep duration in the attenuation creep stage is shorter, which is consistent with the actual situation;

5) η_2 reperents the viscosity coefficient of the viscous-plastic deformation part, which mainly affects the creep rate during the stable creep stage. The larger the η_2 value is, the smaller the creep rate in the stable creep stage will be. From Table 3.6, it is found that as for the same structure plane under the same normal stress, η_2 would decreases as the shear force increases. As for the same discontinuity, η_2 increases gradually with the increase of the normal stress, due to the weakening of the structure plane induced by the increase of the normal stress. While as for different discontinuities under the same normal force, η_2 shows no obvious changes.

3.6 An improved NISHIHARA model in studying the creep behavior

Since the same samples under different shear stresses exhibit different creep behaviors, it is difficult to well understand the associated mechanical behaviors using only one unified constitutive model. In view of this, an improved NISHIHARA model, which can reflect the different creep behaviors of discontinuities subjected to different shear stresses, is established.

3.6.1 Improvement and establishment of the model

Though the NISHIHARA model could describe the creep test results, there still have some limitations in its mechanism exploration and in fitting the curves.

1) Instantaneous deformation would occur in every loading level. In general, the instantaneous deformation includes both instantaneous elastic deformation and instantaneous plastic deformation. Xia Caichu [145] (1987) conducted creep tests on shale samples and found that the instantaneous plastic deformation caused by the micro-crack closure in the rock becomes obvious when the load increases to a certain level, thereafter, it increases finitely with the increased stress. Considering that natural discontinuities often exist some micro-defects / cracks, plastic deformation will be inevitably appeared during the loading process. However, such instantaneous plastic deformation is not considered into the NISHIHARA model. To this end, the elastic component in the NISHIHARA model is modified.

The detailed improvements for the NISHIHARA model are shown in Figure 3.51. When processing the data, the instantaneous deformation ε_0 could be replaced by σ / E_0, which could offer more accurate calculation conditions for model parameter inversion in the creep deformation part.

Figure 3.51 Modified Hoke model

2) From Figure 3.51, it is observed that under a low shear stress, the curves fitting by the NISHIHARA model, especially the attenuation creep stage, are not satisfied, and differences could be easily observed between the fitting data and the testing data. Therefore, from a mathematical point of view, the extended Kelvin model is used instead of the Kelvin model to describe the acceleration creep stage of the samples subjected to relatively low shear stress. The detailed approach is: under the relatively low shear stress, the single Kelvin model is replaced by two Kelvin models in series. The improved NISHIHARA model can greatly improve the limitation of a single Kelvin model in describing the rapid attenuations during the attenuation creep stage. The specific improvements are shown in Figure 3.52.

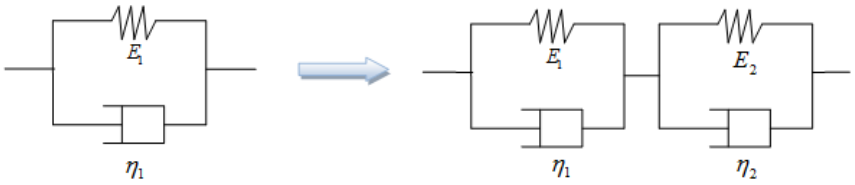

Figure 3.52 Modify Kelvin models

3) When the applied shear stress is larger than the long-term strength, as time progresses, in addition to viscoelastic deformations, viscous-plastic deformations would also develop. The viscous-plastic deformation is the primary cause of the progressive damage of the structural surface, which deteriorates the strength of the structural surface and affects the mechanical parameters of the structural surface. Some researchers have studied the variation effect of mechanical parameters in rock rheological behaviors; however, due to the significant difference in rock properties, those revealed evolutions still hardly to be coupled into the constitutive models. In addition, the stale creep stage is indeed not strictly linear; therefore, the viscous element in the viscous-plastic body is modified into non-linear characteristics, in order to more accurately describe the nonlinear characteristics during the creep process. Detailed improvements are shown in Figure 3.53.

图 3.53 Modified Bingham model

The relationship among the viscosity coefficient, time and stress is expressed by Eq.3.18, in which *n* is the adjustment factor.

$$\eta = (\sigma - \sigma_\infty) n t^{n-1} / \dot{\varepsilon} \qquad (3.18)$$

By solving the differential equation of Eq.3.18, the creep equation of the nonlinear viscous-plastic body can be obtained as:

$$\varepsilon_3 = \frac{\sigma - \sigma_\infty}{\eta_3} t^n \qquad (3.19)$$

Based on the above analysis, the rheological constitutive models under different stress levels could be obtained respectively. When the stress level is low, the creep behavior of discontinuities could be described using the improved NISHIHARA model, so called H-K-K model, as shown in Figure 3.71. On the other hand, when the stress level is high, the creep behavior of discontinuities could be described using the improved NISHIHARA model shown in Figures 3.54-3.55.

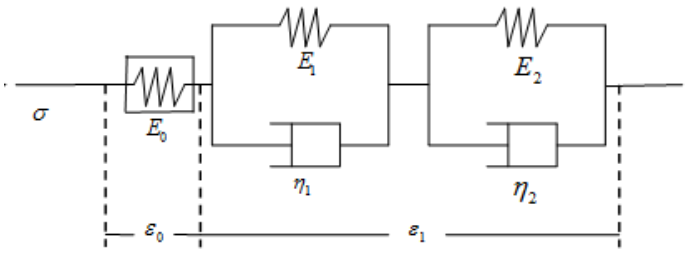

Figure 3.54 H-K-K model for relatively low stress

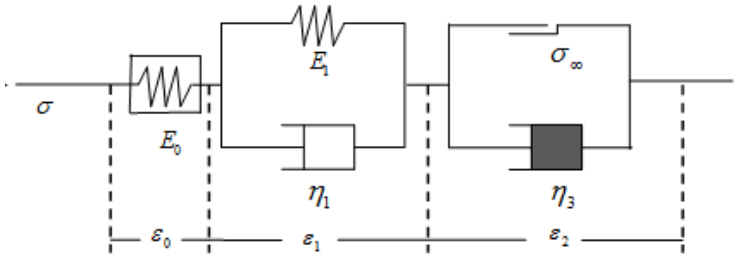

Figure 3.55 Improved Nishihara model for relatively high stress

Based on the above analysis, the creep relation derived from the improved NISHIHARA model could be obtained by combining Eq.3.14 and Eq. 3.15.

When the stress level is smaller than the long-term strength, the creep relation is expressed as Eq. 3.20.

$$\varepsilon = \varepsilon_0 + \frac{\sigma}{E_1}[1-\exp(-\frac{E_1}{\eta_1}t)] + \frac{\sigma}{E_2}[1-\exp(-\frac{E_2}{\eta_2}t)] \quad (3.20)$$

When the stress level is larger than the long-term strength, the creep relation is expressed as Eq. 3.20.

$$\varepsilon = \varepsilon_0 + \frac{\sigma}{E_1}[1-\exp(-\frac{E_1}{\eta_1}t)] + \frac{\sigma-\sigma_\infty}{\eta_3}t^n \quad (3.21)$$

It can be seen from the model that when the stress level is smaller than the long-term strength, the improved NISHIHARA model is composed of two parts: the improved Hook body that characterized the instantaneous deformation and the K-K body that characterizes the attenuation creep deformation. When the stress level is larger than the long-term strength, the improved NISHIHARA model consists of three parts: an improved Hooke body that characterizes instantaneous deformation, a Kelvin body that characterizes the attenuation creep deformation, and a nonlinear viscous-plastic body that characterizes the stable creep.

3.6.2 Model fitting and its parameter evolution analysis

For better comparison, the fitting data obtained from the improved NISHIHARA model and NISHIHARA model, as well as the testing data were summarized in Figure 3.56~3.61. In addition, the involved parameters in the improved NISHIHARA model can derived by the optimum solution method through the software of 1stOpt , the results are shown in Table 3.8.

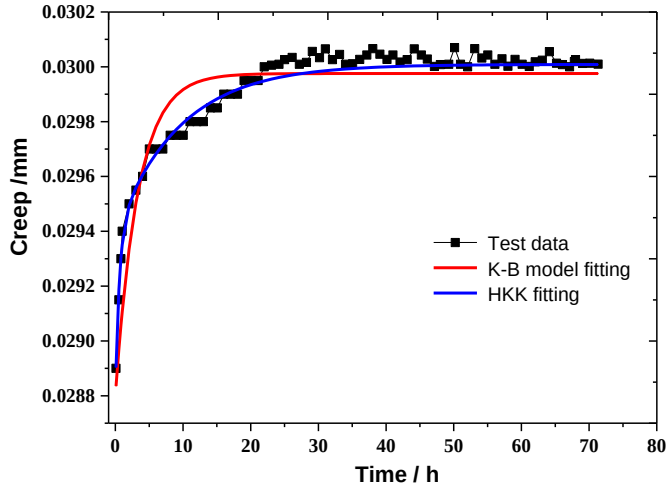

Figure 3.56 Fitting comparison between Nishihara model and modified Nishihara model (1-2.17, 1st level)

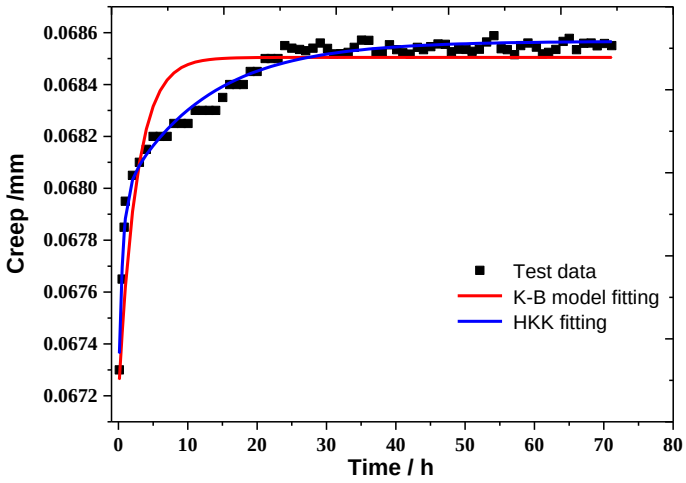

Figure 3.57 Fitting comparison between Nishihara model and modified Nishihara model (1-2.17, 2nd level)

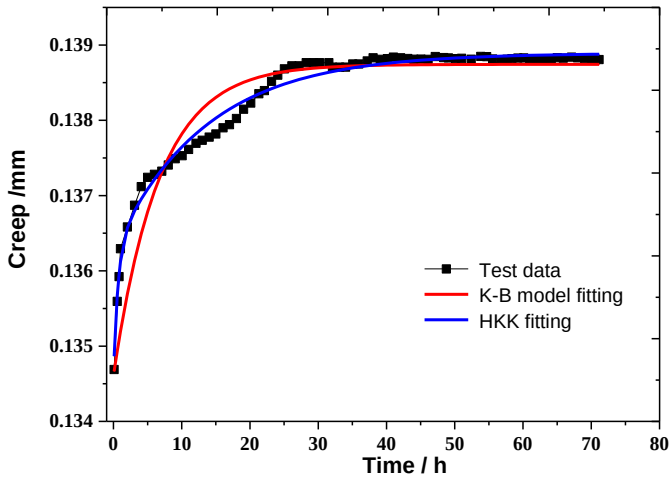

Figure 3.58 Fitting comparison between Nishihara model and modified Nishihara model (1-2.17, 3rd level)

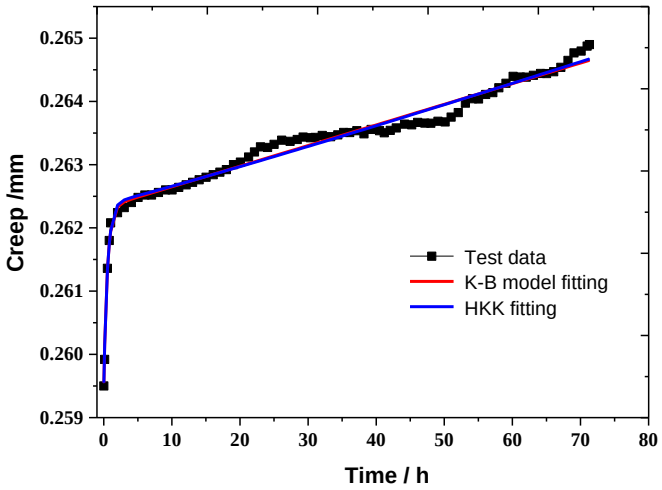

Figure 3.59 Fitting comparison between Nishihara model and modified Nishihara model (1-2.17, 4th level)

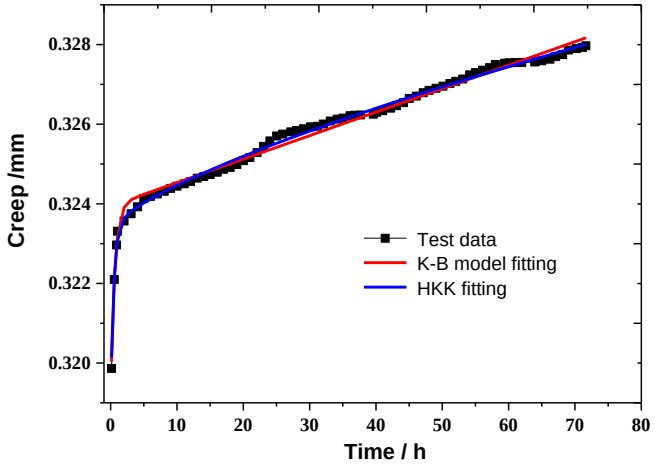

Figure 3.60 Fitting comparison between Nishihara model and modified Nishihara model (1-6.52, 4th level)

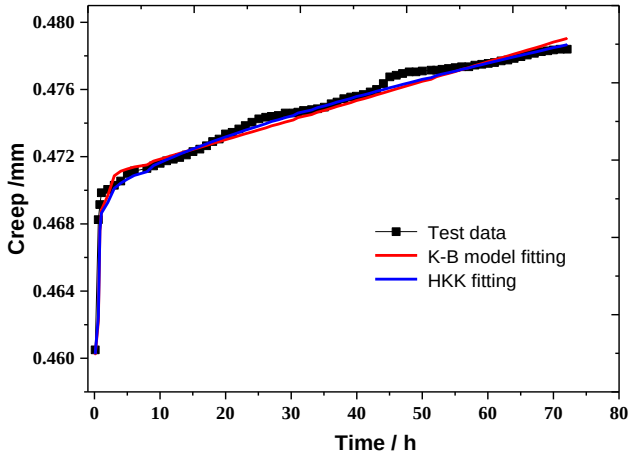

Figure 3.61 Fitting comparison between Nishihara model and modified Nishihara model (10-2.17, 5th level)

Table 3.8 Parameters of modified Nishihara model

Sample	Loading level	τ /MPa	E_1 /GPa	η_1 /(GPa.h)	E_2 /GPa	η_2 /(GPa.h)	η_3 /(GPa.h)	n	Correlation coefficient R
1-2.17	1	0.88	1483.27	856.95	1429.59	13527.22	—	—	0.995
	2	1.06	1064.57	1715.62	2858.34	31728.61	—	—	0.991
	3	1.23	696.02	2363.54	2651.84	40618.21	—	—	0.983
	4	1.41	490.52	265.01	—	—	3602.08	0.66	0.992
	5	1.58	334.18	104.23	—	—	152.6	1.20	0.982
1-4.35	1	1.95	409.11	1124.15	1506.75	539.59	—	—	0.995
	2	2.33	360.74	1503.01	1417.98	12165.72	—	—	0.983
	3	2.72	1539.7	8.08	1524.43	15045.52	—	—	0.971
	4	3.11	929.05	1391.29	—	—	968.02	0.37	0.997
	5	3.5	655.67	659.46	—	—	670.07	0.42	0.995
	6	3.7	191.06	194.63	—	—	8734.61	1.2	0.997
1-6.52	1	2.37	1740.53	4810	5336.39	64262.08	—	—	0.993
	2	2.84	1499.91	1409.35	6600.55	9799.61	—	—	0.982
	3	3.31	754.6	2754.85	66377.72	2961.56	—	—	0.99
	4	3.78	871.78	411.94	—	—	1114.93	0.42	0.998
	5	4.26	815.25	284.35	—	—	777.88	0.47	0.988
	6	4.49	935.67	545.28	—	—	3421.02	0.6	0.99
4-2.17	1	1.1	1798.86	2617.63	961.18	6156.07	—	—	0.995
	2	1.32	654.72	4435.33	1819.56	15.75	—	—	0.995
	3	1.54	628.76	2784.45	16069.87	700.53	—	—	0.984
	4	1.76	6394.53	10329.38	—	—	162.31	0.21	0.987
	5	1.98	649.53	9432.5	—	—	648.44	0.44	0.981
4-4.35	1	2.27	1314.8	3937.34	1393.94	4174.35	—	—	0.979
	2	2.72	2512.31	143.44	1847.80	13449.86	—	—	0.995
	3	3.18	1876.97	5250.91	3313.76	36444.51	—	—	0.998
	4	3.63	1526.41	59.24	—	—	961.53	0.48	0.983
	5	4.09	3292.74	13709.54	—	—	32367.78	0.94	0.995
4-6.52	1	2.66	1736.66	2498.3	4203.54	48303.94	—	—	0.993
	2	3.19	6544.5	1678.84	4858.24	22098.23	—	—	0.976
	3	3.72	3701.92	9.71	2718.78	28465.34	—	—	0.989
	4	4.25	2967.06	92831.2	—	—	120.08	0.04	0.972
	5	4.78	2803.96	7252.55	—	—	6671.78	0.43	0.96
10-2.17	1	1.79	640.66	3379.88	1735.01	2540.56	—	—	0.999
	2	2.15	521.68	2005.32	7695.93	175898.28	—	—	0.999
	3	2.51	655.79	2182.74	5990.53	299776.84	—	—	0.999
	4	2.86	1242.07	292.95	—	—	7573.7	0.67	0.997
	5	3.22	346.31	134.82	—	—	997.91	1.12	0.995
10-4.35	1	3.13	2351.99	1396.04	3607.09	24688.37	—	—	0.991
	2	3.75	1547.14	3263.18	9648.02	159040.73	—	—	0.999
	3	4.38	1945.29	3216.36	14623.57	76517.99	—	—	0.993

	4	5	1123.97	495.53	—	—	6022.05	1	0.995
	5	5.63	1211.21	720.82	—	—	40457.93	1.17	0.98
10-6.52	1	3.95	3559.19	1902.18	6015.38	73478.29	—	—	0.989
	2	4.74	3592.72	1642.66	8787.92	102523.76	—	—	0.989
	3	5.53	1054.1	544.63	12153.69	126635.85	—	—	0.994
	4	6.32	1628.63	719.18	—	—	2331.7	0.46	0.996
	5	7.11	3932.37	579.16	—	—	1674.87	0.49	0.99
	6	7.51	3344.15	1092.96	—	—	10098.3	0.87	0.994

It is found that, the correlation coefficients of the fitting curves obtained from the improved NISHIHARA model are obviously improved, with all of them larger than 0.95. From Table 3.8, it is seen that the evolution of each parameter in the modified NISHIHARA model is generally similar to those observed in the NISHIHARA model; however, the regularity and even the congruity of value are worse than those obtained by the NISHIHARA model.

As for the same discontinuity under the same normal stress, the parameter *n* increases with the increasing of the shear stress, indicating that with the increasing of shear stress, the non-linear property associating with the viscous-plastic deformation becomes more and more distinct.

3.7 Concluding remarks

In this chapter, a series of shear creep tests on different discontinuities of the 1st, 4th and the 10th Barton's standard lines were conducted. The corresponding creep behavior in terms of the whole creep curves, stepwise creep curves, creep rate curves, and isochronous curve were analyzed. The NISHIHARA model was selected to describe the creep properties of discontinuities, and an improved NISHIHARA model is thereafter proposed to better describe the creep properties of discontinuities. The effects of parameters involved in both the NISHIHARA model and improved NISHIHARA model were analyzed. Some conclusions could be therefore drawn as follows:

1) The samples develop to failure without distinctly manifesting the acceleration creep phase. The following reasons are considered: The creep failure of an intact rock under constant external load results from the initiation and evolution of micro-cracks, which finally coalescent into macro-failure along with the stick-slip between the cracks. While as for rock mass with

discontinuities, the sample already coalescent into macro-cracks, i.e. the discontinuity, therefore, when the stress level is higher than a certain value, shear creep would occur, leading to the rapid reduction of the viscous resistance, and hence exhibiting as an apparent instantaneous behavior.

2) The results of the creep rate relation show that at the beginning of loading, the creep rate is mainly related to the applied shear stress level, where a higher shear stress generates a larger initial creep rate. Meanwhile, an empirical formula whose involved parameters have clear physical meaning is suggested to describe the creep rate during the whole creep process, and a satisfied fitting result is obtained.

3) The instantaneous deformation is mainly affected by the shear stress level, which increases with the increased shear stress. Generally, the instantaneous deformation increases almost linearly during the first three or four loading levels where the shear stresses in each level are relatively low. Thereafter, as the increase of the shear stress, especially at the last loading level, the instantaneous deformation would increase more rapidly with the increased shear stress. In addition, the total amount of creep deformation is also increased with the increasing shear stress.

4) The duration for the attenuation creep stage for a sample under a relatively low shear stress is longer than that under a high shear stress, which is due mainly to the full play of viscous deformations between the discontinuities of the sample when it subjected to a low shear stress. Besides, under a relatively low shear stress, the creep would stabilize eventually, while the creep would continuously develop with time even after reaching the stable creep stage when the sample is subjected to a high shear stress. It is worth noted that the stable creep stage in the discontinuity is not strictly evolved linearly, but exhibiting some fluctuations due to the effect of the discontinuity.

5) The isochronous curve that reflecting the stress-strain relation is the link between the instantaneous mechanical behavior and rheological mechanical behavior that considers the effect of time. The isochronous curve could be divided into two stages in terms of the initial linear stage and the followed nonlinear stage where the shear stress increases with the deformation at a gradually decreasing rate. In which, the slope of the initial linear stage reflects the elastic modulus, while the latter non-linear stage reflects the strain softening property of the sample under time effect. These two stages are corresponding to the elastic deformation and yielding deformation in the instantaneous stress-strain curve, which have great significance to understand the non-linear

rheological mechanical behavior of discontinuities. However, since the rock samples used in this thesis are relatively hard, the time effect on the isochronous curve is not so obvious.

6) NISHIHARA model was selected to fitting the testing data and the evolutions of involved parameters in the model were analyzed. The results show that the NISHIHARA model still has some limitations, in describing the creep behavior of discontinuities. For example, NISHIHARA model does not take the instantaneous plastic deformation into account; the attenuation rate at the inflection part of the attenuation creep stage is too rapid when the sample is under a relatively low shear stress; lack of explorations on the non-linear property of involved parameters in the model when the sample subjected to high shear stress, etc. To this end, an improved NISHIHARA model was therefore proposed and the involved parameters were analyzed and compared. It results that a better fitting result could be obtained compared with the original NISHIHARA model.

Chapter 4 Stress relaxation properties of discontinuities

Creep and stress relaxation are two commonest mentioned phenomenon in time-dependent behaviors. Spene and Hult (2001) defined creep as a state caused by prescribed boundary forces while relaxation represents the state caused by prescribed boundary displacements. The current study limits in the stress relaxation field ascribe to the limitation of engineering practice. Furthermore, the study of rheological characteristics mainly focus on three parts, that is creep, stress relaxation and long-term strength, which current study pay less attention to their internal connection and make them independent of each other, especially between creep and stress relaxation. Under unconfined conditions, creep refers to continuously increasing strain with fixed boundary forces, while relaxation refers to the drop in stress with fixed boundary deformation. This demonstrates that creep and relaxation are two intrinsic time-dependent behaviors of material caused by different boundary condition. In other words, the intrinsic time-dependent properties of the material should be consistent, no matter whether it is investigated with the creep test or the relaxation test. In this chapter, stress relaxation behaviors of discontinuities are investigated.

4.1 Test method and conditions

4.1.1 Procedure of isostress cyclic loading

Currently, the main test method for stress relaxation is a single load at various stress levels (Yu et al. 2011; Li et al. 2006). Isostress cyclic loading method (ICL method) is proposed in this work, which can gradually reduce the effect of instantaneous mechanical characteristics with increasing cycle times and reflect the viscous properties of the rock material more accurately. In addition, a more accurate method of determining the rock's long-term strength is proposed in chapter 5 based on this test method.

In the process of stress relaxation, $\sigma_0 = \sigma_r + \sigma_s$, where, σ_0 is the loading stress, σ_r is the residual stress, and σ_s is the relaxation stress. Figure 4.1 illustrates the procedures of isostress cyclic loading method (ICL method). First step is applying the predetermined loading stress σ_0 on the sample and conducting the 1st level of stress relaxation test. The residual stress eventually decreases to a stable value over time, which means the complication of the 1st level. Next step

requires reloading the stress up to σ_0 on the basis of the residual stress σ_r in the 1st level. In here, the relaxed stress in the 1st level is equal to the added stress in the 2nd level. By this analogy, the residual stress of each level can be acquired and recorded as σ_{s1}, σ_{s2}, σ_{s3},… … σ_{sn}, σ_{sn+1}. When $\sigma_{sn} = \sigma_{sn+1}$, the test could be completed.

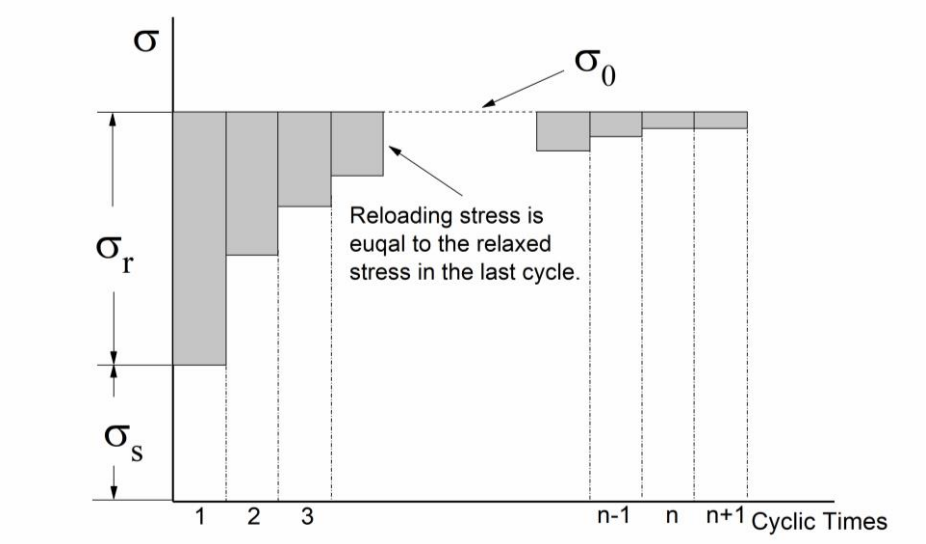

Figure 4.1 Isostress cyclic loading method (ICLM)

In this study, ICLM was applied to the shear stress relaxation test; three types of structural planes and normal forces of 4, 8, and 12 MPa were used, with one sample in each group, and 9 samples in total. Before the stress relaxation test, rapid shear tests were conducted under normal forces of 4, 8, and 12 MPa to determine the instantaneous shear strength. A value equal to 85% of the conventional shear strength at different normal stresses, which is greater than the long-term strength, was taken as the initial shear stress value σ_0 in shear stress relaxation tests.

4.1.2 Test conditions

As previously stated, in the shear relaxation test, firstly, a normal stress was loaded and kept it as a steady value throughout the test; secondly, the shear stress was loaded to a predetermined value σ_0 and kept the corresponding deformation value of the horizontal shear direction unchanged until the stress relaxed to a steady value. Then, the shear stress was increased upward to σ_0 again and

the 2nd level of testing was conducted. By this analogy, six levels of the test were conducted here. The samples were designated as 4-4, 4-8, 4-12, 6-4, 6-8, 6-12, 10-4, 10-8, and 10-12, and each group of samples was loaded for 72.07-84.98 h per level. Test conditions are listed in Table 4.1.

Table 4.1 Test condition of shear stress relaxation test

Sample	JRC	Shear strength /MPa	Normal stress/ MPa	Shear stress/ MPa	Test time per-levels/h
4–4	7	4.01	4	3.41	72.07
4–8	7	7.71	8	6.55	72.07
4–12	7	11.41	12	9.70	84.79
6–4	11	4.41	4	3.75	75.90
6–8	11	8.47	8	7.21	84.58
6–12	11	12.54	12	10.66	84.79
10–4	19	5.38	4	4.57	84.79
10–8	19	8.74	8	7.43	84.08
10–12	19	12.71	12	10.80	84.98

4.2 Stress relaxation curves

4.2.1 Whole process of relaxation curves

Through the compilation of test data, stress relaxation curves under different stress levels were obtained (shown in Figure 4.2). Shear stress relaxation characteristics were studied.

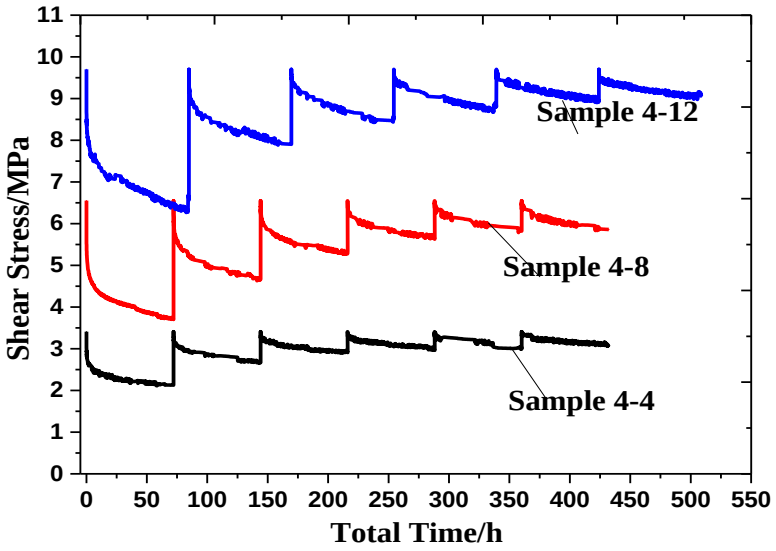

a. **The 4th structural plane**

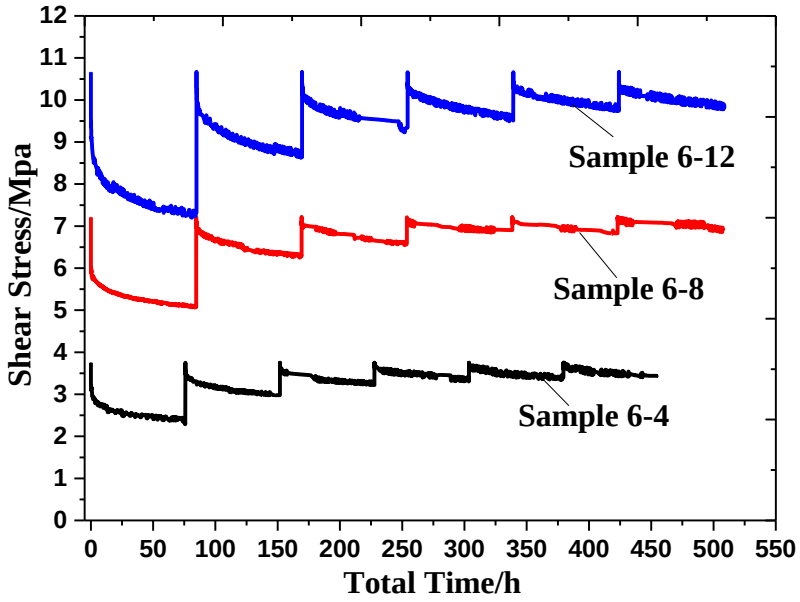

b. **The 6th structural plane**

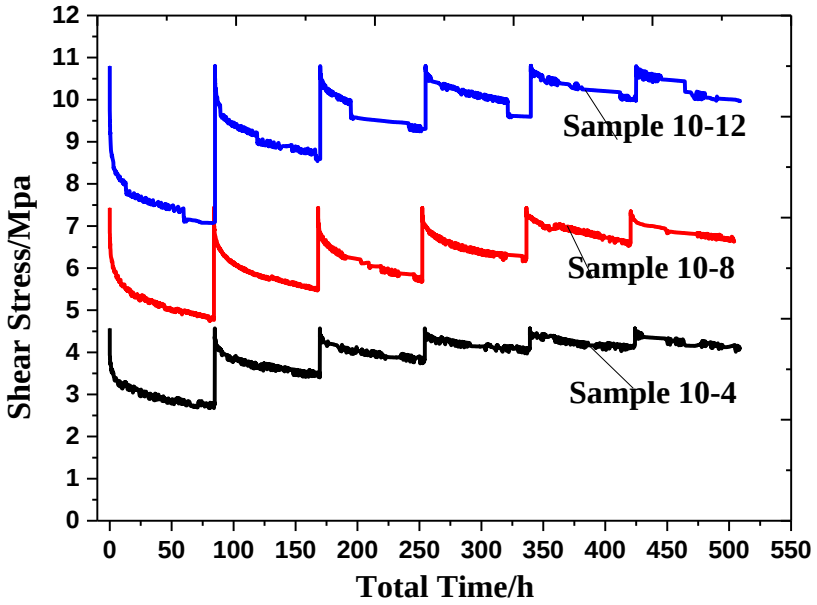

c. **The 10th structural plane**

Figure 4.2 Stress relaxation curves under different stress levels

It can be seen from Figure 4.2, on the whole, the test curves are continuous stress relaxation curves, however, stair-stepping falling phenomenon of stress values occurred occasionally, which is showing as a ladder type curve. Take sample 10-12 as example, stress rapidly dropping was observed on the 3rd level when test for 194.75h, the loading stress suddenly decreased from 9.98

MPa to 9.65 MPa, fell 0.33 MPa which accounts for 19.5% of the total stress relaxation in this level, and also on the 4rd level when test for 321.40h, the loading stress suddenly decreased from 9.97 MPa to 9.68 MPa, fell 0.29 MPa which accounts for 22.1% of the total stress relaxation in this level. Ladder type stress relaxation curve is related to the expansion of crack. In the process of test, with the stair-stepping falling phenomenon of stress, macro-crack expansion was observed at the edge area of the sample.

4.2.2 Stage Division of Stress Relaxation

Based on the stress relaxation curve in Figure 4.2, stress relaxation rate curve can be drawn. Take the 1st level of sample 4-4 as example (see Figure 4.3), at the beginning of the test, shear stress has a rapid decline while stress relaxation rate is relatively larger, then stress relaxation rate gradually slow down and eventually tends to 0, stress value tends to a stable value. The initial stress relaxation rate is 4.27 MPa/h and ten minute later decline to 0.95 MPa/h, one hour later attenuate to 0.12 MPa/h, and eventually attenuate to 0 MPa/h and stress value tends to 2.11 MPa finally.

According to it, the stress relaxation can be divided into three stages: rapid stress relaxation stage, decelerating stress relaxation stage and stable stress stage. Rapid stress relaxation stage generally completes within minutes at the beginning of the test, then enters into decelerating stress relaxation stage, in this stage stress relaxation rate gradually attenuate to 0 MPa/h and eventually enters the stable stress stage. At this point, internal force and external force are equal and the process of stress relaxation is completed.

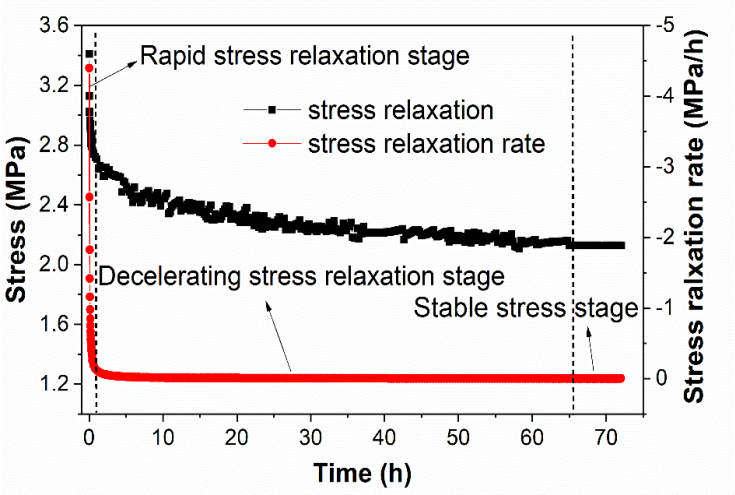

Figure 4.3 Typical stress relaxation curve and stress relaxation rate curve

Stress relaxation is a process in which stress relaxes, as strains constant. It is a process of remaining strain constant by reducing stress. Because the sample is in a state of loading, the effect of loading would promote the development of strain, which appears in two forms: local failure and deformation. Local failure manifests as the expansion of cracks, deformation mainly manifests as the viscous deformation which connects with time. In this case, in order to maintain the strain as a constant, it is bound to release part of elastic deformation by reducing the loading stress to compensate for the development of strain. Local failure and viscous deformation can be regarded as two indirect forms of stress relaxation.

Stress relaxation is a gradually adjusting process between internal force and external force under limited deformation condition. It can be seen as an attenuation process of stress concentration caused by loading. At the beginning of stress relaxation process, the work that external force impacted on the sample is stored in the form of elastic energy and forms stress concentration in partial area of the sample. Stress relaxation can also be seen as a dynamic adjustment process of deformation, the deformation is not a constant value all through but a dynamic adjustment process between the testing machine and the sample itself.

In rapid stress relaxation stage, cracks rapidly expand due to local stress concentrated by loading exceeded the requiring for the crack extension. This process mostly reflects the instantaneous mechanical characteristics of the sample. It is equivalent to the characteristic after the peak of complete stress-strain curves, in which material would be failure with crack extension without increasing the stress. With the stress release, stress relaxation enters into the decelerating stress relaxation stage. In this stage, on one hand, crack extension gradually slows down and continues to release the stress concentration. On the other hand, viscous deformation develops gradually under time effect. When crack extend and viscous deformation develop, part of the elastic deformation would be released to keeping strain value as constant. Finally, stress relaxation enters into stable stress stage, in which stress is a stable value.

4.2.3 Kinematic interactions during relaxation behaviours

Stress relaxation is defined as a state caused by prescribed boundary displacements (Spene and Hult, 2001), in which the initial load acting on material gradually decreases with time under the constant initial deformation. Stress relaxation is divided into three stages, termed as rapid stress relaxation stage, decelerating stress relaxation stage, and stable stress stage, respectively. The rapid stress relaxation stage is transient and generally completed within minutes from the very beginning of the test. In decelerating stress relaxation stage, the relaxation rate gradually attenuates to 0 and eventually enters the stable stress stage, in which the process of stress relaxation is completed.

During the shear relaxation process, the boundary where the shear stress acting on is constrained, and no displacement along the shear direction is allowed. On the other words, there will be no increment in the total strains including elastic, plastic and viscous strains (including viscoelastic and viscoplastic strains) along the shear direction. While the tested material is stressed, it will inevitably cause an adjustment between the reversible (elastic) and irreversible (plastic and viscous) deformation to occur. The strains involved in this process can be expressed by the following Eqs. 4.1 & 4.2.

$$\varepsilon_e + \varepsilon_p + \varepsilon_v = cons. \tag{4.1}$$

$$\dot{\varepsilon}_e + \dot{\varepsilon}_p + \dot{\varepsilon}_v = 0 \tag{4.2}$$

Where ε_e, ε_p and ε_v are the elastic, plastic and viscous strains respectively, and $\dot{\varepsilon}_e$, $\dot{\varepsilon}_p$ and $\dot{\varepsilon}_v$ are the elastic, plastic and viscous strain rate. Viscous deformation related to the loading stress level and the viscous property of testing material will develop over time, which will destroy the boundary condition that holds the deformation as a constant. As a result, the stored elastic deformation in the initial shear loading stage has to be released to compensate the viscous deformation in order to maintain a constant total strain, which will hence promote the stress to release.

In addition to viscous deformation, Li and Xia (2000) and Peng and Podnieks (1972) conducted uniaxial relaxation test on intact rocks and found that stress relaxation is closely related to crack activities, which could promote the stress stored during initial loading stage to release.

While as for discontinuities under shear loading, additional essential contributions to its relaxation behaviors are associated with the frictional resistance and internal kinematic constrains between the contacted surfaces. Prior to the relaxation stage, the asperities on the opposite surfaces of discontinuities are brought together and interlocked by the applied normal stress, the increasing shear stress accumulates on the contacted surface and provokes the internal kinematic behaviors associating with dilatancy in normal direction and crushing and/or breakage between the contacted asperities. Dilatancy in normal direction will be suppressed by the applied normal stress and the morphology of asperities, etc. Generally, higher normal stress, more flat morphology (i.e. smaller undulating angles), and severer asperity crushing would suppress the dilatancy behavior. Due to the intrinsic difference in appearance configuration (e.g. shapes and sizes), inner defects, etc., each asperity on the surface of discontinuities has its own mechanical characteristics. Hence, some asperities with lower strength may firstly be crushed, resulting in the redistribution of stress. While entering into relaxation stage, there is no additional shear stress and the dilatancy behavior would be fully suppressed by the normal stress. Time-dependent deformation (creep) of stressed asperities will nonuniformly develop due to the nonuniformly distributed stress, part of elastic deformation accumulated during shear loading will be released to compensate such deformation and eventually resulting in stress relaxation, as expressed in Eqs. 4.1 & 4.2. Moreover, part of asperities deforms in a relatively higher viscous deformation rate and would be crushed over time, which will also induce stress relaxation. Therefore, viscous deformation and asperity crushing and/or breakage (local failure) could be therefore regarded as two essential behaviors that inducing stress relaxation of discontinuities during the process of shear relaxation, as expressed in Eq. 4-3.

$$\sigma_r(t) = \sigma^{cracking}_{crushing/breakage}(t) + \sigma_{viscous\ deformation}(t) \tag{4.3}$$

Recalling that the process of stress relaxation is divided into three stages, i.e. rapid stress relaxation stage, decelerating stress relaxation stage, and stable stress stage, the mechanism of these three stages can be correspondingly interpreted. In the rapid stress relaxation stage where the stress level is high, some asperities that having been or being failed in the previous shear stage, i.e. reaching the post-peak or peak stress regime of the asperities, continuously to be crushed/broke even though no additional shearing stress is added. Such failures would inevitably cause the stress to release spontaneously, which just behaves similarly to the post-peak regime in the stress-strain

curve of rock materials. Once the rock material has reached its peak failure, it will spontaneously enter its strain softening regime even without any additional loading. Rapid stress relaxation stage reflects a delayed response of the initial loading. With the stress releasing, asperities crushing gradually slow down, and the rock mass enters into the decelerating stress relaxation stage, where the development of time-dependent deformation (i.e. viscous behavior) become working on stress relaxation behaviors. Part of the elastic deformation is released to compensate the viscous deformation resulting in the continuous relaxation of the shear stress. With the time elapsing, the stress relaxes to a value that could cause no more asperity crushing and only limited viscous deformation, and accordingly the rock mass will gradually transit to the stable stress stage. With this, stress relaxation process is completed.

4.3 Stress relaxation behaviours of discontinuities impacted by normal stress and JRC

4.3.1 Stress relaxation and stress relaxation rate curves

Figure 4.4 presents the stress relaxation curves for aforementioned tests, it is observed that the curves generally present continuous, but ladder-type evolutions of stress in some details, marked as “A” as examples in Figure 4.4, are also observed. For a better observation, Figure 4.5 gives a close-up of region “A”. Region “A” in relaxation test of 4-12 presents a sudden stress reduction from 7.41MPa to 7.01MPa accounting for 12.27% of the total relaxed stress. Such phenomenon is considered to be associated with asperity breakage activities. During the test, with such stress reduction, macro-crack expansion was observed occurring at the edge area of the sample, which is in consistence with the testing phenomenon observed by Li and Xia. After the breakage of the conducted asperity, the adjustment between the loading plate and the sample surface is inevitable in order to maintain a constant normal stress, leading to the abrasion and crushing between asperities on the surface of the discontinuities to occur. As a result, the shear stress curve observed in Figure 4.5 is fluctuating with time.

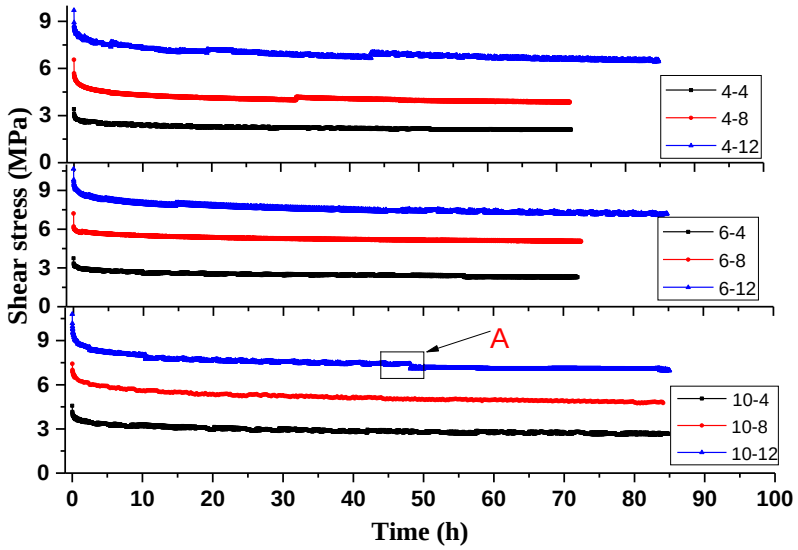

Figure 4.4 Relaxation curves of discontinuities

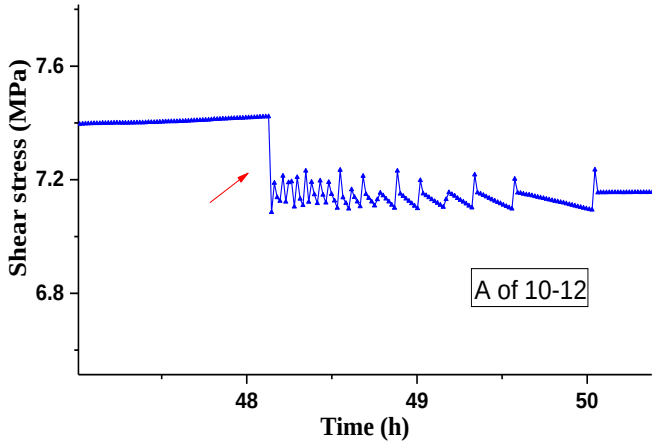

Figure 4.5 A Close-up of the ladder-type stress reduction phenomenon in Figure 4.4

4.3.2 Stress relaxation impacted by normal stress and JRC

For a better observation and comparison of relaxation rate in different conditions, log t-relaxation rate curves are plotted and shown in Figure 4.6 and Figure 4.7, which represent the relaxation rate curves of the same discontinuities with an increasing normal stress from 4MPa to 12MPa (Figure 4.6), and the relaxation rate curves under the same normal stress with an increasing JRC values from 6-8 to 18-20 (Figure 4.7), respectively. It is observed that the relaxation rate increases with the increasing of both normal stress and JRC. Moreover, the difference of stress relaxation rates is relatively large at the rapid relaxation stage and become smaller over time, manifesting in figures is that the relaxation curve tends to overlap with each

other over time. Taking the 4th discontinuity in Figure 4.6 as an example, the initial relaxation rates under the normal stresses of 4, 8 and 12 MPa are 11.98, 9.19 and 4.40 MP/h respectively, after 10 minters, they subsequently decrease to 0.32, 0.24 and 0.12 MP/h respectively, and after 10 h, they further decrease to 0.04, 0.03 and 0.01 MP/h respectively. It is also observed that the difference of stress relaxation rates in Figure 4.6 are greater than that in Figure 4.7, suggesting that the selected JRCs in this study have a slight impact on the stress relaxation rate.

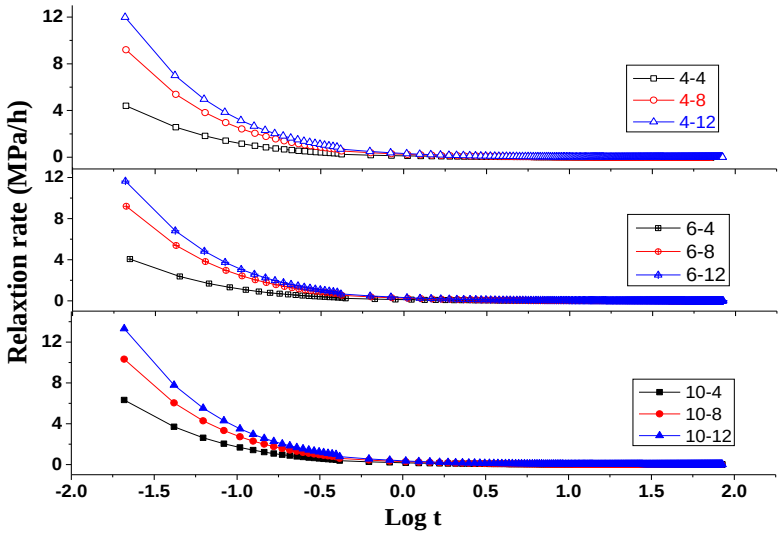

Figure 4.6 Relaxation rate curves at different stresses

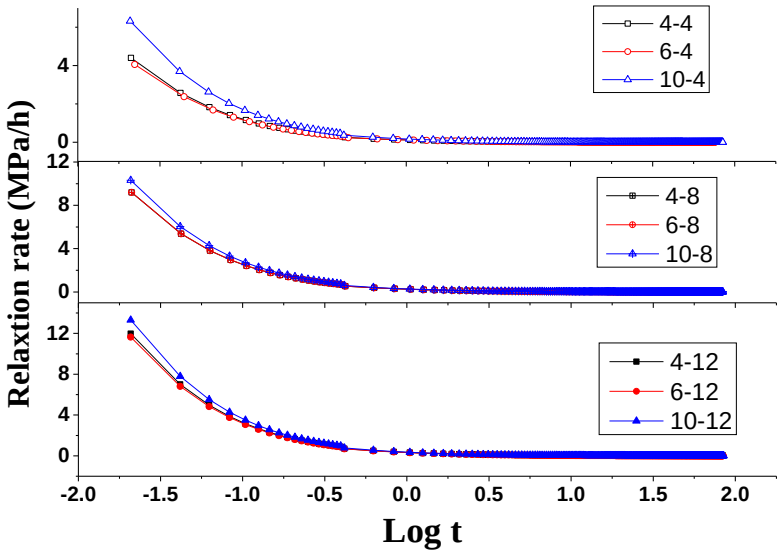

Figure 4.7 Relaxation rate curves at different JRC

In addition, the Relaxation Capacity (*RC*), which is equal to the ratio of relaxed stress, τ_r to the initial loading stress, τ_0, is proposed to represent the ability of relaxation, as expressed in Eq.4.4.

$$RC = \frac{\tau_r}{\tau_0} \tag{4.4}$$

The larger *RC is*, the greater relaxed stress will be. The lower limit of *RC* is 0 and it has an upper limit of 1. The value of *RC*, which depends on the viscous and asperity property of the tested discontinuities, is found between 0.33 and 0.41 in this study. Figure 4-8a illustrates that *RC* decreases with the increasing of the normal stress, while the variation of *RC*, especially the 4th and the 10th discontinuities shown in Figure4-8b, illustrates *RC* increases with the increasing of JRC. The result suggests that for a given material, the shearing relaxation of discontinuities mainly depends on the normal stress and the surface roughness, in which higher normal stress would restrict the stress relaxation, while more rough surfaces would facilitate the stress to release during the relaxation process. This probably due to the kinematic behaviors associating with dilatancy and asperity crushing occurred on the discontinuities. Under a higher normal stress, dilatancy behavior associating with climbing in the normal direction will be well suppressed by the well-established kinematic constrains (such as friction resistance and interlocking between asperities). The suppressed dilatancy increases the contacted area as well as the area of potential failure plane, and hence decreases the potential to crush or break the contact asperities. Such behavior would then improve the mechanical properties of tested discontinuities. While the initial stress level under higher normal stress is quite high, the contacted asperities during the discontinuities are prone to crush and even break over time, facilitating the stress to release, but meanwhile leading to a flatter morphology and larger contact area between the surface of the discontinuities. It seems that under a higher normal stress, kinematic behaviors of suppressed dilatancy and asperity crushing are “competing” with each other to influence the stress relaxation, and the rock mass will not “announce the result” until the comparison and competition of these two behaviors are completed. From Figure 4-8 a, it seems that the suppressed dilatancy plays a more important role in governing the relaxation behavior when increasing the normal stress. However, with the increase of the JRC, the RC increases. Under a higher JRC, asperities crushing/breakage behaviors associating with contact area between the surface of the

discontinuities will be increase, which facilitate the stress to release.

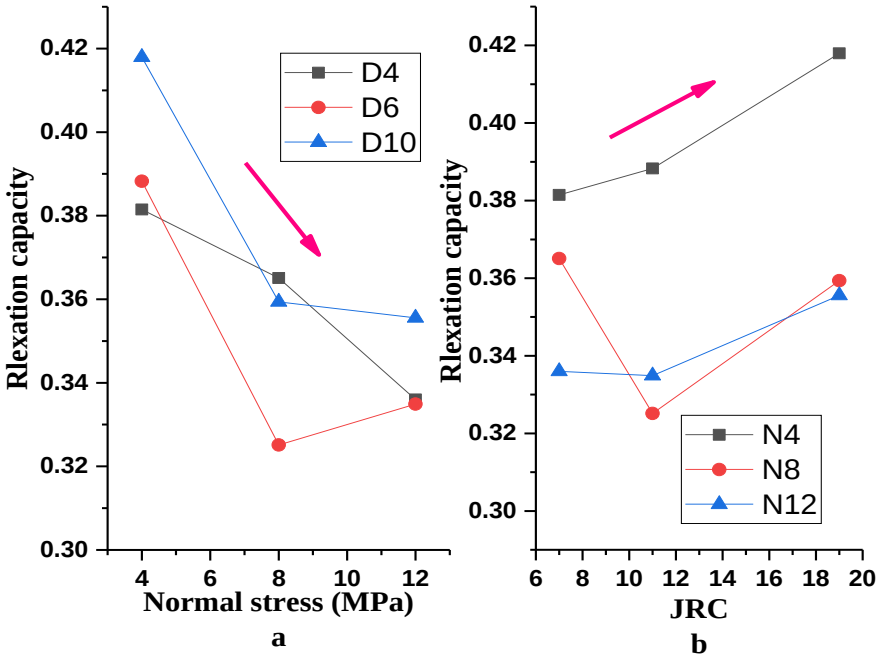

Figure 4.8 Relationship between relaxation capacity (*RC*) and normal stress (a) and JRC(b)

4.3.3 Normal deformation during stress relaxation

Since the normal stress is hold as constant during relaxation tests, an adjustment of the displacement along the normal direction is inevitable. Figure 4.9 shows the corresponding displacement in the normal direction during the entire relaxation history. For briefly, only the result of sample 4-4 is taken for interpretation. It is observed that the normal displacement increases monotonically with the elapsing time during the relaxation process. The displacement increases in a rapid rate at the beginning, and then slows down over time, which corresponds well with the relaxation behaviors in the rapid and attenuation relaxation stages respectively.

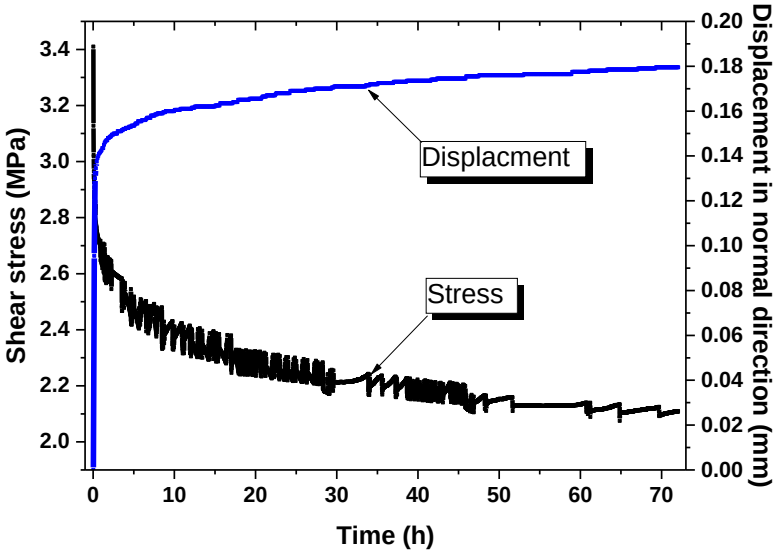

Figure 4.9 Corresponding displacement in normal direction during relaxation

Referring to previous creep tests on same discontinuities poured by same materials, viscous deformation under different stresses in more than 100hours developed within 0.01millimeters. During the relaxation process, time-dependent viscous deformation, though at a much small scale, would develop at a gradual decreasing manner with time, depending on the viscous coefficient and stress level of the materials. While in the rapid relaxation stage, in addition to viscous deformation, some asperities that having been or being failed, i.e. reaching the post-peak or peak stress regime of the asperities, in the previous shearing stage continuous to be crushed/broke even though no additional shearing stress is added. Such failures would inevitably cause the stress to release spontaneously, which just behaves similarly to the post-peak regime in the stress-strain curve of rock materials. Once the rock material has reached its peak failure, it will spontaneously enter its strain softening regime even without any additional loading. Due to such kind of asperity crushing/breakage, the contact connected by the asperity at that moment is lost and the bearing capacity of the discontinuity decreases transiently, as also previously stated in section 3.1. While the loading system has to adjust (reloading) itself correspondingly to maintain the normal stress constant, and consequently manifesting as compressed displacements along the normal direction. From Figure 4.9, it is observed that the compressed displacement along the normal direction during the rapid relaxation stage is up to 0.12 mm, which is much larger than that induced by viscous deformation.

It seems that the behavior of asperity crushing/breakage plays a more predominant role in facilitating stress relaxation during the rapid relaxation stage, where the severest asperity crushing/breakage is indicated occurring just shortly after the shearing loading by the rapid increase of compressed displacements as well as the rapid rate of stress relaxation. Thereafter, with the time elapsing and the decreasing of stress level in shear direction, asperity activities gradually decrease and bears a smaller contribution to the stress relaxation. In addition, viscous deformation continuously contributes to release stress at a gradual decreasing manner with time. With these, the discontinuity enters into the attenuation relaxation stage, manifesting as the gradually decreased compression displacement as well as the decreased relaxation rate. With the completion of asperity crushing/breakage, stress releases into a certain low level, which meanwhile could provoke no more viscous deformation. As a result, relaxation behavior will be ceased and the discontinuity enters into the third stage, i.e. the stable relaxation stage, suggesting by the levelling off shear stress as well as the compressed displacement. Based on the above results, it might be stated that the total stress relaxation, especially in the rapid relaxation stage, seems to be exclusively contributed by the asperity crushing/breakage behavior. While viscous deformation, which depends on the viscous coefficient and the stress level of the material, bears a relatively smaller and gradually decreasing contribution to the total stress relaxation during the entire relaxation history.

4.3.4 Relationship between Stress Relaxation and Creep

The equivalence of creep and stress relaxation is put forward by Liu Xiong 1994 in *"Introduction to Rheology"*, which reveals the inseparable relationship between creep and stress relaxation. The rheology properties of rock are not pure affected by creep or stress relaxation, but effected by their interaction. To some extent, the development of creep promotes stress relaxation, and stress relaxation reduces the requiring stress for further development in creep.

From the perspective of energy, in the process of creep, because of the development of deformation has certain relaxation effect on stress, loading force have to increase to compensate the loss of stress for keeping the stress as a constant, new energy is joint in this process. While in the process of stress relaxation test, part of the elastic deformation must be released to compensate the creep deformation for keeping the strain as a constant, no energy is joint in this process. This is

the reason why in the process of test creep can develop to failure and stress relaxation often tends to be stable. Therefore, creep and stress relaxation should be taken into account comprehensively when studying the characteristics of rock rheology.

4. 4 Cyclic relaxation properties of discontinuities

4.4.1 Stress relaxation curves under cyclic loading

On the basis of Figure 4.2, put the test data of each level in a same time scales, take sample 4-8 for example (see Figure 4.10).

It can be seen from Figure 4.10, with the increasing times of cycle, relaxation stress gradually decreases and finally tends to a stable value, curves tend to overlap and the needed time for stabilization of stress relaxation gradually reduce.

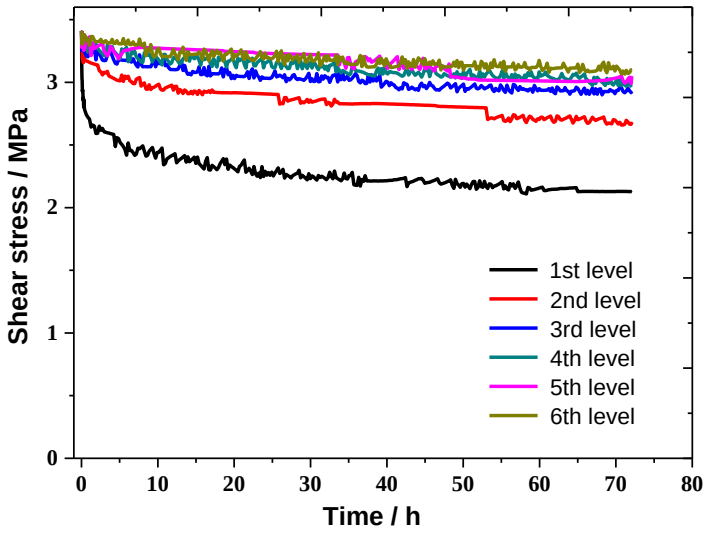

a. Sample 4-4

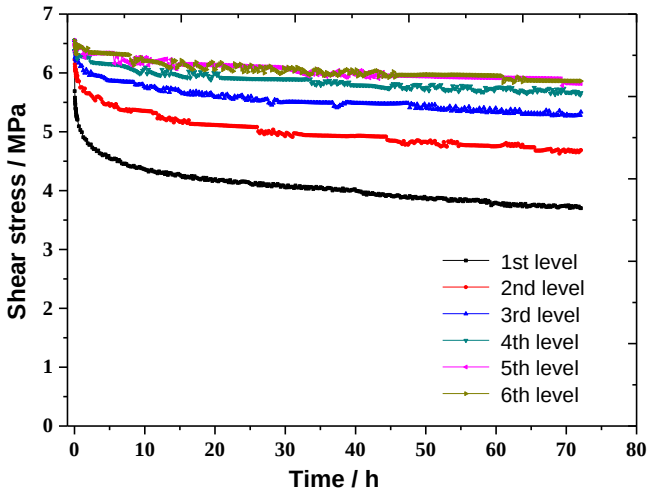

b. Sample 4-8

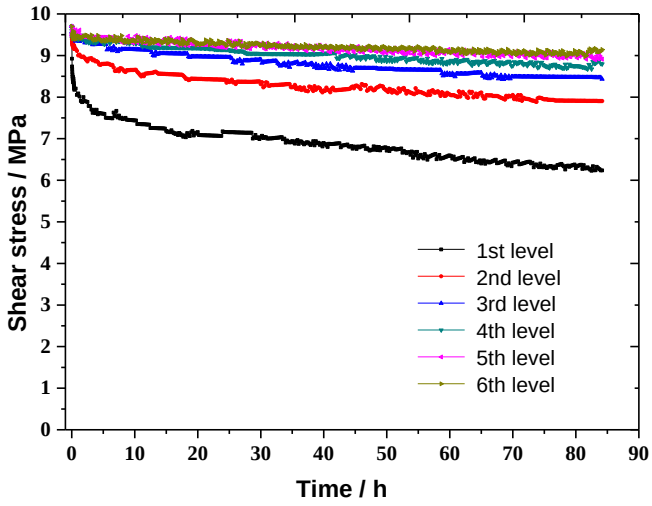

c. Sample 4-12

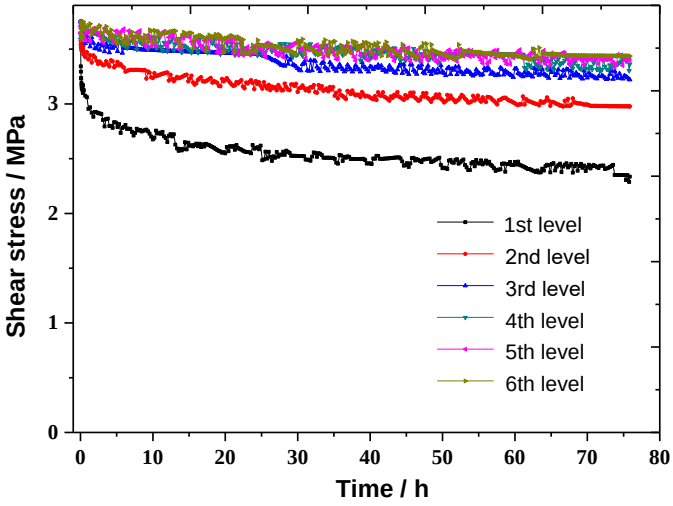

d. Sample 6-4

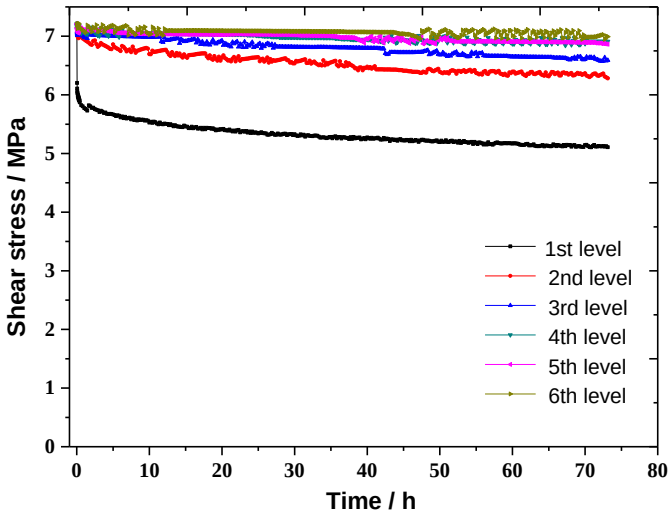

e. Sample 6-8

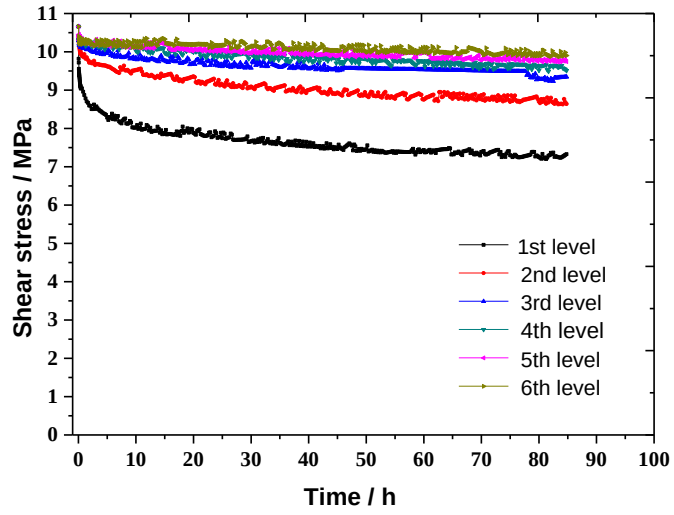

f. Sample 6-12

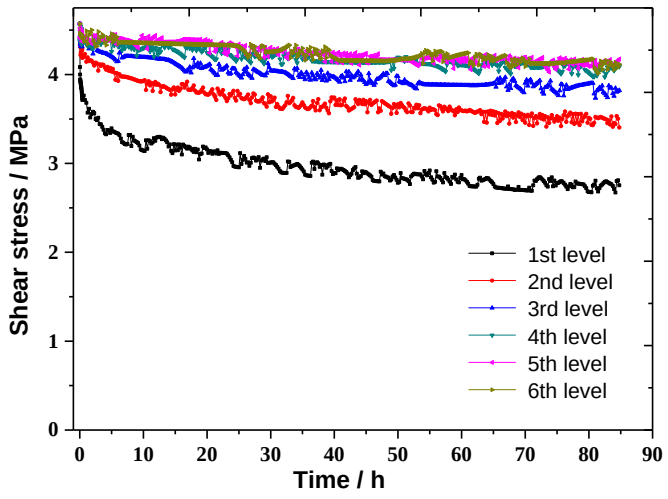

g. Sample 10-4

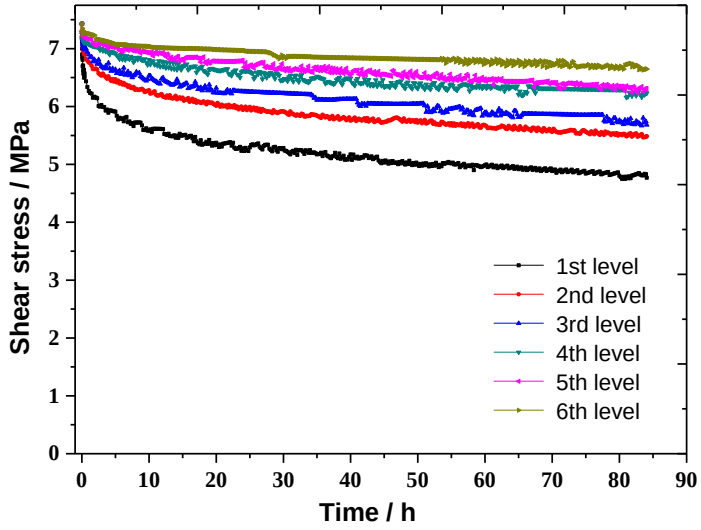

h. Sample 10-8

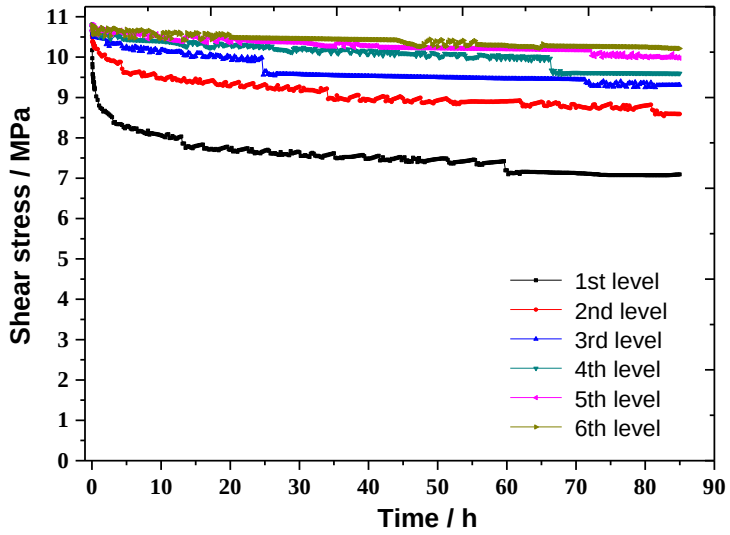

i. Sample 10-12

Figure 4.10 Stress relaxation curves in same time scale (4-8)

In the process of stress relaxation，

$$\sigma_0 = \sigma_s + \sigma_r \tag{4.5}$$

Where: σ_0= loading stress, MPa,

σ_s=residual stress, MPa,

σ_r=relaxation stress, MPa.

With the increasing times of cycle, relaxation stress σ_r gradually decreases, residual stress σ_s gradually increases. The concept of Anti-Relaxation Capacity（ARC） γ which is equal to the ratio of residual stress value and the initial load stress (see Eq.4.6) is proposed in this paper, which can represent the ability of anti-relaxation.

$$\gamma = \frac{\sigma_s}{\sigma_0} = 1 - \frac{\sigma_r}{\sigma_0} \tag{4.6}$$

The bigger ARC, the smaller relaxation stress will be. The maximum ARC is 1. The value of ARC is depended on the growth and evolvement properties of crack and the viscous properties of rock material.

Seen from Table 4.2, the value of ARC gradually tends to a stable value with the increasing times of cycle. The value of ARC, which is obtained under different test condition, gradually tends to be a stable value with the increasing times of cycle. Take sample 4-4 as example，it is 0.619 in 1st level test and they are 0.871, 0.883 and 0.889 respectively in the 4th, 5th and 6th level test. ARC in 6th level test are obtained between 0.889 and 0.938, the maximum gap is 0.049.

Table 4.2 Anti-Relaxation Capacity（ARC）

Sample NO.	Initial Load Stress, MPa	Levels					
		1st	2nd	3rd	4th	5th	6th
4-4	3.41	0.619	0.780	0.848	0.871	0.883	0.889
4-8	6.55	0.565	0.708	0.792	0.864	0.889	0.895
4-12	9.70	0.662	0.804	0.858	0.896	0.905	0.905
6-4	3.75	0.629	0.795	0.859	0.904	0.912	0.917
6-8	7.21	0.680	0.848	0.892	0.913	0.924	0.922
6-12	10.66	0.688	0.811	0.876	0.892	0.915	0.919
10-4	4.57	0.602	0.744	0.836	0.895	0.912	0.908
10-8	7.43	0.642	0.738	0.764	0.838	0.876	0.894
10-12	10.80	0.649	0.781	0.844	0.879	0.920	0.923

4.4.2 Cyclic properties of stress relaxation rate

On the basis of Figure 4.2, stress relaxation rate curves can also be drawn, take sample 4-4 as an example (shown in Figure 4.11 & 4.12).

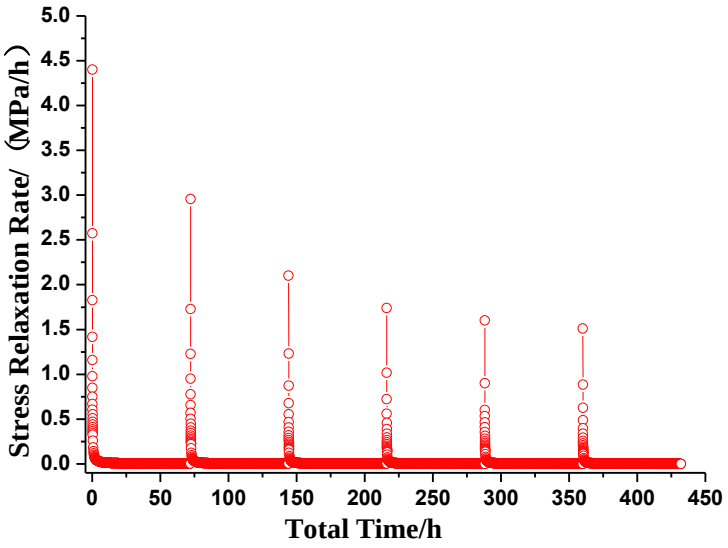

Figure 4.11 Stress Relaxation Rate Curve of Sample 4-4

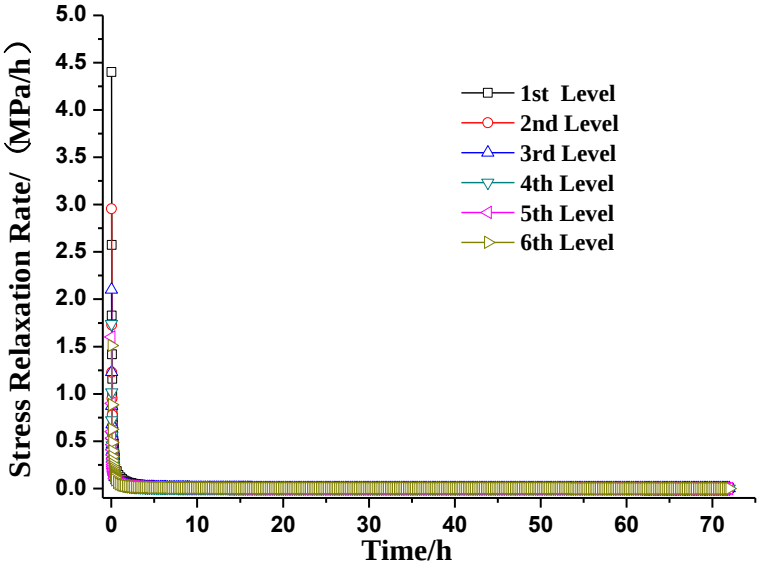

***a*. Full View**

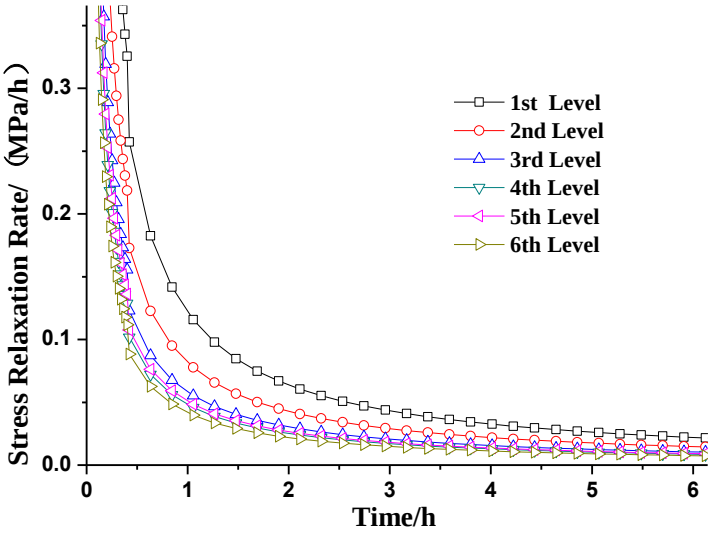

***b*. Partial Enlarged View**

Figure 4.12 Stress relaxation rate curve of sample 4-4 in same time scale

Seen from Figure 4.11, the initial stress relaxation rate gradually decays to a steady value with the increase times of cycle. The initial stress relaxation rate of 1st level is 4.4MPa/h, and the values are1.74, 1.60 and 1.51 respectively in 4th level, 5th level and 6th level. The initial stress relaxation rates of the other samples are shown in Table 4.3.

Table 4.3 Initial Stress Relaxation Rate

Sample NO.	Levels					
	1st	2nd	3rd	4th	5th	6th
4-4	4.40	2.96	2.10	1.74	1.60	1.51
4-8	9.19	7.55	5.58	3.94	3.28	3.28
4-12	11.98	7.65	5.99	4.33	3.33	3.12
6-4	4.06	2.81	1.87	1.56	1.25	1.25
6-8	10.08	7.89	5.99	4.20	3.66	3.54
6-12	11.65	7.99	4.66	3.99	2.99	2.00
10-4	6.32	4.66	2.99	2.00	2.00	2.00
10-8	10.31	8.32	7.32	5.32	5.32	3.33
10-12	13.31	9.32	7.65	5.66	3.66	2.66

Unit：MPa/h

Seen from Figure 4.12, in the decelerating stress relaxation stage, compare the different levels, the variation of stress relaxation rate is larger at the beginning of cyclic loading，and gradually tend to be smaller with the increasing of cyclic times. The curves show that the stress relaxation rate of 1st and 2nd level has a greater discrepancy and the subsequent curves are becoming overlap with the increasing of cyclic times.

Investigate its reason, the indirect form of stress relaxation are crack expansion and viscous deformation. Under isostress cyclic loading, when into the next level，the loading force do work again on the sample and destroy the original stress balance, then a new crack expansion and viscous deformation will adjust to reach a new stress balance. Because of the cyclic stress value remains constant, the main stress relaxation form is gradually transfer from predominantly crack expansion to viscous deformation with the increasing times of cycle. Since viscosity coefficient of the same material is a stable value, the stress relaxation curves tend to overlap eventually. Meanwhile, with the increasing times of the cycle, the Anti-Relaxation Capacity（ARC）γ and stress relaxation rate will be more greatly depend on the viscosity coefficient of material and finally tend to be stable.

4.4.3 Suppressed behaviors in normal direction under ICL

Since the normal stress is hold as constant during relaxation tests, an adjustment of the displacement along the normal direction is inevitable. Figure 4.13 shows the corresponding displacement in the normal direction during the entire relaxation history. For brief, only the result of sample 4-4 is taken for interpretation. It can be also seen that the most obvious change of the normal displacement occurs at the 1st level of shear loading whose increment of normal displacement is 0.184 mm. While with the increasing of loading cycles, the increment of normal displacement becomes smaller and smaller at the latter loading levels, with a increment of 0.0155, 0.009, 0.0065, 0.009 and 0.0045 mm in the 2nd, 3rd, 4th, 5th, and 6th cycle, respectively.

As for the 1st loading level, the normal displacement is observed increases monotonically with the elapsing time. The displacement increases at a rapid rate at the beginning, and then slows down over time, which corresponds well with the relaxation behaviors in the rapid and decelerating relaxation stages respectively. However, with the increase of loading cycles, this tendency becomes

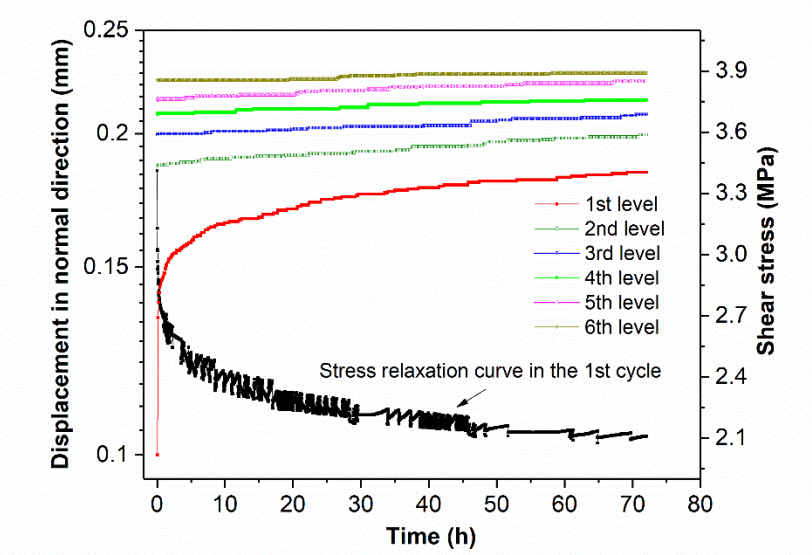

a. Displacement in normal direction during cyclic relaxation

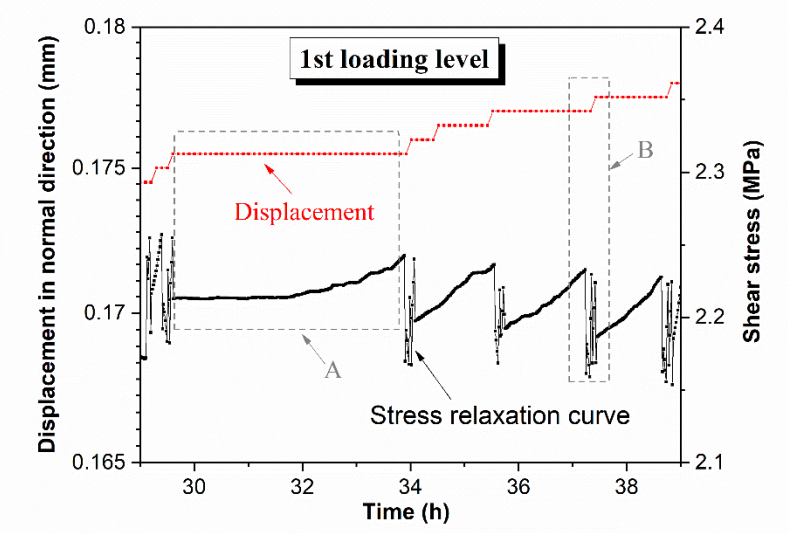

b. Partial enlarged view of Figure 4-13a

Figure 4.13 Displacement in normal direction during cyclic relaxation（sample 4-4）

inapparent. These tendencies are closely related to the stress relaxation properties of discontinuity and will be explained as follow.

In the rapid relaxation stage of the 1st loading level, in addition to viscous deformation, some asperities that having been or being failed (i.e. reaching the peak stress or post-peak regime of the asperities) in the previous shearing stage continuous to be crushed and/or broke even though no additional shearing stress is added. Such failures would inevitably cause the stress to release spontaneously. Due to such kind of asperity crushing and/or breakage, the contact connected by the

asperity at that moment is lost and the bearing capacity of the discontinuity decreases transiently. While the loading system has to adjust (reloading) itself correspondingly in order to maintain a constant normal stress, and consequently manifesting as compressed displacements along the normal direction. Evidence could be observed from Figure 4.13b, where part of the normal displacement-time curve and its corresponding shear relaxation-time relations was enlarged. It can be observed that when the normal displacement is relatively stable (region A that marked by the dash line rectangular in Figure 4.13b), the shear stress is relatively constant and even increase gradually due to the well-established contact of asperities and development of bearing capacity. While a sudden increase at the normal displacement (region B at Figure 4.13b) is always followed by a transient reduction at the shear stress, inducing by asperity crushing and/or breakage.

Returning back to Figure 4.13a, at the first ten minutes' relaxation, it is observed that the compressed displacement along the normal direction during this duration (i.e. the rapid relaxation stage) in the 1st loading level is up to 0.13 mm, which accounts for 70.6% of the total displacement in the 1st loading level. Correspondingly, the shear stress in this duration (i.e. the first 10 minutes) is relaxed by 0.54 MPa at a rapid rate, accounting for 41.2% of the total relaxed stress in this loading level. It seems that the behavior of asperity crushing and/or breakage plays a more predominant role in facilitating stress relaxation during the rapid relaxation stage. Thereafter, with the time elapsing and the decreasing of stress level in shear direction, asperity activities gradually decrease and bear a smaller contribution to the stress relaxation. Meanwhile, the viscous deformation, which depends on the viscous coefficient and the stress level of the material, occurs during the entire relaxation history and continuously contributes to release stress at a gradually decreasing manner with time. With these, the discontinuity enters into the decelerating relaxation stage, manifesting as the gradually decreased compression displacement as well as the decreased relaxation rate. With the completion of asperity crushing and/or breakage, stress releases into a certain low level, which meanwhile could provoke no more viscous deformation. As a result, relaxation behavior will be ceased and the discontinuity enters into the stable stress stage, where the shear stress as well as the compressed displacement are levelling off.

Based on the above results, it might be stated that the total stress relaxation, especially in the rapid relaxation stage, seems to be exclusively contributed by the asperity crushing/breakage behavior. With the increase of loading cycles, since the initial loading stress in each cycle is equal,

asperity crushing and/or breakage gradually dwindle especially at the initial stage of stress relaxation under Kasai effect. While the viscous deformation bears a relatively smaller and relatively stable contribution to the total stress relaxation during the entire relaxation history.

4.5 Constitutive study of stress relaxation properties

Most of rheological constitutive models are built based on creep study, previous study have shown that stress relaxation behavior could be equivalent to creep behavior. Laboratory tests are commonly employed to investigate the time-dependent behavior of discontinuities. In this chapter, Based on relaxation mechanism, a relaxation model was first developed by modifying Burgers model. The parameters for both Burgers model and modified Burgers model（K-M） were determined from each relaxation test.

4.5.1 BURGERS model

Relaxation mechanism analyzed in section 3 is divided into visco-elastic deformation and crack extension. Visco-elastic property is widely described by Kelvin model, and crack extension is always described by a viscous component. Both mechanism induce the development of time-dependent deformation, an elastic component should be in series to stabilize the boundary condition of relaxation. Burgers model could be assembled by these three components, as shown in Figure 4.14.

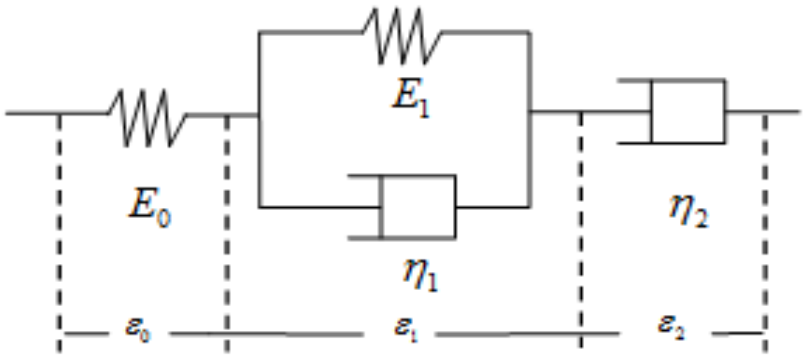

Figure 4.14 Burgers model

$$\sigma = \sigma_0 = \sigma_1 = \sigma_2 \tag{4.7}$$

$$\varepsilon = \varepsilon_0 + \varepsilon_1 + \varepsilon_2 \tag{4.8}$$

In which, Hooke model is displayed as follow:

$$\varepsilon_0 = \sigma_0 / E_0 \tag{4.9}$$

Kelvin model is a parallel combination of a viscous element and an elastic element, and strains generated by these two elements are equivalent. The sum of their corresponding stresses component is displayed in Eq.4.10.

$$\sigma = \sigma_1 = \sigma_{1v} + \sigma_{1h} = \eta_1 \dot{\varepsilon}_1 + E_1 \varepsilon_1 \tag{4.10}$$

Viscous element follows Eq.4.11.

$$\sigma_2 = \eta_2 \dot{\varepsilon}_2 \tag{4.11}$$

Hence, the constitutive equation of Burgers model could be described by Eq.4.12.

$$\sigma + (\frac{\eta_2}{E_0} + \frac{\eta_1 + \eta_2}{E_1})\dot{\sigma} + \frac{\eta_1 \eta_2}{E_0 E_1}\ddot{\sigma} = \eta_2 \dot{\varepsilon} + \frac{\eta_1 \eta_2}{E_1}\ddot{\varepsilon} \tag{4.12}$$

By giving the initial conditions, one can solve the above differential equations to obtain the mathematical expressions of creep constitutive and stress relaxation constitutive. Where, creep constitutive could be displayed by Eq.4.13.

$$\varepsilon = \frac{\sigma}{E_0} + \frac{1 - \exp(-\frac{E_1}{\eta_1}t)}{E_1}\sigma + \frac{t}{\eta_2}\sigma \tag{4.13}$$

Stress relaxation constitutive is relatively complex, which could be displayed by Eq. 4.14.

$$\sigma = \frac{q_2 \varepsilon_0}{p_2(a_1 - a_2)}\left[(\frac{q_1}{q_2} - a_2)\exp(-a_2 t) - (\frac{q_1}{q_2} - a_1)\exp(-a_1 t)\right] \tag{4.14}$$

In which, $a_1 = \frac{p_1 + \sqrt{p_1^2 - 4p_2}}{2p_2}$, $a_2 = \frac{p_1 - \sqrt{p_1^2 - 4p_2}}{2p_2}$, $p_1 = (\frac{\eta_2}{E_0} + \frac{\eta_2}{E_1} + \frac{\eta_1}{E_1})$,

$p_2 = \frac{\eta_2 \eta_1}{E_0 E_1}$, $q_1 = \eta_2$, $q_2 = \frac{\eta_2 \eta_1}{E_1}$.

Burgers model has four parameters, i.e. E_0, E_1, η_1 and η_2. Among them, E_0 refers to elasticity modulus, which could be determined by the slope of the linear part in stress-strain curve during each loading level. Other parameters could be optically estimated by software 1stOpt.Typical fitting curves and estimated parameters could be obtained by means of Burger model simulation, as shown in Figure 4.15 and Table 4.4, respectively.

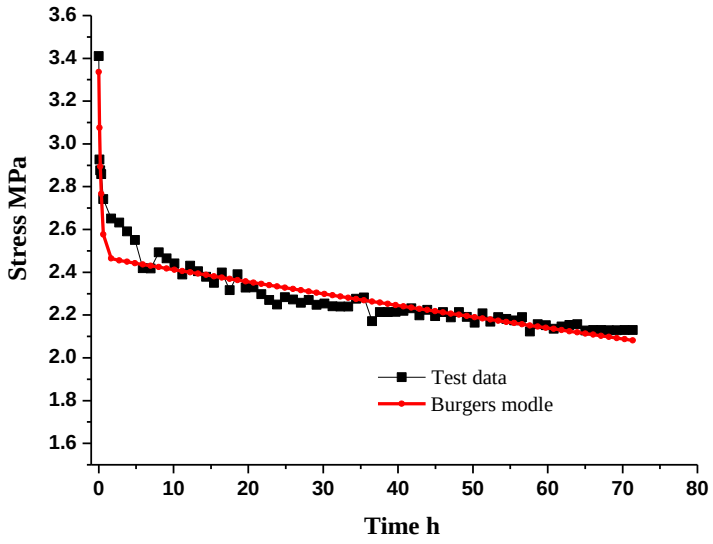

a. 1st level of 4-4

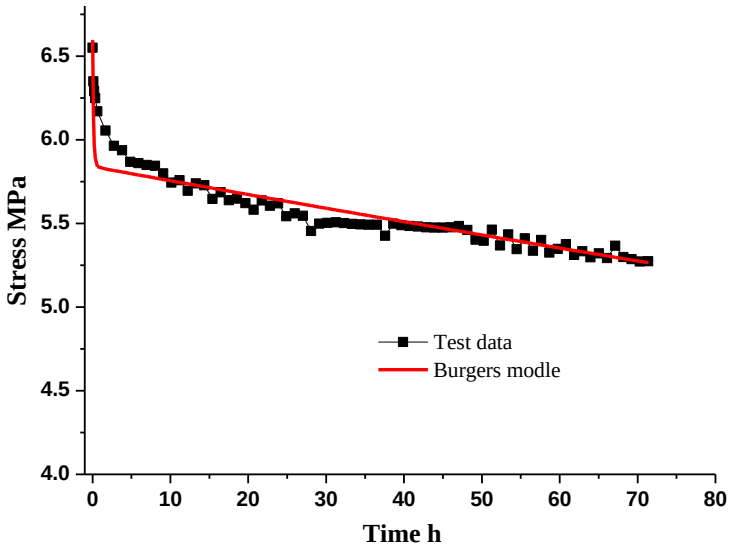

b.3rd level of 4-8

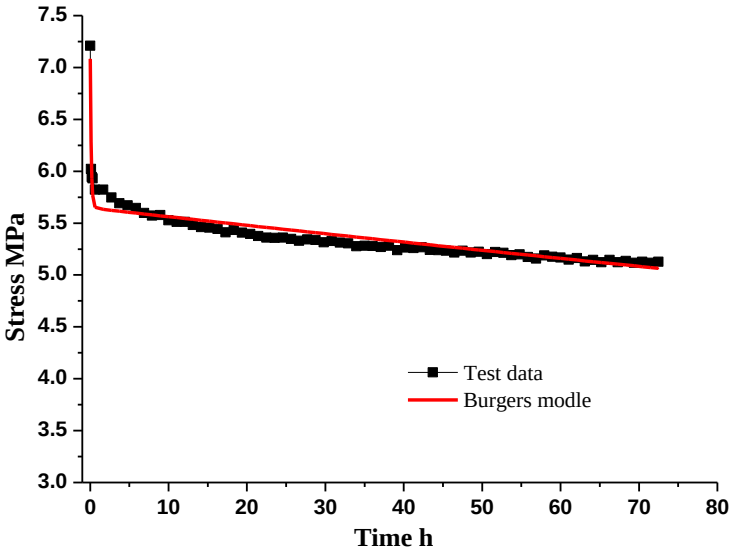

c. 1st level of 6-8

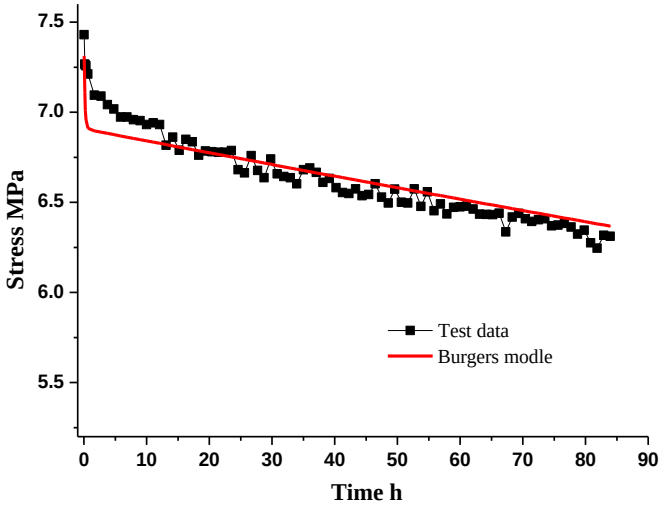

d.5th level of 10-8

Figure 4.15 Fitting curves using Burgers modle

Table 4.4 Burgers parameters

Sample	Levels	E_0/GPa	E_1/GPa	η_1/(GPa.h)	η_2 /(GPa.h)	R
4-4	1	8.834	23.303	9.529	2662.04	0.944
	2	7.939	55.59	17.461	5161.538	0.929
	3	7.569	82.439	24.48	7684.623	0.925
	4	7.349	109.052	31.109	9413.372	0.919
	5	7.209	136.818	38.558	8846.837	0.904
	6	7.089	144.512	40.166	10772.794	0.910
4-8	1	11.644	26.643	7.459	2599.359	0.923
	2	10.791	51.146	8.72	4138.056	0.903
	3	10.455	85.959	11.591	6425.292	0.893
	4	10.25	133.07	16.146	9834.553	0.888
	5	10.139	191.754	19.242	12182.769	0.878
	6	10.031	195.942	19.023	12072.434	0.877
4-12	1	16.928	59.018	8.735	6146.367	0.887
	2	15.324	132.187	12.343	11933.391	0.867
	3	14.653	233.505	13.658	16080.166	0.850
	4	14.265	300.272	18.989	22665.509	0.853
	5	14.017	380.029	24.438	29797.559	0.853
	6	13.837	377.735	36.655	43097.706	0.871
6--4	1	7.591	21.224	7.68	2816.8	0.942
	2	6.977	49.294	14.358	5220.331	0.928
	3	6.726	87.94	23.735	8535.164	0.918
	4	6.585	126.32	32.68	10412.367	0.907
	5	6.505	133.317	35.031	13180.925	0.917
	6	6.427	155.917	40.034	13051.169	0.907
6-8	1	10.077	36.394	5.956	5263.879	0.927
	2	8.984	134.851	21.199	9859.735	0.877
	3	8.453	213.921	33.39	14802.023	0.871
	4	8.165	357.534	53.266	30088.877	0.88
	5	8.007	371.678	53.318	39994.336	0.894
	6	7.875	585.783	83.663	59933.393	0.891
6-12	1	22.925	80.799	9.194	9470.017	0.889
	2	20.441	170.318	19.203	16703.302	0.865
	3	19.399	250.772	25.859	30216.765	0.872
	4	18.801	330.819	35.269	35581.209	0.864
	5	18.379	376.812	37.761	47555.738	0.872
	6	18.098	412.119	37.133	71940.591	0.892
10-4	1	7.866	20.648	7.024	2441.66	0.929
	2	7.191	43.764	8.932	4295.187	0.912

	3	6.862	69.755	13.238	7372.483	0.910
	4	6.672	102.332	19.224	11637.021	0.911
	5	6.557	126.863	19.375	11544.77	0.899
	6	6.482	117.074	19.009	11381.37	0.903
10-8	1	8.882	31.025	5.418	2900.595	0.895
	2	7.748	56.436	7.444	3820.833	0.870
	3	7.242	52.528	8.566	4415.824	0.877
	4	6.908	73.325	11.556	6403.763	0.874
	5	6.703	88.651	14.485	6432.933	0.865
	6	6.564	123.401	19.005	10706.931	0.869
10-12	1	17.604	58.079	6.762	6218.673	0.884
	2	15.63	126.978	14.889	11034.823	0.858
	3	14.774	210.353	26.719	14245.998	0.847
	4	14.257	349.436	44.539	20431.898	0.853
	5	13.918	499.123	62.759	31756.858	0.849
	6	13.697	554.518	66.225	42809.879	0.846

From Figure 4.15 and Table 4.4, it could be seen that:

1) Burgers model could be used to describe stress relaxation property. Correlation coefficients for each above mentioned parameters, i.e. E_0, E_1, η_1 and η_2, are within 0.84 ~ 0.94.

2) As for the elasticity modulus E_0, it could be seen from Tab.4.9 that for the same sample, E_0 tends to gradually reduce with the increase of cyclic loading number, while its variation is within a small range. The main reason is that in ICLM, cyclic stress is remaining constant, while the strain level is gradually increasing. For the same discontinuity, E_0 tends to gradually increase with the increase of normal stress. The main reason is that with the increase of normal stress, the influence of discontinuity on mechanical properties of rock mass is gradually weakened, and the rigidity along the shear direction is gradually increased.

3) As for the viscoelastic modulus of creep relaxation E_1, it could be seen from Table 4.3 that for the same sample, E_1 tends to gradually increase with the increase of cyclic loading number. For the same discontinuity, E_1 tends to gradually increase with the increase of normal stress. The main reason is considered to be that during the process of loading, the gradually increased strain level results in the enhancement of discontinuity stiffness. The larger the E_1 is, the greater the corresponding stress relaxation rate will be during deceleration stage of stress relaxation.

4) As for the viscosity coefficient of viscoelasticity deformation η_1, which has a significant impact on deceleration stress relaxation stage, it could be seen from Tab.4.9 that for the same sample,

η_1 tends to gradually increase with the increase of cyclic loading number. It suggests that with the increase of cyclic loading number, the relaxation rate of discontinuity is gradually reducing during attenuation stage of stress relaxation.

5) As for the viscosity coefficient of crack relaxation η_2, which has a significant impact on deceleration stress relaxation stage, it also could be seen that for the same sample, η_2 tends to gradually increase with the increase of cyclic loading number. Analogously, with the increase of cyclic loading number, the relaxation rate of discontinuity is gradually reducing during attenuation stage of stress relaxation. Besides, it is seen that η_2 seems to asymptotically constant until approaching the last 2~3 loading level, demonstrating that with the increase of cyclic loading, stress relaxation rates also tend to stabilize.

4.5.2 K-M model

Since the parameters in burgers model is linear model, Stress will completely attenuate to 0, which cannot fully reflect the practice. In relative larger stress, Burgers model can't describe the stress relaxation caused by crack extension. In the process of stress relaxation, no matter the stress relaxation caused by creep or crack extension, it is necessary to compensate for the displacement with a rebound deformation. In this section, we suggest a nonlinear K-M model to describe stress relaxation properties as shown in figure 4-16. In the K-M model, K is used to describe stress relaxation caused by creep and M is used to describe stress relaxation caused by crack extension.

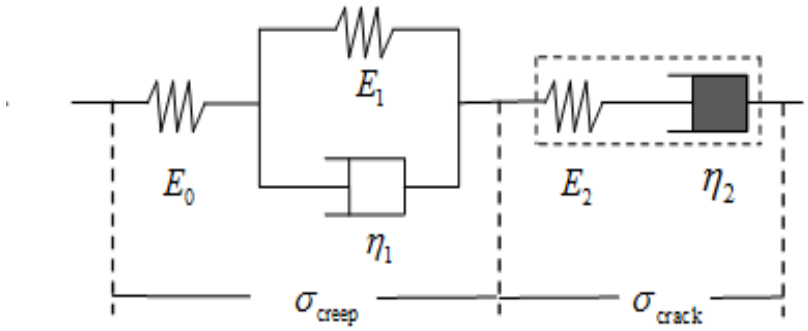

Figure 4.16 K-M model

We would like to note that, no matter the stress relaxation induced by creep or crack extension, the modules of rebound deformation is equal, i.e. $E_0 = E_2$.

In K-M model, stress relaxation is described by K model and M model satisfying the following Eqs. 4.15 and 4.16.

$$\sigma = (E_0 - \frac{E_0 E_1}{E_0 + E_1}) \exp(-\frac{E_0 + E_1}{\eta_1} t)\varepsilon_0 + \frac{E_0 E_1}{E_0 + E_1}\varepsilon_0 \qquad (4.15)$$

$$\sigma(t) = E_2 \exp(-\frac{E_2}{\eta_2} t^n)\varepsilon_0 \qquad (4.16)$$

In which, E_2 is rebound modulus, t is time, n is adjustment coefficient，ε_0 is strain condition. From Eqs.n 4.15 and 4.16, stress relaxation constitutive equation can be obtained as follow.

$$\sigma = (E_0 - \frac{E_0 E_1}{E_0 + E_1}) \exp(-\frac{E_0 + E_1}{\eta_1} t)\varepsilon_0 + \frac{E_0 E_1}{E_0 + E_1}\varepsilon_0 + E_2 \exp(-\frac{E_2}{\eta_2} t^n)\varepsilon_0 \qquad (4.17)$$

Where $E_0 = E_2$.

Typical fitting curves and estimated parameters could be obtained by means of K-M model simulation, as shown in Figure 4.17 and Table 4.4, respectively.

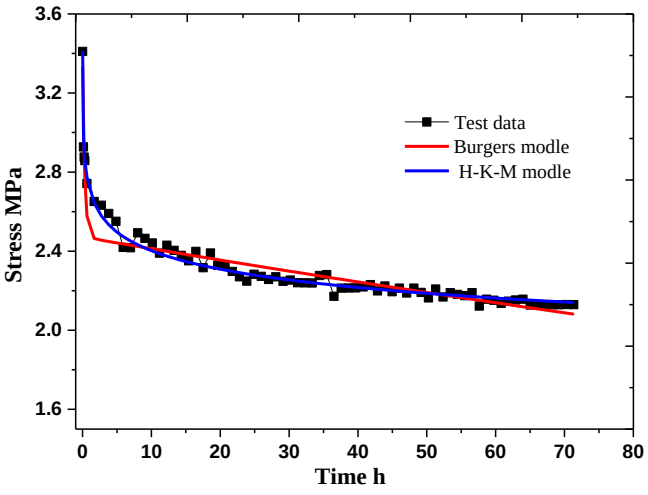

a. 1st level of 4-4

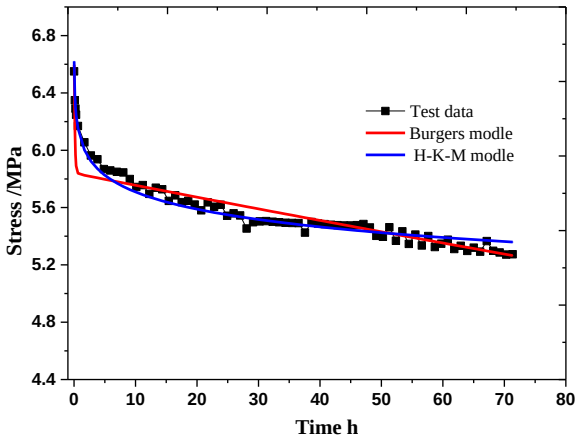

b. 3rd level of 4-8

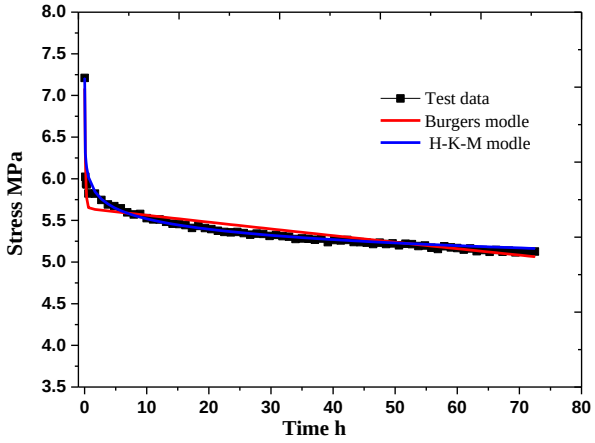

c. 1st level of 6-8

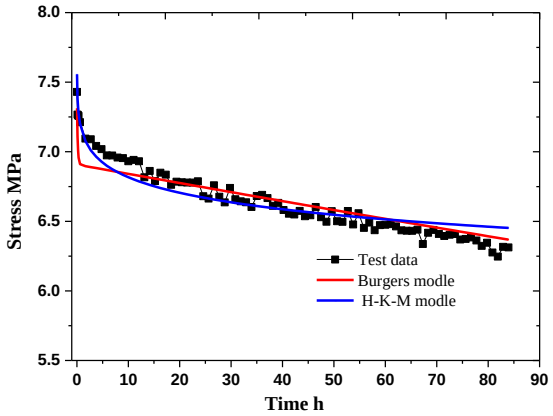

d.5th level of 10-8

Figure 4-17 Fitting curves using Burgers model and K-M model

Table 4-5 K-M parameters

Samples	levels	E_0 & E_2 /GPa	E_1 /GPa	η_1 /(GPa.h)	η_2 /(GPa.h)	n	R
4-4	1	8.834197	5.034075	0.12466	10.554141	0.108364	0.991
	2	7.939464	4.025957	2.68E-15	14.733357	0.078572	0.997
	3	7.569367	7.422399	0.005931	21.684649	0.069477	0.989
	4	7.349138	7.372196	0.00298	34.001517	0.078231	0.986
	5	7.209302	7.675362	0.001848	29.843600	0.768630	0.988
	6	7.089397	7.699982	0.004733	27.558306	0.900854	0.973
4-8	1	11.644444	5.573146	0.173001	14.157458	0.118172	0.998
	2	10.790774	7.65174	0.000143	14.030133	0.096399	0.992
	3	10.454908	8.905287	0.007396	24.890555	0.085237	0.983
	4	10.250391	8.306968	0.005604	39.357665	0.080315	0.985
	5	10.139319	9.165122	0.00619	71.066389	0.101086	0.990
	6	10.030628	10.057412	0.000861	75.847680	0.106299	0.969
4-12	1	16.928447	11.441279	0.191027	20.250629	0.102199	0.998
	2	15.323855	16.418272	2.00E-16	34.001752	0.075580	0.996
	3	14.652568	12.911219	2.60E-12	90.959530	0.108077	0.989
	4	14.264706	14.604702	2.53E-13	104.856120	0.092655	0.993
	5	14.017341	15.28658	2.19E-12	126.330260	0.085897	0.987
	6	13.837375	17.180106	5.32E-12	96.801288	0.071171	0.990
6-4	1	7.591093	4.526011	0.125856	8.910016	0.095271	0.998
	2	6.976744	5.340282	3.17E-15	9.611869	0.066360	0.997
	3	6.726457	5.892161	1.55E-06	22.005185	0.064558	0.990
	4	6.584723	6.851449	7.49E-15	42.894726	0.085892	0.993
	5	6.504770	7.145974	1.24E-13	33.191259	0.059558	0.989
	6	6.426735	7.649011	7.62E-14	52.792037	0.083489	0.991
6-8	1	10.076869	7.143804	0.182949	11.251040	0.068226	0.998
	2	8.984424	8.643045	8.11E-14	41.861489	0.083273	0.992
	3	8.452521	9.788221	8.37E-15	74.197298	0.090655	0.988
	4	8.165345	10.625846	0.001836	90.871697	0.059704	0.994
	5	8.006663	12.228425	0.005313	30.275047	0.019856	0.997
	6	7.875478	11.804089	1.95E-14	73.437851	0.027293	0.987
6-12	1	22.924731	15.664286	0.316916	26.810648	0.090184	0.998
	2	20.441035	11.87814	5.18E-15	35.283911	0.065630	0.996
	3	19.399454	24.63828	0.113254	20.597204	0.035759	0.984
	4	18.800705	7.078795	5.99E-14	50.747819	0.041476	0.983
	5	18.379310	25.932801	0.123422	19.095172	0.022965	0.98
	6	18.098472	26.034413	0.254492	18.564438	0.015303	0.981
10-4	1	7.865749	4.392596	0.060316	9.640266	0.114814	0.997
	2	7.191188	6.977793	0.060478	8.316005	0.084031	0.993
	3	6.861862	8.652462	0.002865	7.253781	0.053856	0.991

	4	6.671533	8.947622	0.04522	7.082100	0.035755	0.992
	5	6.556671	9.202297	0.045789	6.964984	0.035729	0.988
	6	6.482270	8.99831	0.044943	6.880411	0.035760	0.988
10-8	1	8.882247	6.027164	0.056847	10.888077	0.115328	0.991
	2	7.747654	8.677005	7.89E-15	14.354032	0.098090	0.992
	3	7.241715	9.623789	1.07E-14	17.388528	0.095774	0.991
	4	6.908415	10.85435	3.13E-11	22.524037	0.083596	0.995
	5	6.702751	10.990712	4.08E-13	36.666431	0.112779	0.990
	6	6.563604	11.961635	1.23E-14	38.454554	0.079919	0.984
10-12	1	17.603912	11.381316	0.217744	21.064175	0.102021	0.991
	2	15.629522	16.075244	3.76E-14	36.263745	0.083559	0.982
	3	14.774282	18.974751	0.003303	88.587078	0.117967	0.984
	4	14.257426	19.635911	4.00E-14	26.377508	0.047084	0.989
	5	13.917526	20.405497	5.70E-14	311.771849	0.154147	0.989
	6	13.696893	22.663449	1.06E-10	221.082061	0.099485	0.979

From Figure 4.17 and Table 4.5, we can see that:

1) K-M model can better characterize stress relaxation mechanism and stress relaxation test data as well, and their fitting correlation coefficients are over 0.980.

2) Parameters E_0 and E_2 refer to rebound elastic modulus of stress relaxation, which have impact on the stress level in both initial and rapid stress relaxation stages. It can be seen from Tab.4.11 that for the same sample, with the increase of cyclic loading number, E_0 and E_2 tend to gradually decrease. The initial stress level remains no change, while the sample's elasticity is gradually weakening, for the reason that as the increase of cyclic loading number. For the same discontinuity, with the increase of normal stress, E_0 and E_2 tend to gradually increase. This is because the increase of normal stress weakens the influence of discontinuity on sample's mechanical property.

3) Parameter E_1 denotes the viscoelastic modulus of stress relaxation caused by viscoelasticity creep deformation. It could be seen from Table 4.5 that for the same sample, with the increase of cyclic loading number, E_1 tends to fluctuates within a certain range. The main reason is considered to be that during the process of stress relaxation, stress varies within a small range and the stress relaxation effect caused by viscoelastic deformation is relatively small, hence viscoelasticity creep relaxation is relatively stable for each loading level. For the same discontinuity, E_1 tends to gradually increase with the increase of normal stress.

4) η_1 represents the viscosity coefficient of viscoelasticity creep deformation, whose impact

mainly acts in the deceleration stress relaxation stage. It could be seen from Table 4.5 that for the same sample, with the increase of cyclic loading number, η_1 is essentially small and varies within a small range. It suggests that the difference of viscoelasticity creep relaxation in each loading level is relatively small.

5) η_2 is the viscosity coefficient of non-linear Maxwell element. From Table 4.5, it also can be seen that for the same sample, η_2 tends to gradually increase with the increase of cyclic loading number and finally η_2 seems to asymptotically stabilize to a constant. Analogously, for the same discontinuity, with the increase of normal stress, η_2 *also* tends to gradually increase, which is consistent with the characteristics of crack relaxation.

6) Parameter *n* mainly has an impact on the stress relaxation rate in the second half of the stress relaxation curves. It could be seen from Table 4.5 that for the same sample, *n* is initially large, while with the increase of cyclic loading number, it tends to gradually decrease. Finally, n become stable until reaching the fifth or sixth level of stress relaxation test, which is consistent with the stress relaxation rate during the last half of the stress relaxation curve.

Base on the above analysis, it is obvious that K-M model not only can better simulate the test data, but also can satisfactorily characterize the test data from the prospective of mechanism.

4.6 Summary

In this chapter, isostress Cyclic Loading Method (ICLM) is proposed to study shear stress characteristic, which can reduce the influence of instantaneous mechanical characteristics with the increasing times of cycle and reflect the viscous properties of rock material more accurately. According to the test, stress relaxation can be divided into three stages: rapid stress relaxation stage, decelerating stress relaxation stage and stable stress stage. Stress relaxation appears in two indirect forms: local failure and viscous deformation. The kinematic interactions of discontinuities in terms of asperity crushing and/or breakage and viscous deformation are stated governing the fundamental relaxation behaviors of discontinuities subjected to shear relaxation. Stress relaxation is dominantly contributed by asperity crushing and/or breakage in rapid relaxation stage, which gradually transferred to be contributed by viscous deformation in decelerating relaxation stage. From the perspective of energy, there is new energy jointed in the process of creep, while no energy

is jointed in the process of stress relaxation. This is the reason why in the process of test creep can be developed to failure and stress relaxation often tends to be stable.

The concept of Anti-Relaxation Capacity (ARC） γ which is equal to the ratio of residual stress value and the initial load stress is proposed in this paper, which can represent the ability of anti-relaxation. With the increasing times of the cycle, the Anti-Relaxation Capacity（ARC）γ and stress relaxation rate will be more greatly depend on the viscosity coefficient of material and finally tend to be a stable value.

Burgers model was adopted to describe stress relaxation properties and the parameters of burgers model were determined, which shown that burgers model could be used in stress relaxation properties, meanwhile stress will relaxed to 0 and linear properties of burgers model cannot reflect stress relaxation well. A new nonlinear model (K-M model) was proposed in this study, which could describe stress relaxation well, and the parameters in K-M model were studied.

Chapter 5 Long-term strength of discontinuities

Long-term strength behaviors of discontinuities contained in rock mass is crucial for assessing the long-term stability of rock engineering. Stress relaxation property and its relation to long-term strength have been rarely investigated. In the present study, multiple of stress relaxation tests were performed on artificial samples under biaxial shear conditions using Isostress Cyclic Loading Method (ICLM), a novel method is put forward to determine long-term strength of discontinuities. Meanwhile, stepwise shear creep tests at constant normal stress were also conducted, as mentioned in chapter 3 the evolution laws of creep rate under variant stress levels and isochronous stress-strain curves are analyzed and these laws are utilized to determine the long-term strengths of discontinuities. Long-term strengths from aforementioned methods show that the long-term strength determined by the creep rate law is within a range and its accuracy largely depends on the steps of loading stresses used in the tests, and by isochronous stress-strain curves, long term strength is regarded as equivalent to the yielding strength after taking the time-effect into account, this result, however, is suspected to be conservative. The proposed method based on stress relaxation considering the influence of creep could obtain the long-term strength of rock mass more accurate.

5.1 Determination of long-term strength based on relaxation test

5.1.1 Potential correlation between relaxation behaviors and long-term strength

Long-term strength is usually defined as a stress threshold that could be observed during the creep process of rock mass. Bowden (1984) reported that the creep properties of rock discontinuity were rather similar to that of intact rock. When the applied stress is beyond the long-term strength, the rock mass fails in a limited time even if the loading stress remains constant. In this limited time, viscous deformation experiences three stages, i.e. transient creep stage, steady state creep stage and

accelerating creep stage. While when the applied stress is below the long-term strength, the viscous deformation could be stable with elapsing time, i.e. when the stress is equal to or lower than the long-term strength, viscous deformation is limited, and this limited deformation occurs only in the transient creep stage, as illustrated in Figure5-1. Accordingly, the long-term strength could be determined within a range by comparing the creep curves under different stresses (Zhang et al., 2016). It is indicated that the evolution of viscous deformation for a given material is impacted by the applied stress level whether is larger or lower than its long-term strength.

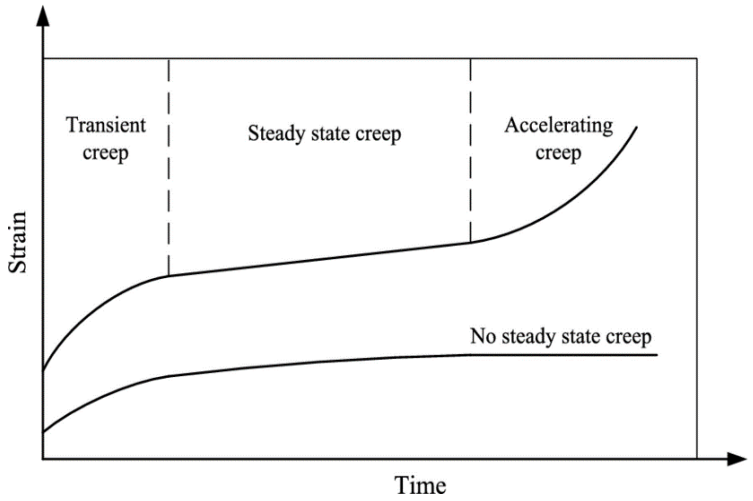

Figure 5.1 Illustration of typical creep curves (Jiang et al. 2013)

The difference between creep and stress relaxation is that the stress conditions in creep are constant, while the stress conditions in stress relaxation are decreasing. In the process of stress relaxation, though the total deformation is fixed, viscous deformation depended on the applied stress level and the viscous property of tested material will also develop at a decreasing manner over time. Without considering the influence of asperity crushing and/or breakage on stress relaxation, the viscous behavior of rock mass would be the dominant factor that governing the behavior of stress relaxation. Limited viscous deformation represents limited stress relaxation and no further development of viscous deformation represents the completion of stress relaxation behaviors. Assuming that the evolution of viscous deformation during the stress relaxation process is analogous to that in creep. That is, when the stress is beyond the long-term strength, the viscous deformation will also experience three similar stages, identically termed as transient stage, steady stage and accelerating stage, respectively. While when the stress is lower than the long-term strength,

viscous deformation is limited and only occurs in the transient stage. It is conceivable that the shear stress at a high level would be relaxed by viscous deformation with time and ultimately be stable at a residual stress which is equal or lower than long-term strength. If viscous deformation during the time that stress relaxed from a relatively large value to the long-term strength has passed through the transient stage, the stress is expected to be released and terminated at the long-term strength.

5.1.2 Indication of isostress cyclic loading procedure

According to the above discussion, in order to eliminate the influence of asperity crushing and/or breakage during relaxation, iso-stress cyclic loading (ICL) method considering the Kaiser effect (Tensi 2004) is proposed to conduct stress relaxation tests, as mentioned in chapter 4. Kaiser effect is firstly discovered by Kaiser in metals, and then confirmed in rocks *(Goodman 1963)*. It has been experimentally demonstrated that acoustic waves produced in the material under cyclic loading/unloading has a specific feature whereby the acoustic emission activity is zero or close to background level when the stress magnitude of the cyclic load remains below the previously attained maximum stress. The generation of acoustic waves is believed to be linked with the crack (breakage) and/or crush activities of rock mass (Filimonov et al. 2001; Hazzard and Young 2003; Li and Nordlund 1993; Tuncay and Ulusay 2008). Figure 5.2 illustrates the process of the ICL method (same with Figure 4.1). In stress relaxation process,

$$\sigma_0 = \sigma_r + \sigma_s \tag{5.1}$$

Where, σ_0 is the initially applied stress, σ_r is the relaxed stress (decreased stress from the initially applied stress), and σ_s is the residual stress. The first step is applying the predetermined loading stress that is larger than the long-term strength on the sample and conducting the 1st level of stress relaxation test. The residual stress eventually decreases to a stable value over time, which means the completion of the 1st level. The second step is reloading the stress up to the initially applied stress on the basis of the last residual stress. That is, the added stress in the 2nd level is equal to the relaxed stress in the 1st level. By this analogy, the residual stress of each level is recorded as σ_{r1}, σ_{r2}, σ_{r3}, … … σ_{rn}, σ_{rn+1}. *When* $\sigma_{rn} = \sigma_{rn+1}$, the test could be terminated.

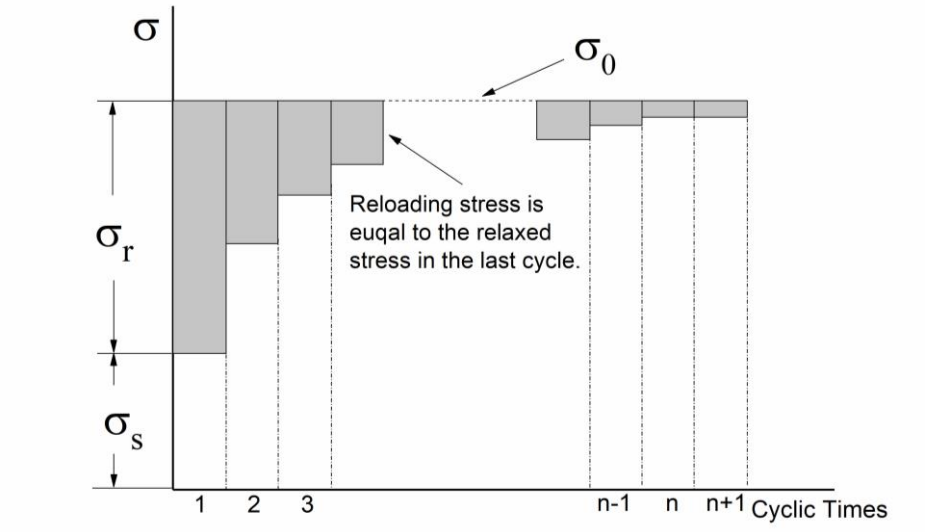

Figure 5.2 Procedure of iso-stress cyclic loading (ICL) method

Stress relaxation is stated to be induced by viscous deformation and asperities crushing and/or breakage. In each cycle using ICL method, the initial stress in the last cycle could be regarded as the previous maximum stress loading on the discontinuity. Asperity crushing and/or breakage during relaxation is expected to be dwindled under Kaiser effect, if so the dominant inducer of stress relaxation will gradually transfer from asperities crushing and/or breakage to viscous deformation. Since the viscosity coefficient of a given material is relatively stable, the stress relaxation behaviors controlled by viscous deformation will tend to be consistent with the increased loading cycles, and if the transient stage of viscous deformation in relaxation test has been completed, the ultimate residual stress is expected to be the long-term strength. More interpretations will be present in section 5.

5.1.3 Long-term strength obtained from stress relaxation method

In the stress relaxation test, rapid stress relaxation stage in which the concentrated stress accumulated in the process of loading is quickly released by crack expansion is more a response to instantaneous mechanical characteristics. Then the test enters into decelerating stress relaxation stage in which the stress relaxation form changes from crack extension to viscous deformation. At this point, the corresponding residual stress value can be divided into two cases: smaller than long-term strength and greater than long-term strength. Combine with studying results of creep,

when residual stress is smaller than the long-term strength, over time the material will only cause attenuation creep and eventually into the stable creep stage that the creep rate is 0. When residual stress is greater than long-term strength, over time material will enter into the stable creep stage that the creep rate is not 0. For keeping the deformation value as a constant, the stress have to be relaxed to the value that only can cause the creep rate equal to 0 in stable creep stage. Viz. the termination condition of the stress relaxation test is stress value less than or equal to the long-term strength. By means of isostress cyclic loading, reduce the influence of crack extension in stress relaxation, and to ensure that the relaxation stress mostly depend on vicious deformation, inevitably the residual stress value would gradually tend to be long-term strength.

Based on the analysis, through Shear stress relaxation test that use samples with artificial joint surface selected the 4th, 6th and 10th discontinuity lines from Barton's ten standard lines, long-term strength trend curve can be drawn in Figure 5.3 and long-term strength can easily be obtained from it (shown in Table 5.1).

Meanwhile, in order to study the strength loss during the cyclic loading process, the samples were exposed under constant temperature and humidity for a period when testing was completed and then conducted the instantaneous shear strength test. The test results show that the instantaneous strength loss is little and the loss rate is within 0.5%~2.4%. Specific data are shown in Table 5.1.

Based on Anti-Relaxation Capacity（ARC） and initial loading shear stress, the long-term strength of the rock can also be determined. As following formula:

$$\tau_{\infty} = \gamma \times \tau_{\mathrm{i}} \tag{5.2}$$

$$\frac{\tau_{\infty}}{\tau} = \gamma \times \frac{\tau_{\mathrm{i}}}{\tau} \tag{5.3}$$

Where:

τ_{i}= initial loading shear stress, MPa,

γ=Anti-Relaxation Capacity（ARC）,

τ_{∞}= long-term strength, $\tau_{\mathrm{i}} > \tau_{\infty}$.

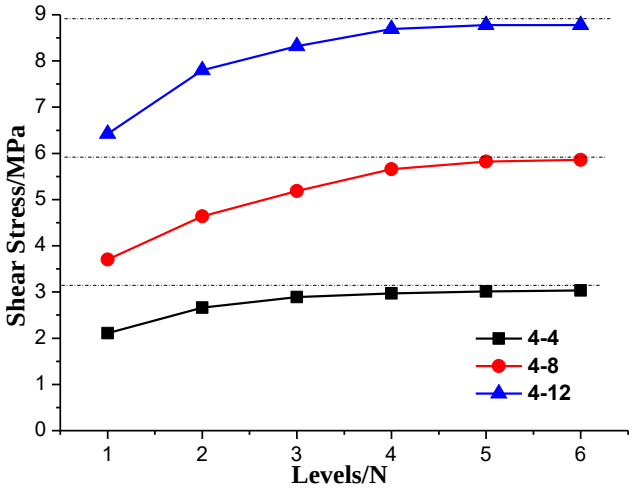

a. **The 4th structural plane**

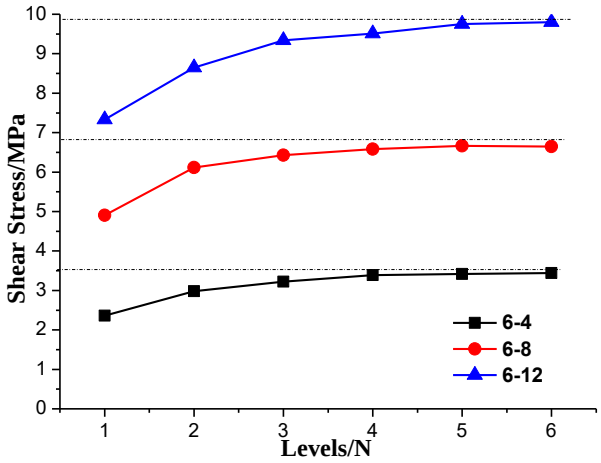

b. **The 6th structural plane**

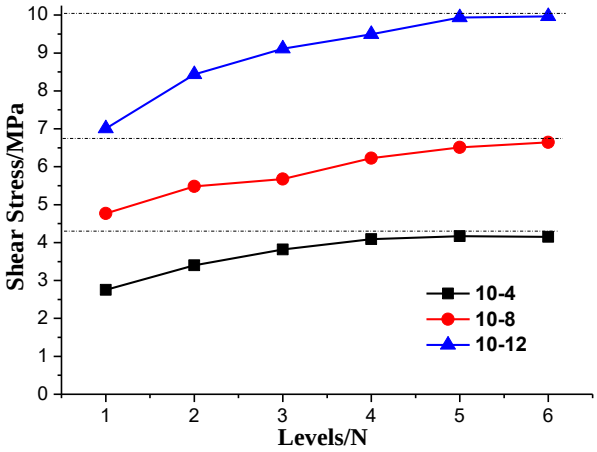

c. **The10th structural plane**

Figure 5.3 Trend curve of long-term strength

Table 5.1 Long-term strength and instantaneous strength

NO.	Normal Stress σ_n,MPa	Instantaneous Strength τ,MPa	Instantaneous Strength τ',MPa	Long-term Strength τ_∞,MPa	τ_∞/τ	τ_∞/τ'
4-4	4.00	4.01	3.96	3.05	0.761	0.770
4-8	8.00	7.71	7.67	5.88	0.763	0.767
4-12	12.00	11.41	11.30	8.80	0.771	0.779
6-4	4.00	4.41	4.33	3.46	0.785	0.799
6-8	8.00	8.47	8.40	6.67	0.787	0.794
6-12	12.00	12.54	12.44	9.82	0.783	0.789
10-4	4.00	5.38	5.25	4.17	0.775	0.794
10-8	8.00	8.74	8.60	6.66	0.762	0.774
10-12	12.00	12.71	12.50	9.99	0.786	0.799

τ' is instantaneous strength after the stress relaxation test.

It can be seen from Table 5.1 that the ratio of long-term strength to instantaneous strength is similar, between 0.761 and 0.787. According to shear strength formula of Coulomb：$\tau = \sigma_n \tan\varphi + c$, the linear fitting for instantaneous strength and long-term strength curves drawn respectively, which achieved a well-fitting result that correlation coefficients square are all up to 0.99 (shown in Figure 5.4 & Table 5.2). Cohesion and internal friction angle correspond to different samples are gained in Table 5.2, compared the long-term strength with the instantaneous strength, the reduction of internal friction angle is between 14.94% and 16.32% and the reductions of cohesion force are 48.39%, 27.50%and 30.43% respectively.

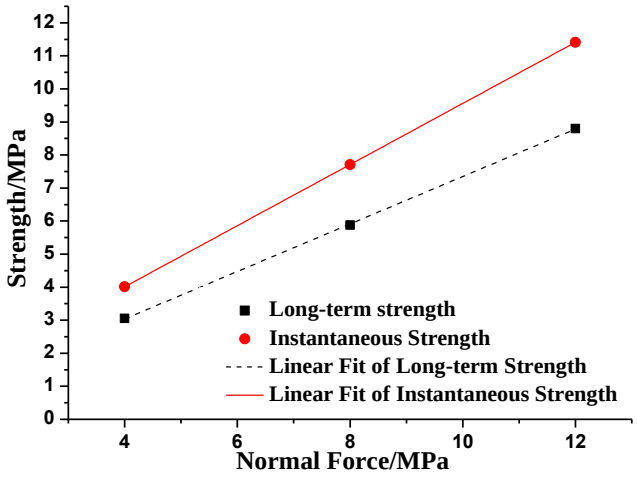

***a.* The 4th structural plane**

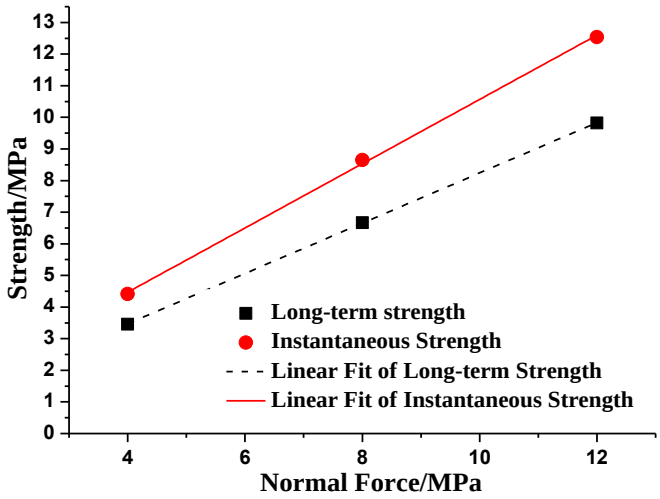

b. **The 6th structural plane**

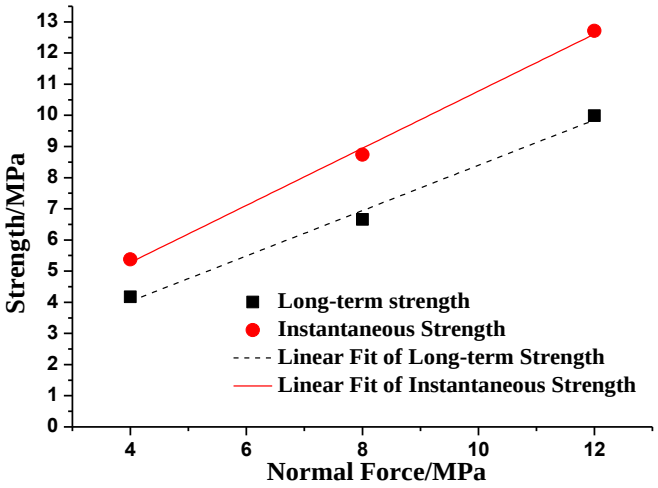

c. **The 10th structural plane**

Figure 5.4 Coulomb formula fitting curve of instantaneous strength and long-term strength

Table 5.2 Fitted Parameter by Coulomb Shear Strength Formula

No. of Structural Planes	Strength-Type	Cohesive Force,MPa	Internal Friction Angle,°	R^2
4	Instantaneous Strength	0.31	42.77	0.99
	Long-Term Strength	0.16	35.79	0.99
6	Instantaneous Strength	0.40	45.45	0.99
	Long-Term Strength	0.29	38.66	0.99
10	Instantaneous Strength	1.61	42.49	0.99
	Long-Term Strength	1.12	36.05	0.99

With the achievement of creep, from the perspective of stress relaxation, the method to determinate the long-term strength is proposed. On the one hand, the Isostress Cyclic Loading Method (ICLM) that can gradually reduce the influence of stress on further expansion of crack and increase the Anti-Relaxation Capacity (ARC) which led that stress relaxation form mostly rely on the viscous deformation. On the other hand, considering the termination condition of the stress relaxation, it can be inferred that the stress is bound to be less than or equal to long-term strength. The research method proposed in this paper can effectively eliminate manual interference and more accurately determine the long-term strength than existing methods. The testing time and needing loading levels can be determined by the needing time that the test enter into stable stress stage and the times that the Anti-Relaxation Capacity（ARC）tend to be stable.

5.2. Determination of long-term strength based on creep test

5.2.1 Relationship of creep rate and long-term strength

Conventional study shows that under a constant loading condition the deformation of rocks usually experiences three creep stages, termed as primary creep, secondary creep and tertiary creep. Existing creep test have shown that only primary creep stage occurs when loading stress is smaller than long-term strength, i.e. the creep rate in secondary creep stage is 0, and when the loading stress is larger than the long-term strength, creep will enter into the secondary creep stage in which creep rate is not 0 and the rock would be failure eventually. Thus, we can determine long-term strength through whether the creep rate in secondary creep stage is equal 0. We can see that the long-term strength determined by creep rate is not an accurate value but within a range whose size depends on the size of stress classification in creep test. A smaller stress classification, a more accurate rang of long-term strength will be.

Take sample 4-2.17 as an example, the whole process of creep loading is demonstrated in Figure 5.5, while the enlarged creep curves of the 3rd and 4th levels and corresponding creep rate curves are shown in Figure 5.6 & Figure 5.7, providing "close-up" of creeping process with the elapsed time for better observation. Through the observation of creep curve under different stress,

we can obtain that only primary creep stage occurs when the stress levels are 0.5 τ , 0.6 τ and 0.7 τ , and secondary creep stage, in which creep rate is larger than 0, occurs when the stress levels are 0.8 τ and 0.9 τ . Therefore, the long-term strength can be deduced within the range of 0.7 τ and 0.8 τ .

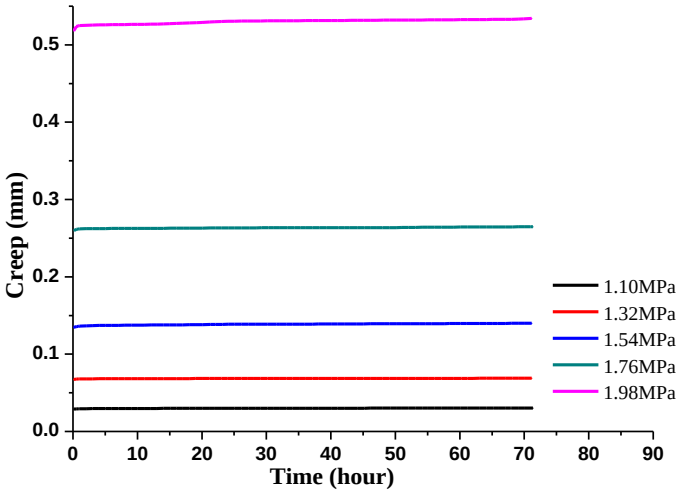

Figure 5.5 Creep curves under different stresses（4-2.17）

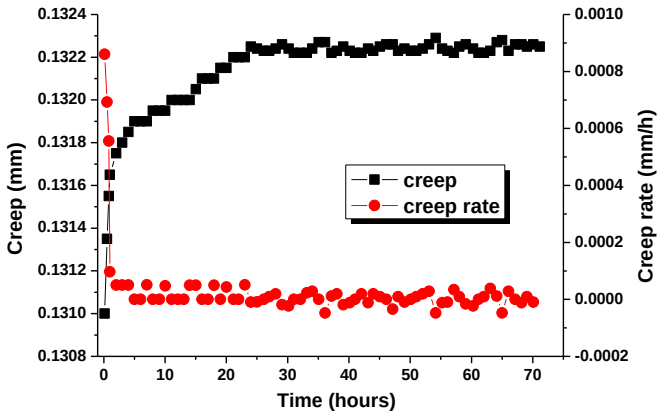

Figure 5.6 Creep curve of the 3rd loading level (4-2.17)

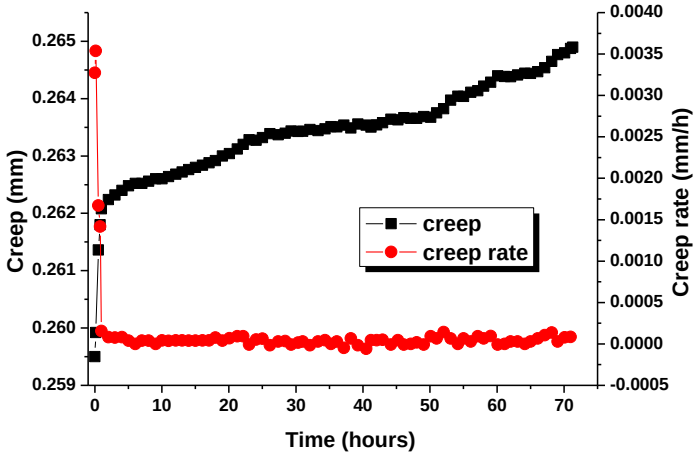

Figure 5.7 Creep curve of the 4th loading level (4-2.17)

5.2.2 Isochronous stress-strain curves

The study of transient mechanical properties mainly concerns the relationship between stress and strain, while the study of rheological properties mainly concerns about the relationship among stress, strain and time. In the creep study, the stress-strain relations at a certain moment, so called isochronous curve, could be transformed by processing the creep-time curve of rocks subjected to different stress levels. On this basis, the isochronous curve could reflect the stress-strain relationship under time effect, and is the link between the instantaneous mechanical properties and the rheological mechanical properties under time effect.

In transient mechanics, the stress-strain curve is divided into four stages, i.e. compaction stage, elastic deformation stage, plastic yield stage and post-peak failure stage. In which, the stress level in the compaction phase is stated could not cause the creep to develop. There would be hence no creep-time curve, not to mention the isochronous stress-strain curve. Besides, in the post-peak stage, the failure mechanism is relatively complicated, and the sample undergoes through accelerated creep stage, which would inevitably make the derivation of the isochronous time intervals difficult and lead to the unavailability of the isochronous stress-strain curve. Therefore, only two stages, i.e. the elastic deformation stage and the plastic yield stage, are applicable to process their corresponding creep-time curves into isochronous stress-strain curves. It is considered important to study the evolution of isochronous curves under time effect, which is

expected to provide beneficial reference to the understanding of the nonlinear characteristics of creep process and the establishment of nonlinear constitutive model of creep.

It is worth noted that, in the instantaneous mechanics, there exists an inflection point at the creep-time curve where the sample transits from the elastic deformation stage (manifesting as linear curve) to the plastic yield stage (manifesting as nonlinear curve). This inflection point is representing the yielding point of the tested rock material. Therefore, previous researchers further inferred that there should also be existed an inflection point between these two stages when time effect is of concern. On this basis, a method for calculating the long-term strength of rock was therefore proposed by pioneers. Details regarding the long-term strength determination will be also discussed latter.

The schematic diagram shown in Figure 5.8 illustrates the method on how to derive the isochronous curve from creep-time curve, in which, the right side of the vertical axis in Figure 5.8 shows the creep-time curve of rock at different stress levels, and the left side shows the corresponding isochronous curve. After obtaining a series of creep-time curves under different stress levels, a line pointed to a specific time moment (i.e. t_1) is drawn parallel to the vertical axis, which intersects the corresponding series of shear stress values (i.e. σ_1, σ_2, σ_3,…. σ_n) at the creep-time curve. By plotting the corresponding parallel lines, passing these shear stress values, to the horizontal axis, a series of isochronous shear-strain curves, i.e. isochronous curves, could be therefore obtained. By this principle, nine groups of corresponding isochronous curves could be derived from the nine groups of creep-shear tests on discontinuities, as shown in Figure 5.9.

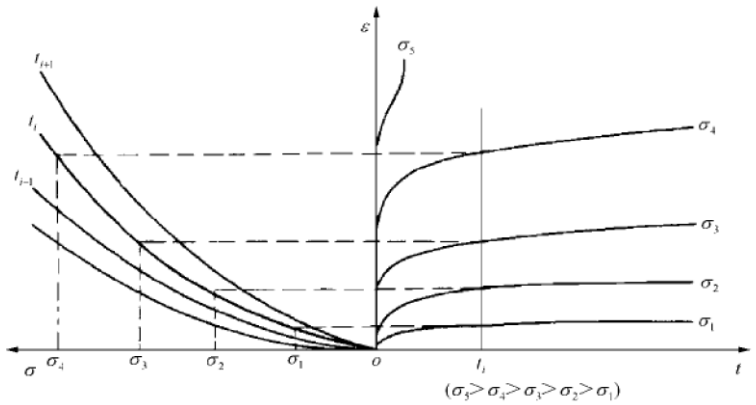

Figure 5-8 Illustration to draw isochronous stress-strain curves (Sun, 2007)

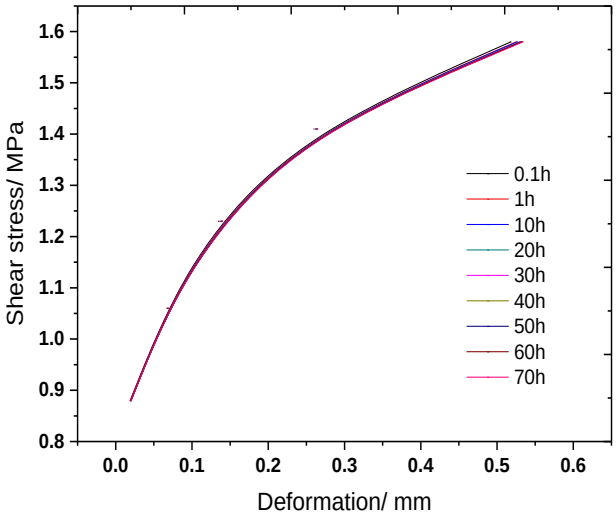

a. 1-2.17

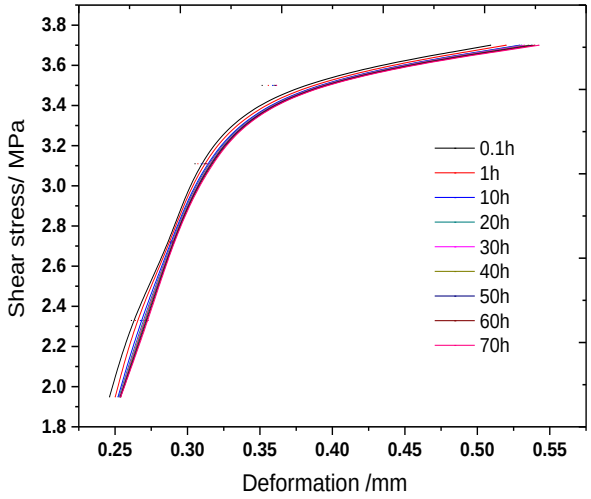

b. 1-4.35

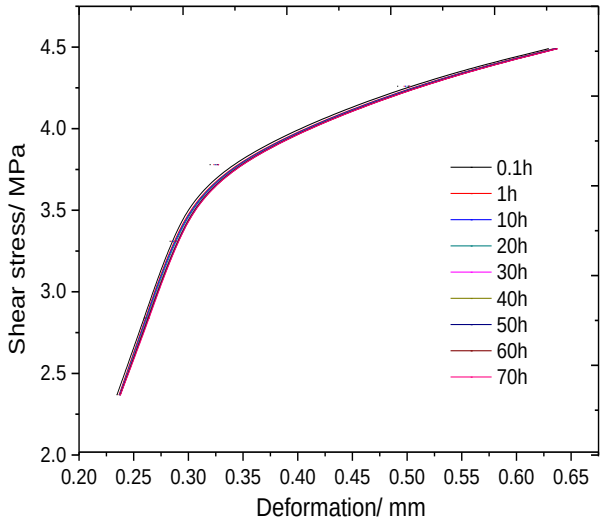

c. 1-6.52

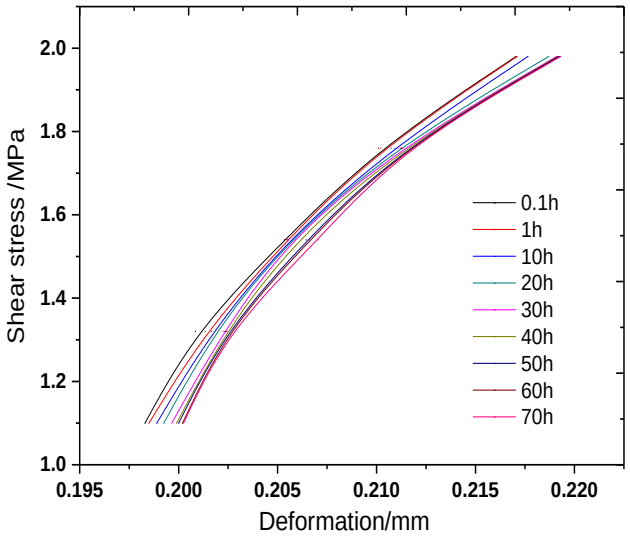

d. 4-2.17

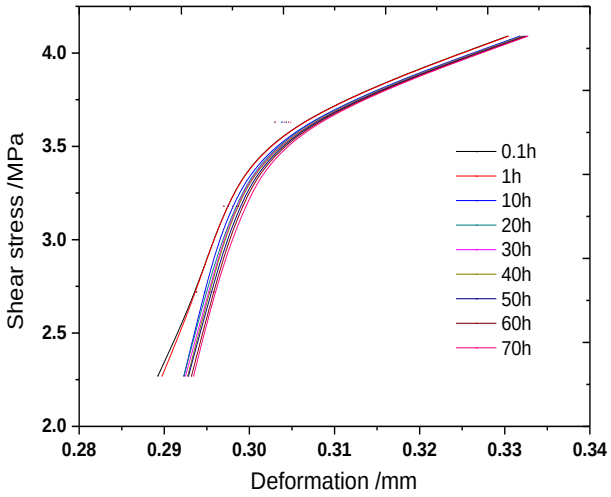

e. 4-4.35

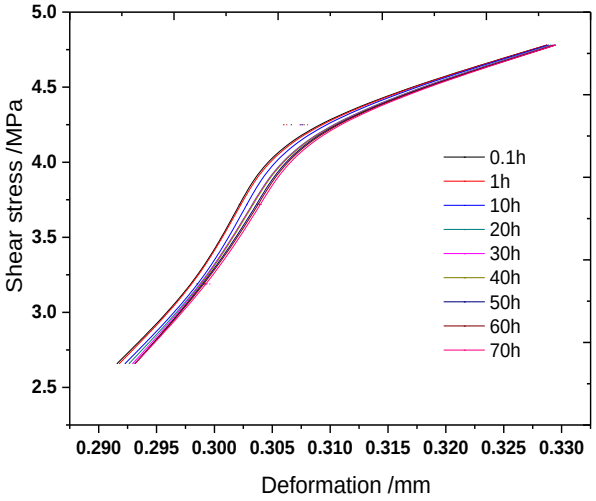

f. 4-6.52

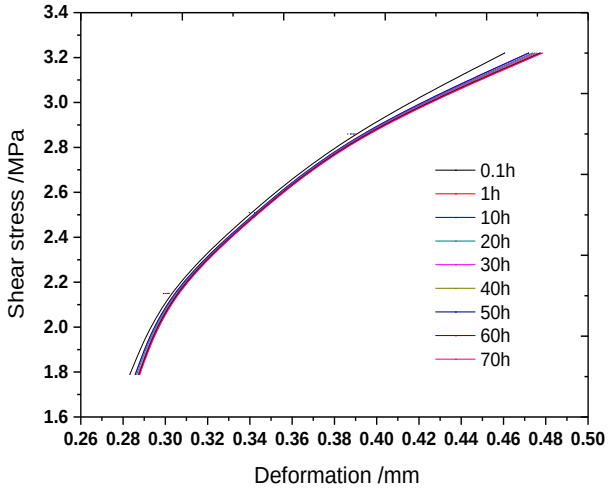

g. 10-2.17

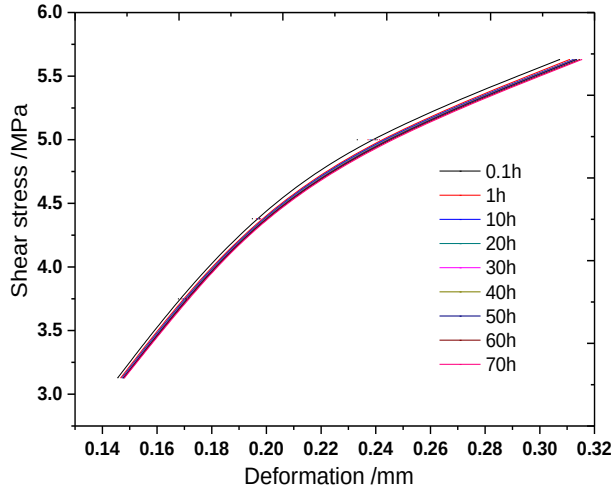

h. 10-4.35

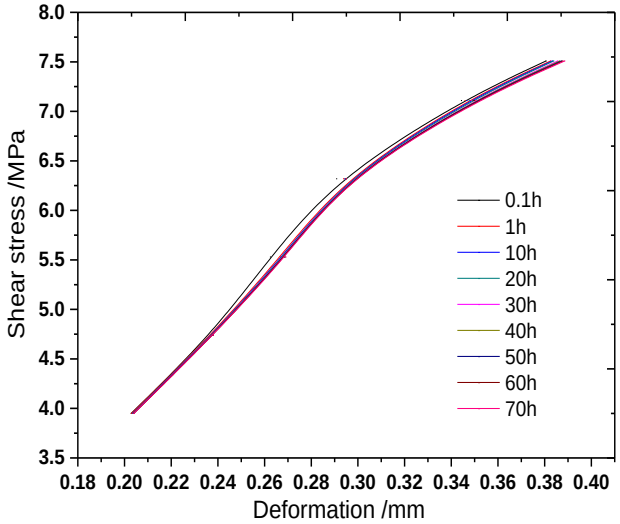

i. 10-6.52

Figure 5.9 Isochronous stress-strain curves

From Figure 5.9, it is observed that:

1) Generally, the isochronous curve could be divided into two stages: an initial linear deformation stage followed by a nonlinear deformation stage. That is, the shear stress at the 1st, 2nd, and 3rd loading levels increases almost linearly with the increased deformation, while the shear stress tends to decrease gradually at an decreasing rate with the deformation, exhibiting as strain softening;

2) The samples used in this research are relatively hard, and hence their aging characteristics are not obvious. As a result, for a given sample, the isochronous curves with time are approximately overlapping with each other;

3) The isochronous curve is initially linear, indicating that the deformation is mainly composed of viscoelastic deformation. The slope of this linear segment is the elastic modulus of the structural surface under the time effect. This parameter gradually decreases with time but at a decreasing rate. By considering the time effect, Xu H. (1997) defined the asymptotically stabilized elastic modulus as the long-term elastic modulus;

4) The isochronous curve in the latter part exhibits nonlinear characteristics, indicating that with the development of shear stresses, in addition to viscoelastic deformations, part of viscous-plastic deformations of the discontinuities are also developed. Such viscous-plastic deformations also reflect the deterioration of the discontinuity itself.

5.2.3 The property of isochronous curve

Isochronous stress-strain curves are always utilized to analyze the nonlinear characteristics, and also be adopted in determination of long-term strength which has been compiled into "specifications for rock tests in water conservancy and hydroelectric engineering" China, SZ264-2001. Isochronous curve consists of two stages: linear stage and nonlinear stage and there is a turning point between them, the corresponding stress of the turning point would decrease over time and tend to a stable value that is long-term strength. The turning point is also termed as the starting point of viscoplastic deformation, and the long-term strength is defined as the transition point from viscoelastic deformation to viscoplastic deformation. Based on the creep curves under

different stress, isochronous stress-strain curves can be drawn, here we take sample 4-4.35 as an example (see Figure 5.10).

From the asymptotic value of isochronous curves, long-term strength can be obtained as shown in Table 5.3. The ratio of long-term strength and strength most lies between 0.7 and 0.8 except sample 4-2.17, and its average is 0.735. The obtained results have a certain hop. Isochronous stress-strain curves are generally consistent, but also present diversity change. As the material used in pouring the sample is relatively hard, the interval of isochronous curve is so small that human factor should be not ignored in determining the asymptotic value of turning point in isochronous curves.

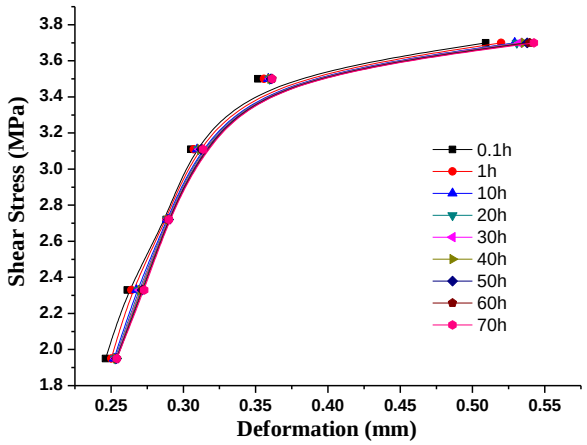

4-4.35 (full view)

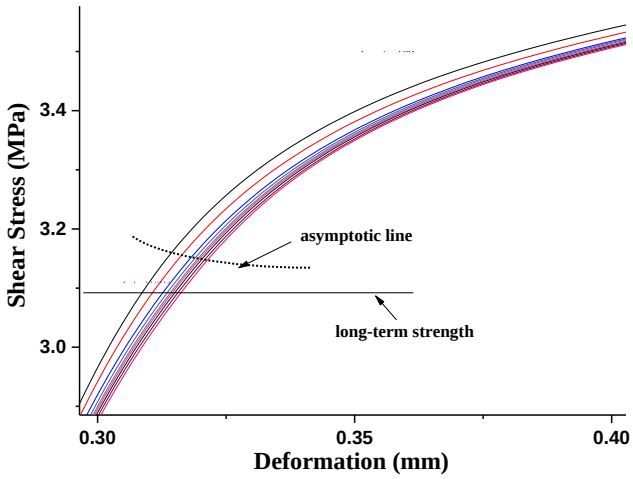

4-4.35 (partial enlarged view)

Figure 5.10 Isochronous curves of 4-4.35

Isochronous curve can be viewed as the stress-strain curve considering time-effect. Instantaneous mechanism properties mainly focus on the relationship of stress and strain, while rheological properties consider the relationship of stress, strain and time. We often divide the conventional stress-strain curves into four stages, compaction stage, elastic stage, plastic yielding stage and failure stage after the peak. Comparing with isochronous stress-strain curve, as the stress in compacting stage could not cause creep deformation and no corresponding stage to isochronous stress-strain curve. The mechanism of failure stage after peak is complicated and difficult to get a series of corresponding points from creep curves. Therefore, only two stages, elastic stage and plastic yielding stage, can be corresponded to isochronous curve, elastic stage corresponds to the linear stage in isochronous curve and plastic yielding stage corresponds to nonlinear stage. The turning point in isochronous stress-strain curve is equal to the yielding point considering time effect in stress-strain curve. The rationality of taking the asymptotic value of yielding point considering time-effect as long-term strength is suspected in this study, as the long-term strength is the strength value considering time-effect and not the yielding point considering time-effect. As a consequence, the obtained long-term strength by isochronous curve method would be conservative.

Table 5.3 Long-term strength determined by isochronous stress-strain curves

Sample	Normal stress /MPa	Conventional strength /MPa	Long-term strength /MPa	τ_∞ / τ
4-2.17	2.17	1.76	1.12	0.636
4-4.35	4.35	3.90	3.09	0.792
4-6.52	6.52	4.74	3.50	0.738
10-2.17	2.17	3.58	2.70	0.754
10-4.35	4.35	6.26	4.63	0.740
10-6.52	6.52	7.90	6.07	0.768

5.3. Discussion and summary

The potential correlation between relaxation behavior and long-term strength is discussed and an iso-stress cyclic loading method (ICL method), which could reduce the influence of asperity activities on relaxation behaviors under Kaiser effect, is hence proposed to determine the long-term strength. Accordingly, long-term strength of discontinuities were determined by ICL method. The

result shows that, with the increasing of cyclic times, the stress relaxation behavior gradually decreases to a steady state of evolution, which is regarded causing by the gradually decreasing portion of stress relaxation induced by the dwindling asperities crushing and/or breakage under Kaiser effect. The determined long-term strengths using ICL method, with an average value of 77.5 % to their corresponding conventional strengths, are well consistent with the long-term strengths determined by shear creep tests. Besides, the linear fitting curves of obtained long-term strengths for different discontinuities present a good agreement to the Coulomb's shear strength formula with decreased internal friction angle and cohesion forces, comparing to their corresponding conventional shear strengths. Based on the revealed results, it could be stated that the proposed ICL method could effectively and accurately determine the long-term strength of discontinuities.

And then, the evolution laws of creep rate under different stress levels and isochronous stress-strain curves were utilized to determine long-term strength of rock mass respectively. The result based on three aforementioned method are different, average ratios of long-term strength and conventional strength are shown in Table 5.4, which are 0.700~0.800, 0.735 and 0.776 respectively.

Table 5.4 Comparison of different methods determining long-term strength

Method-based	Average ratio of long-term strength to conventional strength
Creep rate	0.700~0.800
Isochronous stress-strain curves	0.735
Stress relaxation (ICLM)	0.776

Long-term strength determined by transition creep method is not a single value but a range value the size of which depends on the size of stress classification in creep test. A smaller stress classification, the long-term strength interval value will be more accurate. Isochronous stress-strain curves correspond to elastic stage and yielding plastic stage in stress-strain curve of instantaneous loading. Long-term strength determined by isochronous curves method affected by human factor, as the turning point is not so obvious and also diversity present in the obtained isochronous curves. In addition, taking the yielding strength considering time factor as long-term strength is not right,

which should be the strength considering time factor. Long-term strength obtained by isochronous curve method would be conservative.

Chapter 6 Conclusions

Rock mass, as an engineering material, is a complex geological material containing numerous discontinuities such as geological faults, joints, fractures, etc. Discontinuities are among the most important factors that governing the mechanical behavior of a rock mass. Investigated data has demonstrated that the failure of the rock engineering along discontinuities is always not a brittle behavior but progressive damage after years or decades by creep and stress relaxation. Currently, intensive emphasis has been put on studying the time-dependent behaviors of rock masses through laboratory creep tests. However, stress relaxation behaviors and its correlation with long-term strength has been rarely investigated. A series of conventional shear tests, shear creep tests and shear relaxation tests under different normal stresses were performed on artificial discontinuities with different Joint Roughness Coefficient (JRC). Special interests of this study are given to understand the time dependent behaviors of discontinuities, especially stress relaxation behaviors, and their relationship with long-term strength of discontinuities. The main conclusions could be drawn as follows.

1. Creep properties of tested discontinuities

1) The samples develop to failure without distinctly manifesting the acceleration creep phase. The following reasons are considered: the creep failure of an intact rock under constant external load results from the initiation and evolution of micro-cracks, which finally coalescent into macro-failure along with the stick-slip between the cracks. While as for rock mass with discontinuities, the sample already coalescent into macro-cracks, i.e. the discontinuity, therefore, when the stress level is higher than a certain value, shear creep would occur, leading to the rapid reduction of the viscous resistance, and hence exhibiting as an apparent instantaneous behavior.

2) The results of the creep rate relation show that at the beginning of loading, the creep rate is mainly related to the applied shear stress level, where a higher shear stress generates a larger initial creep rate. Meanwhile, an empirical formula whose involved parameters have clear physical meaning is suggested to describe the creep rate during the whole creep process, and a satisfied

fitting result is obtained.

3) The instantaneous deformation is mainly affected by the shear stress level, which increases with the increased shear stress. Generally, the instantaneous deformation increases almost linearly during the first three or four loading levels where the shear stresses in each level are relatively low. Thereafter, as the increase of the shear stress, especially at the last loading level, the instantaneous deformation would increase more rapidly with the increased shear stress. In addition, the total amount of creep deformation is also increased with the increasing shear stress.

4) The duration for the attenuation creep stage for a sample under a relatively low shear stress is longer than that under a high shear stress, which is due mainly to the full play of viscous deformations between the discontinuities of the sample when it subjected to a low shear stress. Besides, under a relatively low shear stress, the creep would stabilize eventually, while the creep would continuously develop with time even after reaching the stable creep stage when the sample is subjected to a high shear stress. It is worth noted that the stable creep stage in the discontinuity is not strictly evolved linearly, but exhibiting some fluctuations due to the effect of the discontinuity.

5) The isochronous curve that reflecting the stress-strain relation is the link between the instantaneous mechanical behavior and rheological mechanical behavior that considers the effect of time. The isochronous curve could be divided into two stages in terms of the initial linear stage and the followed nonlinear stage where the shear stress increases with the deformation at a gradually decreasing rate. In which, the slope of the initial linear stage reflects the elastic modulus, while the latter non-linear stage reflects the strain softening property of the sample under time effect. These two stages are corresponding to the elastic deformation and yielding deformation in the instantaneous stress-strain curve, which have great significance to understand the non-linear rheological mechanical behavior of discontinuities. However, since the rock samples used in this thesis are relatively hard, the time effect on the isochronous curve is not so obvious.

6) NISHIHARA model was selected to fitting the testing data and the evolutions of involved parameters in the model were analyzed. The results show that the NISHIHARA model still has some limitations, in describing the creep behavior of discontinuities. For example, NISHIHARA model does not take the instantaneous plastic deformation into account; the attenuation rate at the inflection part of the attenuation creep stage is too rapid when the sample is under a relatively low

shear stress; lack of explorations on the non-linear property of involved parameters in the model when the sample subjected to high shear stress, etc. To this end, an improved NISHIHARA model was therefore proposed and the involved parameters were analyzed and compared. It results that a better fitting result could be obtained compared with the original NISHIHARA model.

2. Stress relaxation properties of tested discontinuities

1) The ICL method is proposed to study shear stress characteristics, which can reduce the effect of instantaneous mechanical characteristics with increasing cycle times and reflect the viscous properties of rock material more accurately than existing methods. According to the test, stress relaxation can be divided into three stages: The rapid stress relaxation stage, decelerating stress relaxation stage, and stable stress stage. Stress relaxation appears in two indirect forms: Local failure (asperity crushing and break-off) and viscous deformation.

2) The ARC, which is equal to the ratio of the residual stress value to the initial load stress, is proposed in this paper to represent the anti-relaxation ability. The ARC, and stress relaxation rate depend more strongly on the viscosity coefficient of the material with increasing cycle times and finally tend to reach a stable value σ_0.

3) Burgers model was adopted to describe stress relaxation properties and the parameters of burgers model were determined, which shown that burgers model could be used in stress relaxation properties, meanwhile stress will relaxed to 0 and linear properties of burgers model can not reflect stress relaxation well. A new nonlinear model (K-M model) was proposed in this study, which could describe stress relaxation well, and the parameters in K-M model were studied.

3. Long-term strength of discontinuities

1) With the achievement of creep, from the perspective of stress relaxation, the ICLM is proposed to determine the long-term strength. This method can effectively eliminate manual interference and more accurately determine the long-term strength than existing methods. The testing time and required loading levels can be determined based on the time required for the test to enter a stable stress stage, and the levels of the ARC tend to be stable.

2) The ratios of the long-term strength to the instantaneous strength gradually increase as the normal force and roughness coefficient increase. The main reason here is that the effect of the structural plane is gradually weakened with the normal force and roughness coefficient increase.

Use of the Coulomb shear strength formula, $\tau = \sigma \tan \phi + c$, to fit the instantaneous strength and long-term strength yielded a well-fitting result, with correlation coefficients as high as 0.99.

References

Ashby, M. F., and Sammis, C. G. (1990). The damage mechanics of brittle solids in compression. Pure Appl. Geophys., 133(3), 489–521.

Atkinson, B. K. (1984). Subcritical crack growth in geological materials. J. Geophys. Res. B: Solid Earth, 89(B6), 4077–4114.

Aubertin M, Gill D E, Ladanyi B. (1991）An internal variable model for the creep of rock salt Rock Mechanics and Rock Engineering, 24(2): 81-97.

Barton, N., Choubey, V. (1977). The shear strength of rock joints in theory and practice. Rock mechanics, 10(1-2), 1-54.

Barton N. (2013). Shear strength criteria for rock, rock joints, rockfill and rock masses: Problems and some solutions. Journal of Rock Mechanics and Geotechnical Engineering, 5(4), 249-261.

Barton N. (1973). Review of a new shear-strength criterion for rock joints. Engineering geology, 7(4): 287-332.

Barton N, Choubey V. (1977). The shear strength of rock joints in theory and practice. Rock mechanics, 10(1-2): 1-54.

Barton N. (1978). Suggested methods for the quantitative description of discontinuities in rock masses. ISRM, International Journal of Rock Mechanics and Mining Sciences & Geomechanics Abstracts, 15(6).

Bieniawski Z T. (1967) Mechanism of brittle fracture of rock: part I—theory of the fracture process[C]//International Journal of Rock Mechanics and Mining Sciences & Geomechanics Abstracts. Pergamon, 4(4): 395-406.

Bieniawski Z T. (1967) Mechanism of brittle fracture of rock: part II—experimental studies[C]//International Journal of Rock Mechanics and Mining Sciences & Geomechanics Abstracts. Pergamon, 4(4): 407-423.

Bieniawski, Z. T. (1967). Stability concept of brittle fracture propagation in rock. Engineering Geology, 2(3), 149-162.

Bowden, R. K. (1984). Time-Dependent Behavior of Joints in Shale. MA. Sc. thesis, University of Toronto, Ontario.

Brantut, N., Baud, P., Heap, M. J., and Meredith, P. G. (2012). Micromechanics of brittle creep in rocks. J. Geophys. Res. B: Solid Earth, 117(B8).

Brantut, N., Heap, M. J., Meredith, P. G., and Baud, P. (2013). Time-dependent cracking and brittle creep in crustal rocks: A review. J. Struct. Geol., 52, 17–43.

Brouard, B., Berest, P., de Greef, V., Béraud, J. F., Lheur, C., Hertz, E. (2013). Creep closure rate of a shallow salt

cavern at Gellenoncourt, France. International Journal of Rock Mechanics and Mining Sciences, 62, 42-50.

Charles, R. J. (1958). Static fatigue of glass. I. J. Appl. Phys., 29(11), 1549–1553.

Chen L, Wang C P, Liu J F, et al. (2014) A damage-mechanism-based creep model considering temperature effect in granite. Mechanics Research Communications, 56: 76-82.

Chin H P, Rogers J D. (1987) Creep parameters of rocks on an engineering scale[J]. Rock mechanics and rock engineering, 20(2): 137-146.

Chandler, N. A. (2013). Quantifying long-term strength and rock damage properties from plots of shear strain versus volume strain. International Journal of Rock Mechanics and Mining Sciences, 59, 105-110.

Costin, L. S. (1985). Damage mechanics in the post-failure regime. Mech. Mater., 4(2), 149–160.

Cui, X. H., Fu, Z. L. (2006). Test study on rock creep properties and its long-term strength. Chinese Journal of Rock Mechanics and Engineering,25(5), 1021-1024. (in Chinese)

Damjanac, B., Fairhurst, C. (2010). Evidence for a long-term strength threshold in crystalline rock. Rock Mechanics and Rock Engineering, 43(5), 513-531.

Fabre, G., Pellet, F. (2006). Creep and time-dependent damage in argillaceous rocks. International Journal of Rock Mechanics and Mining Sciences, 43(6), 950-960.

Filimonov, Y. L., Lavrov, A. V., Shafarenko, Y. M., Shkuratnik, V. L. (2001). Memory effects in rock salt under triaxial stress state and their use for stress measurement in a rock mass. Rock mechanics and rock engineering, 34(4), 275-291.

Goodman, R. E. (1963). Subaudible noise during compression of rocks. Geological Society of America Bulletin, 74(4), 487-490.

Goodman R E. (1989). Introduction to rock mechanics[M]. New York: Wiley.

Heap, M. J., Brantut, N., Baud, P., and Meredith, P. G. (2015). Time-dependent compaction band formation in sandstone. J. Geophys. Res. B: Solid Earth, 120(7), 4808–4830.

Hazzard, J. F., Young, R. P. (2000). Simulating acoustic emissions in bonded-particle models of rock. International Journal of Rock Mechanics and Mining Sciences, 37(5), 867-872.

Huang, X., Haimson, B. C., Plesha, M. E., Qiu, X. (1993, June). An investigation of the mechanics of rock joints—Part I. Laboratory investigation. International Journal of Rock Mechanics And Mining Sciences & Geomechanics Abstracts, 30(3), 257-269). Pergamon.

Hutson, R. W., Dowding, C. H. (1990, April). Joint asperity degradation during cyclic shear. International Journal of Rock Mechanics and Mining Sciences Geomechanics Abstracts. 27(2), 109-119. Pergamon.

Jang H S, Kang S S, Jang B A. (2014). Determination of joint roughness coefficients using roughness parameters[J]. Rock mechanics and rock engineering, 47(6): 2061-2073.

Jiang, Q., Qi, Y., Wang, Z., Zhou, C. (2013). An extended Nishihara model for the description of three stages of sandstone creep. Geophysical journal international, 193(2), 841-854.

Jing, L., Stephansson, O., Nordlund, E. (1993). Study of rock joints under cyclic loading conditions. Rock Mechanics and Rock Engineering, 26(3), 215-232.

Lacroix, P., Amitrano, D. (2013). Long-term dynamics of rockslides and damage propagation inferred from mechanical modeling. Journal of Geophysical Research: Earth Surface, 118(4), 2292-2307.

Lee, H. S., Park, Y. J., Cho, T. F., You, K. H. (2001). Influence of asperity degradation on the mechanical behavior of rough rock joints under cyclic shear loading. International Journal of Rock Mechanics and Mining Sciences, 38(7), 967-980.

Li, C., Nordlund, E. (1993, January). Assessment of Damage in Rock by the Kaiser Effect of Acoustic Emission. In The 34th US Symposium on Rock Mechanics (USRMS). American Rock Mechanics Association.

Li, Y., Xia, C. (2000). Time-dependent tests on intact rocks in uniaxial compression. International Journal of Rock Mechanics and Mining Sciences, 37(3), 467-475.

LI Yongsheng (1995) Creep and relaxation of four kinds of rocks under uniaxial compression tests[J], Chinese Journal of Rock Mechanics and Engineering, Vol. 14, No.1, pp.39-47.

LI You, ZHU Weishen, PENG Yi, LI Ni and HUANG Chaoqiang (2006) Multi-axial experimental study on creep and relaxation properties of red sandstone from somewhere[J], Rock and Soil Mechanics, Vol.27, No.8, pp.1248-1252.

Liu A, Shen M, Jiang J, Zhang Q. (2014) Determining long-term strength of rock with discontinuities using shear stress relaxation test. Chinese Journal of Rock Mechanics and Engineering, 09:1916-1924. (in Chinese).

Liu A, Shen M., Jiang J. (2015). Investigation of the shear stress relaxation characteristics of a structural plane using the isostress cyclic loading method. Geotechnical Testing Journal, 38(2), 219-228.

Liu, M. Y., and Xu, C. Y. (2000). Rheological properties of anhydrite and determination of its long-time strength. China Mining Magazine, 9(2), 53-55. (in Chinese)

Liu, X. (1994). Introduction to Rock Rheology, Geological Publishing House, Beijing, China. (in Chinese)

LIU Jinghui, WANG Changshan and YANG Honghai. (1996) Method to determine the rheological test long-term strength for soft intercalations[J], Site Investigation Science and Technology, Vol. 4, No.5, pp.3-7.

LIU Xiong, (1994) Introduction to rock rheology[M], Beijing: Geological Publishing House, pp.40-43&194-207.

（in Chinese）

Lacroix P, Amitrano D (2013) Long-term dynamics of rockslides and damage propagation inferred from mechanical modeling. J Geophys Res 118(4):2292–2307.

Lockner, D. A. (1993). Room temperature creep in saturated granite. J. Geophys. Res. B: Solid Earth, 98(B1), 475–487.

Lockner D. (1993) The role of acoustic emission in the study of rock fracture. International Journal of Rock Mechanics and Mining Sciences & Geomechanics Abstracts. Pergamon, 30(7): 883-899.

Malan D F. (1999) Time-dependent behavior of deep level tabular excavations in hard rock[J]. Rock Mechanics and Rock Engineering, 32(2): 123-155.

Malan K. (1997) Time-dependent behavior of hard rock in deep level gold mines[J]. Journal of the Southern African Institute of Mining and Metallurgy, 97(3): 135-147.

Main, I. G. (2000). A damage mechanics model for power-law creep and earthquake aftershock and foreshock sequences. Geophys. J. Int., 142(1), 151-161.

Martin, C. D., and Chandler, N. A. (1994). The progressive fracture of Lacdu Bonnet granite. Int. J. Rock Mech. Min. Sci., 31(6), 643-659.

Miura K, Okui Y, Horii H (2003) Micromechanics-based prediction of creep failure of hard rock for long-term safety of high-level radioactive waste disposal system. Mech Mater 35(3):587–601.

Molladavoodi, H., and Mortazavi, A. (2011). A damage-based numerical analysis of brittle rocks failure mechanism. Finite Elem. Anal. Des.,47(9), 991–1003.

Mortazavi, A., and Molladavoodi, H. (2012). A numerical investigation of brittle rock damage model in deep underground openings. Eng. Fract. Mech., 90, 101-120.

Munday, J. G. L., Mohamed, A. E., and Dhir, R. K. (1977). A criterion for predicting the long-term strength of rock. Conf. Rock Engineering, Univ. of Newcastle-upon-Tyne, Newcastle upon Tyne, U.K., 127-135.

Nabarro F R N. (2004) Do we have an acceptable model of power-law creep? Materials Science and Engineering: A, 387: 659-664.

Nara, Y., Takada, M., Mori, D., Owada, H., Yoneda, T., and Kaneko, K. (2010). Subcritical crack growth and long-term strength in rock and cementitious material. Int. J. Fract., 164(1), 57-71.

Paraskevopoulou, C., Perras, M., Diederichs, M., Amann, F., Löw, S., Lam, T., Jensen, M. (2017). The three stages of stress relaxation-Observations for the time-dependent behaviour of brittle rocks based on laboratory testing. Engineering Geology, 216, 56-75.

Park J W, Song J J. (2009) Numerical simulation of a direct shear test on a rock joint using a bonded-particle model. International Journal of Rock Mechanics and Mining Sciences, 46(8), 1315-1328.

Pang Z, Hu J. (2006) Shear creep and long-term strength test research on unconformity plane. Rock and Soil Mechanics, 27(supplement): 1179-1182. (in Chinese).

Peng, S., Podnieks, E. R. (1972, November). Relaxation and the behavior of failed rock. In International Journal of Rock Mechanics and Mining Sciences & Geomechanics Abstracts, 9(6), 699-700. Pergamon.

Plesha, M. E. (1987). Constitutive models for rock discontinuities with dilatancy and surface degradation. International Journal for Numerical and Analytical Methods in Geomechanics, 11(4), 345-362.

Peng S, Podnieks E R. (1972) Relaxation and the behavior of failed rock[C]//International Journal of Rock Mechanics and Mining Sciences & Geomechanics Abstracts. Pergamon, 9(6): 699-700.

Peng S S. (1973) Time-dependent aspects of rock behavior as measured by a servocontrolled hydraulic testing machine[C]//International Journal of Rock Mechanics and Mining Sciences & Geomechanics Abstracts. Pergamon, 10(3): 235-246.

Read RS (2004). Twenty years of excavation response studies at AECL's Underground Research Laboratory. Int J Rock Mech Min Sci 41(8):1251–1275.

Ranalli, G. (1995): Rheology of the Earth. Chapman & Hall, London.

Salganik, R. L., and Gotlib, V. A. (2000). Continuum versus discontinuum damage mechanics of creep caused by microcracking. Int. J. Fract.,101(3), 181–201.

Shen, M., Chen, H., and Zhang, Q. (2012). Method for Determining Long-Term Strength of Discontinuity Using Shear Creep Test, Chin. J. Rock Mech. Eng., Vol. 31, No. 1, pp.1-7.

SHEN M, ZHANG Q. (2008) Study of creep characteristics of regular rock mass discontinuity. Chinese Journal of Rock Mechanics and Engineering, 27: 3973-3979.

Shen M, Zhang Q Z. (2010) Experimental study of shear deformation characteristics of rock mass discontinuities[J]. Chin J Rock Mech Eng, 29(4): 713-9.

Shen M, Chen H. (2011）Testing study of long-term strength characteristics of red sandstone[J]. Rock and Soil Mechanics, 32(11)：3301-3305. (in Chinese).

Spence J, Hult J. (1973) Simple approximations for creep relaxation[J]. International Journal of Mechanical Sciences, 15(9): 741-755.

Shao J F, Zhu Q Z, Su K. (2003) Modeling of creep in rock materials in terms of material degradation[J]. Computers and Geotechnics, 30(7): 549-555.

SHEN Mingrong and ZHANG Qingzhao, (2010). Study on the shear creep characteristic of greenschist discontinuity[J], Chinese Journal of Rock Mechanics and Engineering, Vol. 29, No.6, pp.1149-1155.

Su C, Herbert E G, Sohn S, et al. (2013) Measurement of power-law creep parameters by instrumented indentation methods. Journal of the Mechanics and Physics of Solids, 61(2): 517-536.

SUN Jun, (2007). Rock rheological mechanics and its advance in engineering applications, Chinese Journal of Rock Mechanics and Engineering, Vol. 26, No.6, pp.1081-1106.

Tensi, H. M. (2004). The Kaiser-effect and its scientific background. Journal of Acoustic Emission, 22, s1-s16.

Tsai, L. S., Hsieh, Y. M., Weng, M. C., Huang, T. H., Jeng, F. S. (2008). Time-dependent deformation behaviors of weak sandstones. International Journal of Rock Mechanics and Mining Sciences, 45(2), 144-154.

Tuncay E, Ulusay R. (2008). Relation between Kaiser effect levels and pre-stresses applied in the laboratory[J]. International Journal of Rock Mechanics and Mining Sciences, 45(4): 524-537.

XU Weiya and YANG Shengqi, (2005). Test study on shear rheological behavior of jointed rock mass and the model investigations, Chinese Journal of Rock Mechanics and Engineering, Vol. 24, No. Supp.2, pp.5536-5542.

Xu, T., Tang, C. A., Zhao, J., Li, L. C., and Heap, M. J. (2012). Modelling the time-dependent rheological behaviour of heterogeneous brittle rocks. Geophys. J. Int., 189(3), 1781–1796.

Xue, Y., Mishra B., Gao, D. (2017). Numerical and Laboratory Analysis of Relaxation Tests for Determining Time-Dependent Properties of Rock. Geotechnical and Geological Engineering, 35, 615-629.

Yahya O M L, Aubertin M, Julien M R. (2000). A unified representation of the plasticity, creep and relaxation behavior of rocksalt[J]. International Journal of Rock Mechanics and Mining Sciences, 37(5): 787-800.

YU Huaichang, ZHOU Min and LIU Handong, (2011). Experimental investigation on stress relaxation properties of silty mudstone under triaxial compression[J], Chinese Journal of Rock Mechanics and Engineering, Vol. 30, No.4, pp.803-811.

Zhang H, Wang Z, Zheng Y, et al. (2012). Study on tri-axial creep experiment and constitutive relation of different rock salt[J]. Safety science, 50(4): 801-805.

Zhang, H. B., Wang, Z. Y., Zheng, Y. L., Duan, P. J., and Ding, S. L. (2012). Study on triaxial creep experiment and constitutive relation of different rock salt. Saf. Sci., 50(4), 801–805.

Zhang, Q. Z., Shen, M. R., Ding, W. Q., and Carl, C. (2012). Shearing creep properties of cements with different irregularities on two surfaces. J. Geophys. Eng., 9(2), 210-217.

Zhang, Q. Z., Shen, M. R., and Clark, C. (2011a). Shearing mechanical properties of structural planes of a regular

tooth rock. Mater. Test., 53(9), 540-545.

Zhang, Q. Z., Shen, M. R., and Wen, Z. (2011b). Investigation on mechanical behavior of a rock plane using rheological tests. J. Mater. Civ. Eng., 10.1061/(ASCE)MT.1943-5533.0000269, 1220-1226.

Zhang, Q. Z., Shen, M. R., and Ding, W. Q. (2015). The shear creep characteristics of a green schist weak structural marble surface. Mech. Adv. Mater. Struct., 22(9), 697-704.

Zhang Q, Shen M, Ding W, et al. (2012). Shearing creep properties of cements with different irregularities on two surfaces[J]. Journal of Geophysics and Engineering, 9(2): 210.

Zhang Q, Shen M, Zhi W. (2011). Investigation of mechanical behavior of a rock plane using rheological tests[J]. Journal of Materials in Civil Engineering, 23(8): 1220-1226.

Zhang, Q. Z., Shen, M. R., Jang, B. A., Ding, W. Q. (2016). Creep behavior of rocks with rough surfaces. Journal of Materials in Civil Engineering,

Zhang, Y, Xu,W. Y., Gu, J. J., andWang,W. (2013). Triaxial creep tests of weak sandstone from fracture zone of high dam foundation. J. Cent. South Univ., 20(9), 2528-2536.

ACKNOWLEDGEMENT

Firstly, I would like to express my greatest appreciation to my supervisor **Associate Prof. JIANG Jing-cai** for his guidance and consistent encouragement during the past several years. Without his consistent and illuminating guidance, it is hard for me to fulfill this thesis.

My sincere acknowledgement also gives to my supervisor in Tongji University Prof. **SHEN Mingrong** for his enlightening insights and constructive suggestions, which deepen my understanding toward the fundamental of rock mechanics.

My appreciation is also extended to my senior, **Dr. ZHANG Qingzhao** for his recommendations in my research. His kind support made it possible for me to smoothly process my research.

I would like to thank all of the laboratory members for their friendship. With a special mention to **Dr. TIAN Guanghui, Dr. WANG Zhen**, who have kindly supported me along the way. It was my fortune to have the opportunity to work my research with all of them.

Last but not the least, I would like to give my deepest gratitude to my family members, my parents, my wife, who have provided me through moral and emotional support in my life. Without their selfless love and support, I would never be the person of my present being.

LIU ANG
Feb. 2018